AFIT/DS/PH/78-1

AD A056542

LEVEL II ① 2

D D C
JUL 19 1978
RECEIVED
F

⑨ Doctoral thesis,

⑥

ANOMALOUS TRANSPORT COEFFICIENTS DUE TO THE

ION-ION TWO-STREAM PLASMA MICROINSTABILITY.

DISSERTATION

⑭ AFIT/DS/PH/78-1   ⑩ Robert C. Backstrom
Captain   USAF

⑪ 25 May 78   ⑫ 186p.

012225

78 07 07 005

ANOMALOUS TRANSPORT COEFFICIENTS DUE TO THE

ION-ION TWO-STREAM PLASMA MICROINSTABILITY

DISSERTATION

Presented to the Faculty of the School of Engineering

of the Air Force Institute of Technology

Air University

in Partial Fulfillment of the

Requirements for the Degree of

Doctor of Philosophy

by

Robert C. Backstrom, B.S., M.S.

Captain   USAF

78 07 07 005

$0/2\ 225$

ANOMALOUS TRANSPORT COEFFICIENTS DUE TO THE

ION-ION TWO-STREAM PLASMA MICROINSTABILITY

by

Robert C. Backstrom, B.S., M.S.

Captain   USAF

Approved:

Chairman

Philip E. Nielsen	12 May 1978
Charles J Bridgman	12 May 1978
Allen M. Hunter, II	12 May 1978
George H Nickel	17 May 1978
William A. Davis	25 May 1978

Accepted:

J S Przemieniecki   25 May 1978
Dean, School of Engineering

Preface

This dissertation is the result of my application of quasilinear plasma theory to the high altitude nuclear explosion debris-air coupling problem. Although I have written the dissertation with this problem in mind, the plasma theory and numerical techniques are applicable to a wide range of physical problems in geophysics and in controlled thermonuclear reactor research. I have written the dissertation with both the reader familiar with quasilinear theory and the reader with only a limited knowledge of plasma physics in mind. The experienced reader can omit the physical discussion sections in Chapter II and all of the derivations in the Appendices without loss in continuity. These discussions are primarily for the inexperienced reader wishing to learn quasilinear theory. I have assumed that this reader, who wishes to understand all of the derivations, has some basic knowledge of plasma physics including Vlasov theory. If not, the references given throughout the dissertation contain the necessary information. For the reader interested in the computer program, I have included an outline of the entire program in Appendix G.

I wish to thank the people at the Air Force Weapons Laboratory, the Naval Research Laboratory, and the Air Force Institute of Technology whose assistance was invaluable in completing my work. I especially thank my coworkers; J. Janni, G. Cable, D. Hollars, G. Radke, and G. Kuller for guidance and for allowing me to work almost full time on the dissertation. I am grateful to H. Murphy, M. Havens, D. Amos, and R. Conley for providing the routines which are incorporated into the program. I thank Drs. P. Nielsen and K. Papadopoulos for their invaluable technical assistance. I am grateful to N. Calder whose fine art

AFIT/DS/PH/78-1

work appears in the figures. I especially thank C. Fields, M. Harville, G. Perea, and M. Barnett for their endless hours of typing assistance. Finally, I thank my wife, Conra Sue, and my children; Eric, Carl, and Katrina; for their physical and moral assistance in completing this dissertation.

<div style="text-align: right">Robert C. Backstrom</div>

AFIT/DS/PH/78-1

Contents

List of Figures

List of Tables

Notation

AMU	atomic weight (atomic mass units)
$\vec{B}$, B	magnetic field (gauss)
$\overleftrightarrow{D}$, D	diffusion coefficient (cm^2/sec^3)
$\vec{E}$, E	electric field (statvolt/cm)
$\mathcal{E}$	spectral wave energy (ergs in 3D or ergs/cm in 2D)
J	current density (statcoulomb/cm^2-sec)
P	pressure (dynes/cm^2)
T	temperature (degrees Kelvin)
V	volume (cm^3)
V_{DA}	computer velocity mesh translation constant (cm/sec)
V_R	initial relative velocity between the debris and air ion beams (cm/sec)
V_α	species average velocity (cm/sec)
W	energy (ergs) or energy density (ergs/cm^3)
$Z_r(x)$	plasma dispersion function $= \frac{1}{\sqrt{\pi}} \int_{-\infty}^{\infty} \frac{dz\, e^{-z^2}}{z - x}$
a	sound speed (cm/sec) $= \sqrt{\frac{\gamma \times T}{m}}$
c	speed of light (cm/sec) $= 3.00(10^{10})$
c_α	thermal speed of species α (cm/sec)
$c_{\alpha\theta}$	thermal speed of species α in wave propagation direction (cm/sec)
e	elementary charge (statcoulomb) $= 4.8(10^{-10})$
f	distribution function (sec^3/cm^6 in 3D or sec^2/cm^5 in 2D)
i	$\sqrt{-1}$
$\vec{k}$, k	wave propagation vector (cm^{-1}) $= 2\pi/$wavelength
m	mass (gm)
n	number density (cm^{-3})

x

q   number of elementary charges (q = 1 means singly charged)

t   time (sec)

u_x, u_z computer velocity mesh coordinates

v_{xo}, v_{zo} computer velocity mesh scale constants (cm/sec)

$\vec{v}$, v   particle velocity (cm/sec)

v_{ac} ion acoustic speed (cm/sec) $= \sqrt{\dfrac{\gamma_e \times T_e}{m_i}}$

v_{alf} Alfvén wave speed (cm/sec) = $\sqrt{\dfrac{B^2}{4\pi n_i m_i}}$

$\vec{v}_{ph}$ wave phase velocity (cm/sec) $= \dfrac{\omega_r}{k^2}\vec{k}$

$\vec{x}$ particle location (cm)

x, y, z   particle location (cm)

α denotes particle species (debris, air, or electrons)

β_e electron beta $= \dfrac{1.5 n_e m_e c_e^2}{B^2/8\pi}$

γ ratio of specific heat at constant pressure to that at constant volume

ϵ_α plasma dielectric of species α

θ angle between the streaming direction and the wave propagation direction (degrees)

χ Boltzmann constant (erg/degree Kelvin) = $1.38(10^{-16})$

λ electron gyro radius vs wavelength parameter $= \frac{1}{2} k_x^2 \rho_{Le}^2$

$\lambda_{D\alpha}$ Debye length for species α (cm) = $c_\alpha/\omega_{p\alpha}$

ν_c anomalous collision frequency (sec^{-1}) $= \dfrac{\left.\frac{\partial\, mom/vol}{\partial t}\right|_{anom}}{m_A n_A(V_A - V_D)}$

π pi = 3.14

ρ_{Le} average electron gyro (Larmor) radius (cm) = $\dfrac{\sqrt{\frac{2 \times T_{e\alpha}}{m_e}}}{\Omega_e}$

ρ_{Li} ion gyro radius (cm) = $\dfrac{V_i}{\Omega_i}$

τ_{norm} time normalization constant (sec) = ω_{pD}^{-1}

ψ angle between velocity point of interest and wave propagation direction (degrees)

ω complex wave frequency (radians/sec)

Ω gyro frequency (sec^{-1}) = $\dfrac{q|e||\vec{B}|}{mc}$

ω_p plasma frequency (sec^{-1}) = $\sqrt{\dfrac{4\pi n_o q^2 e^2}{m}}$

ω_{LH} lower hybrid frequency (cm^{-1}) = $\omega_{pi}\Big/\sqrt{1 + \dfrac{\omega_{pe}^2}{\Omega_e^2}}$

0 subscript   denotes zero order quantity

1 subscript   denotes first order quantity

i subscript   imaginary part or ion species

r subscript   real part

D, A, or e
subscript   species: debris, air, or electrons

α subscript   species

AFIT/DS/PH/78-1

Abstract

Improved calculations of the anomalous transport coefficients due
to the ion-ion two-stream plasma instability are presented. The coeffi-
cients describe the transfer of momentum and energy between the ion
species by the electric fields generated by unstable waves. The calcula-
tions use electrostatic quasilinear theory in two dimensions to trace
the time evolutions of the two ion species. The evolutions are continued
until the transport coefficients reach their maximum values. The evolu-
tions are done for homogeneous plasmas with warm ion beams and a single
hot electron background distribution. The electrons may or may not be
magnetized by a uniform magnetic field perpendicular to the ion streaming
motion. Because the calculations are two dimensional, the unstable ion-
ion waves do not necessarily propagate in the streaming direction. The
presentation includes derivations of quasilinear theory from Vlasov's
and Poisson's equations and several physical discussions regarding the
quasilinear equations. The analytical forms of the anomalous transport
coefficients are also derived. A detailed discussion of the computer
program, IONION, which was written to numerically solve the quasilinear
equations is included. Several test evolutions are done for plasmas
which could characterize the early time nuclear debris cloud surrounding
a nuclear detonation in the terrestrial exosphere. The two ion species
represent the nuclear debris ions in the expanding cloud and the ionized
ambient air being overrun by the debris. The results of the evolutions
indicate that a fair amount of momentum transfer from the debris to the
air occurs when the relative velocity between them is less than the
characteristic wave phase velocity of the plasma, the ion acoustic speed

or the Alfvén speed (respectively for unmagnetized or magnetized electrons). On the other hand, little transfer occurs when the relative velocity is higher than the characteristic speed.

ANOMALOUS TRANSPORT COEFFICIENTS DUE TO THE

ION-ION TWO-STREAM PLASMA MICROINSTABILITY

I. Introduction

Exospheric nuclear bursts inject large numbers of radioactive
fission debris nuclei into the terrestrial magnetosphere. These radio-
active nuclei decay emitting copious numbers of energetic electrons
which often are trapped in the magnetosphere. These energetic electrons
(beta particles) supplement the naturally occurring Van Allen radiation
belts greatly enhancing the flux (electrons/cm^2/sec) of high energy
electrons. (A general discussion of the magnetosphere and trapped radia-
tion is in Ref 1.) Because the beta electrons typically have energies
of the order of 1 MeV, satellites passing through the enhanced belts can
be damaged. This damage problem is particularly severe to the large
scale integrated circuitry being introduced on current and future
satellites as these components often have a relatively low radiation
damage threshold. The problem is of great interest to the agencies who
manage satellite systems, and much effort has been expended to improve
the beta radiation prediction capability.

The topic of this dissertation is an outgrowth of the following
facet of the beta electron injection process: the possible mixing of
the nuclear debris with exospheric air ions by the ion-ion instability.
This instability could occur during the initial outward expansion of the
debris. This expansion lasts about a second after the detonation of the
nuclear device. If the instability occurs and successfully causes the
mixing, the air would accelerate to the debris expansion velocity.
This acceleration of the air is called debris-air coupling. The coupling
problem is discussed in more detail in the next section of this chapter.

1

In the sections of this chapter following that discussion, the dissertation calculation of the ion-ion instability is outlined. Although the dissertation addresses only the ion-ion instability in the context of debris-air coupling, the calculative procedure is applicable to a wide range of physical problems in the fields of geophysics and controlled thermonuclear reactor research.

Debris-Air Coupling Problem

The SPECTER/SAFER computer program, which has been developed jointly by the Air Force Weapons Laboratory (AFWL) and the Lockheed Palo Alto Research Laboratory, calculates the accumulated radiation fluence in electrons per square centimeter received by a satellite from a given exospheric nuclear burst. (The base of the exosphere is considered to be at an altitude of 100 km.) The program first calculates the initial expansion of the nuclear debris as it pushes against the residual atmosphere and the magnetic field of the earth to form a debris-air bubble. The cross section of a typical bubble which surrounds the burst point is shown in Fig. 1. The program then calculates the extension of the ionized debris along the magnetic field lines affected by the bubble. This extension proceeds until the majority of the debris following the field lines ends up in the upper atmosphere of the earth at the conjugate regions shown in the figure. The program calculates the beta decay of the debris as it moves and then calculates the formation of the radiation belts. Finally, the program computes the fluences received by satellites moving through the belts.

One of the factors causing uncertainties in the final fluences calculated by the program is the uncertain fraction of the ambient air which is accelerated to the debris expansion velocity. This acceleration

2
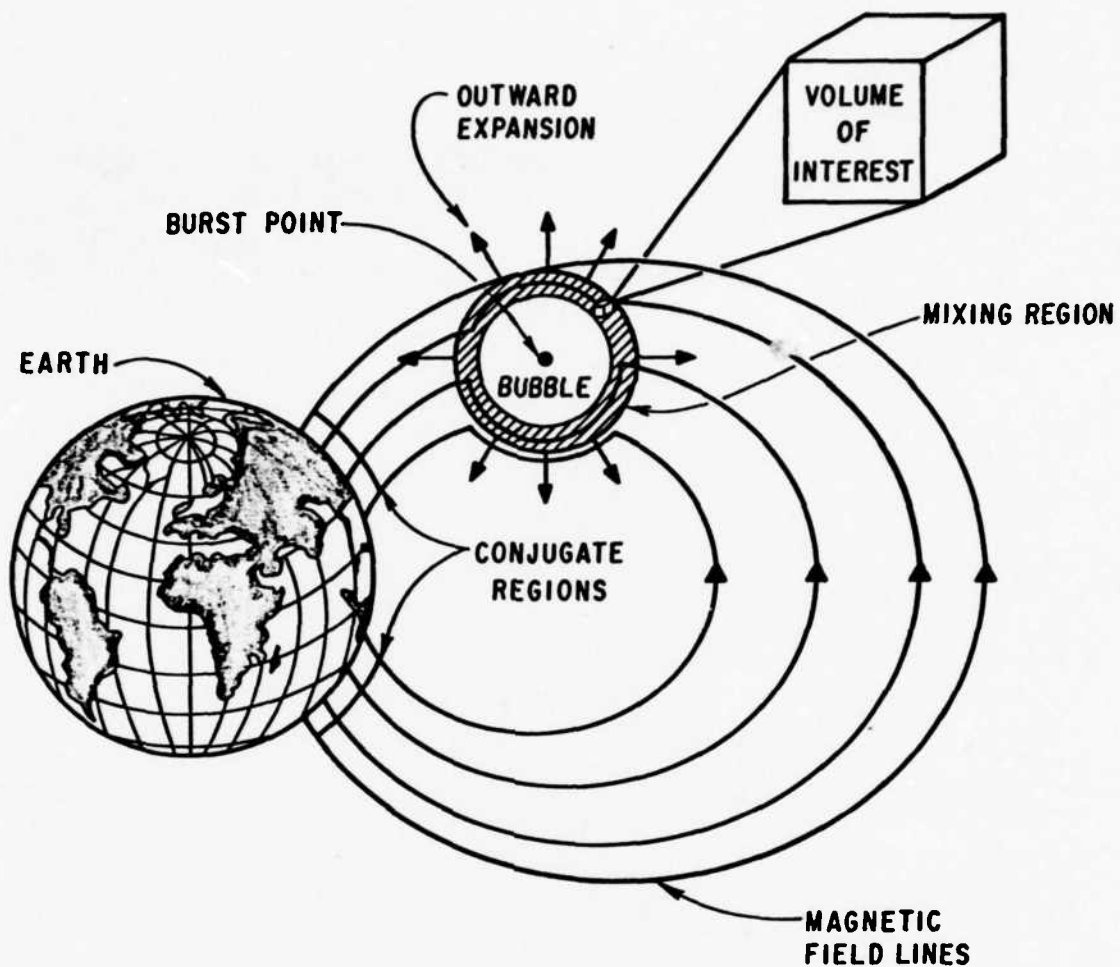
Fig. 1. The Formation of a Debris-Air Bubble in the Exosphere.

during the initial bubble formation is the result of a transfer of
momentum and energy from the expanding debris ions to the air atoms which
have been ionized by x-rays and ultraviolet radiation from the bomb.

If the amount transferred is small, the debris expands outward
impeded only by the magnetic field forming a relatively large bubble. If
the reverse holds, most of the air is accelerated to the expansion
velocity. This accumulation of moving mass rapidly slows the outward
expansion so the bubble is smaller. The resulting radiation belts are
then smaller and more intense significantly affecting the fluences
received by orbiting satellites. For example, a sample calculation has

3

shown that the radius of the bubble from a one kiloton detonation at 400 kilometers is cut in half when the fraction of air coupled to the debris is increased from zero to unity (Ref 2).

The actual fraction of debris-air coupling is calculated by KLYSMA, a large hydrodynamic computer program written by the Naval Research Laboratory (NRL). (Examples on the nature of hydrodynamic theory and some references on the subject are in Chapter II of the dissertation.) The coupling cannot be due to conventional binary collisions in which the debris and air ions simply collide with each other. At the air ion densities characteristic of even a fully ionized exosphere, the average distance an individual debris ion travels between binary collisions is of the order of hundreds of kilometers. This distance is larger than a typical debris-air bubble. However, the coupling can be due to collective interactions between electromagnetic fields and the plasma species: debris, air, and electrons. In collective interactions, large numbers of the plasma particles collectively participate to transfer momentum and energy among them via the fields. The program KLYSMA includes several of these interactions by incorporating anomalous transport coefficients into its hydrodynamic equations. The term "anomalous" means the transport coefficients, which appear in the hydrodynamic equations in the same manner as those due to ordinary binary collisions, actually refer to collective interactions.

One of the most important of the collective interactions causing coupling is the ion-ion two-stream plasma microinstability (Ref 3: 1-2). In a plasma instability, available energy from a nonequilibrium feature is explosively converted into rapidly growing electromagnetic waves. These waves then alter the plasma tending to drive it toward an equilib-

rium configuration. The energy source for the ion-ion two-stream insta-
bility is the relative velocity between the debris and air ions. The
two ion species form the streams or beams of this instability, and the
growing waves tend to reduce their relative velocity. The term "micro-
instability" means the external appearance of the plasma is unchanged
by this instability. Rather, the instability alters the velocity dis-
tributions of the ions. (A velocity distribution describes the probabil-
ity that a plasma particle is traveling at a given velocity. Typically,
the probability distribution is in a gaussian shape--the Maxwell-Boltzman
distribution. The average velocity of the gaussian is the beam velocity,
and the spread around the mean is the thermal velocity which is related
to the temperature. Each plasma species has its own distribution, and
the integral of its distribution over all possible velocities equals the
species density in particles per unit volume.)

Dissertation Calculation

The anomalous transport coefficients from the ion-ion instability
have been included in KLYSMA. The coefficients are obtained from one-
dimensional calculations which assume all of the growing electromagnetic
fields generated by the instability propagate in the radial direction
(the local expansion direction). For reasons which are discussed later,
these one-dimensional calculations are inadequate for large expansion
velocities.

Thus, the objective of this dissertation is to calculate improved
anomalous transport coefficients due to the ion-ion two-stream plasma
microinstability. The plasma parameters used in the calculations such
as the species densities, magnetic field strengths, temperatures, and
relative velocities are chosen to be representative of those which could

5

be found in the solution of a debris-air coupling problem. The calcula-
tions are done simulating both large and small expansion velocities. In
the next few sections, the general nature of the dissertation calculations
is outlined. First, the method used to obtain the anomalous coefficients
is described. Next, the type of plasma and the assumptions used are
outlined. And finally, how the dissertation advances the state of the
art is explained.

   Calculative Method. The calculative method is to solve for wave-
particle interactions the set of electrostatic quasilinear equations
described in the next chapter. In quasilinear theory, a spectrum of weak,
unstable waves is assumed to slowly modify the spatially averaged velocity
distributions of the plasma species. As the averaged distributions
change, the oscillation frequency and wave amplitude growth rate of each
of the unstable wave modes in the spectrum slowly change. Eventually,
the modifications saturate when the waves can no longer change the
distributions.

   The analytical set of equations is solved numerically on a Control
Data Corporation (CDC) 7600 computer using a computer program expressly
written for this task. A particle simulation calculation is not done
because the analytical approach saves computer time and gives better
physical insight. The computer solution follows the changes of the
species distributions with time. This following of the changes in time
is called the evolution of the plasma. Periodically during the evolution,
the wave mode frequencies and growth rates are updated by solutions of
the dispersion relation, one of the equations described in the next
chapter. The calculation is called quasilinear because linear plasma
theory, the solutions of the dispersion relation, is used not only for

6

the initial species distributions but also for distributions which have been evolved in time.

This dissertation includes the evolution of the species distributions for plasmas which generate unstable ion-ion waves. The distributions are evolved in time until the growing transport coefficients, which are related to the wave energies, peak and then begin to decline indicating the approach to quasilinear saturation. Saturation of the ion-ion instability can occur in the debris-air coupling problem because the typical instability growth time of about one microsecond is much shorter than the typical bubble expansion time. The transport coefficients return to zero at saturation, but quasilinear theory is then no longer valid. The dissertation calculations, therefore, give upper limits to the coefficients to help determine whether debris-air coupling is possible and to help estimate the coupling rate. The evolutions are necessary to determine the maximum values of the transport coefficients because these values cannot be accurately estimated from the initial growth rates of the unstable waves. Two different plasmas generating waves with the same growth rates can couple quite differently. An example of this is in Chapter IV.

Plasma Type. The transport coefficients are found for the following type of plasma: (1) The species distributions are initially spatially homogeneous so the calculation represents what is taking place in a small volume in the mixing region near the outer edge of the debris bubble. (See Fig. 1.) The few-kilometer-thick mixing region is much smaller than the bubble size and is where the debris-air mixing takes place. The homogeneous approximation is relatively good when the unstable mode wavelengths and the coupling length (the distance the debris

7

moves during the evolution to saturation) are much less than the mixing
region size. (2) There are no ambient electric fields. (3) A uniform
magnetic field is in the z direction which is perpendicular to the debris
streaming in the x direction. If the debris expansion velocity is
approximately equal to or greater than the Alfvén speed, the magnetic
field of the earth is nearly perpendicular to the local expansion
direction nearly everywhere in the mixing region which forms the edge of
the bubble. This occurs because the Alfvén speed is the speed a low
frequency disturbance can propagate in a magnetized plasma. (This speed
is discussed further in Chapter II.) The bubble expansion is such a low
frequency disturbance, and as a result, the terrestrial field often piles
up on the outside of the bubble as shown in Fig. 1. (The field cannot
easily penetrate the interior of the bubble because it is filled with a
hot, nearly perfectly conducting plasma.) Therefore, the chosen plasma
magnetic field configuration can reasonably represent the compressed
field of the earth in a small volume in the mixing region. (4) The
debris and air ions are assumed to be initially in separate Maxwellian
velocity distributions with the relative velocity between them being the
bubble expansion velocity. These distributions are "warm," meaning that
the ion thermal velocities may be comparable to the relative velocity.
Also, the ion distributions may each have a separate temperature in the
x and z directions. The densities, atomic weights, and ionization levels
of the ion species are not restricted although the densities will usually
be comparable because experience has shown that most of the coupling
occurs at that time (Ref 4). (5) All of the electrons are assumed to be
in a single background Maxwellian distribution possibly with different
x and z direction temperatures. These electrons from both ion species

are assumed to have been mixed together by some faster acting process such as an electron-ion instability. Their distribution thermal velocities will be larger than the ion relative velocities in agreement with the results of electron-ion instability computer simulations (Refs 5 and 6). (6) The dissertation calculation assumes that each ion species is fully ionized at a given ionization level. No neutral particles are included. These approximations are reasonable because most of the ions of each species in a hot plasma tend to be at the same ionization level and because collisions are ignored so neutral particles cannot influence the ions.

Calculation Assumptions. Several basic assumptions are made in the solution of the quasilinear equations. First, the equations are assumed to be valid, meaning that the species distributions change relatively slowly because the wave electromagnetic fields are relatively weak. This condition permits the use of perturbation theory because the changes in the distributions during their evolutions are always perturbations to a known zero order, time independent solution. (See Ref 7: 66-67 for a typical example of perturbation theory.) Quasilinear theory neglects small, high order effects such as the coupling of energy from one wave mode into another. Each wave mode is assumed to remain independent from all of the rest.

The calculation is done in two dimensions. The velocity space distributions of the ions are evolved in the v_x-v_z plane interacting with plane waves having propagation directions in the k_x-k_z plane. Slab geometry, not cylindrical symmetry, has been assumed for the ion distributions and the waves so their coordinates are strictly Cartesian. This means the shape of the ion distributions and the nature of the wave

9

spectrum are unchanged by a translation in the y direction. The calculation would have been one dimensional if the waves propagated only in the k_x direction and interacted with distributions which were functions of v_x only. The reason why the calculation has to be done in two dimensions is that for large relative velocities the unstable wave modes propagate nearly perpendicular to the ion streaming direction.

The electrons are "adiabatic," meaning their distribution does not change with time. The initial type of plasma is chosen so the ion-ion instability dominates over electron-ion instabilities such as the ion acoustic or the modified two-stream instability. The ion-ion instability does not affect the electron distribution so it always is the original Maxwellian.

The two dimensionality of the calculation is relaxed for the electrons when the magnetic field significantly affects their motions. In these magnetized cases, their motions around the field in the v_x-v_y plane are averaged assuming cylindrical symmetry. This process is valid when the wave frequencies are much less than the electron gyro frequency. (A gyro frequency, which is defined in the next chapter, is the rate a charged particle orbits around a magnetic field line. See also Ref 7: 153-156.) Because the electrons are adiabatic, the only change to the quasilinear equations when the field becomes significant is to the electron dielectric term in the wave dispersion relation.

The calculation is assumed to be electrostatic, meaning the magnetic field of each wave vanishes because the curl of its electric field is zero. The electric field of an electrostatic wave is always in the wave propagation direction. For the magnetized cases, a test criterion is evaluated to see if the neglect of the electromagnetic terms in the

dispersion relation introduces a significant amount of error. Electro-static wave modes often grow much faster than electromagnetic modes so they can be expected to dominate the evolution (Ref 3: 29).

The ions are always assumed to be "unmagnetized," meaning they do not see the magnetic field. This approximation is a good one as long as the wave frequency is much greater than the ion gyro frequencies, and the ion gyro radii are much greater than the mode wavelengths and the coupling length.

Relativistic effects are ignored. The relative velocities of interest are at least two orders of magnitude less than the velocity of light.

<u>Advancement of the State of the Art</u>. The complete two-dimensional quasilinear evolutions which are done in this dissertation advance the state of the art. Calculations for the ion-ion instability have been done for two cold, equally dense beams of the same ion species (Refs 8 and 9). The calculations in Reference 8 are done in one dimension using hydrodynamic theory which ignores the effects of the species temperatures. Stability is predicted for large relative velocities. The computer simulation calculations in Reference 9 are done for a magnetic field free plasma and for a ion to electron mass ratio of 25. The Landau damping and/or growth effects (which are explained in the next chapter) on the waves due to the nonzero thermal velocities of the ion distributions are not adequately included in either of these results. Conversely, the dissertation calculations emphasize these effects. Also, the dissertation calculations can be done for cases where the two ion beams have different densities, types of particles, temperatures, and ionization levels. Cases where the electrons are magnetized or unmagnetized can be evolved

11

in two dimensions. This two dimensionality of the dissertation calculations permits the use of unstable wave modes which propagate in directions other than the streaming direction and permits the following of the time evolutions of the species distributions in two dimensions.

Interestingly, before the quasilinear evolutions could be done, linear theory (the use of the dispersion relation for the initial distributions) had to be developed in sufficient generality to be of use in the quasilinear evolutions. A multi-dimensional magnetic-field-free dispersion relation solution for warm ion beams has been done (Ref 10).

Certainly, no large scale numerical solution of the quasilinear equations has been done to include as many effects as are included in the dissertation calculations. The program written to do these calculations was a major undertaking, and none like it exists. These calculations evolve particles both resonant and nonresonant with the waves (Resonant particles have velocities approximately equal to the wave phase velocities as will be explained later.), include the temperatures of the ion beams, include the electron temperature, account for two dimensionality, and include an ambient magnetic field. The availability of a computer with the speed of the CDC 7600 so that the millions of necessary integrations could be done in a reasonable amount of time was extremely helpful in allowing this degree of completeness.

The above discussion regarding the advancement of the state of the art completes the introduction of the topic of this dissertation. First, the background motivation of this topic, the exospheric nuclear detonation debris-air coupling problem, was presented. Next, the dissertation objective and the calculative methods used to reach that objective were described. Then, the type of plasma and the calculation assumptions

were presented. And finally, why this dissertation is a significant advance in the field of plasma physics was explained.

The remainder of the dissertation is as follows: In the next chapter, the equations of quasilinear theory are presented, and their physical significances are explained. In Chapter III, the solution procedure is described. In Chapter IV, the results of the dissertation calculations are presented, and their physical significances are explained. Finally, in the last chapter, the results are summarized and recommendations for further study are made.

II. The Equations of Quasilinear Theory

In this chapter, the equations for electrostatic quasilinear wave-
particle interactions are presented. Most of the algebraic details in
the derivations are included in several appendices. Several additional
derivations are also included in this chapter to give the reader a feel
for what the equations mean physically.

Quasilinear Equations

The equations of electrostatic quasilinear theory governing the
evolution of the debris and air distributions are derived from a simul-
taneous solution of Vlasov's and Poisson's equations (Ref 11: 27 and 34):

$$\frac{\partial f_\alpha}{\partial t} + \vec{v} \cdot \frac{\partial f_\alpha}{\partial \vec{x}} + \frac{q_\alpha e}{m_\alpha}\left[\vec{E} + \frac{\vec{v} \times \vec{B}}{c} \right] \cdot \frac{\partial f_\alpha}{\partial \vec{v}} = 0 \tag{1}$$

$$\frac{\partial}{\partial \vec{x}} \cdot \vec{E} = 4\pi \sum_\alpha q_\alpha e \int_{-\infty}^{\infty} d\vec{v}\, f_{\alpha 1} \tag{2}$$

where $f_\alpha(\vec{x}, \vec{v}, t)$ = distribution function of species α

$$= f_{\alpha 0}(\vec{v}, t) + f_{\alpha 1}(\vec{x}, \vec{v}, t) \tag{3}$$

$\vec{E}$ = electric field = $\vec{E}_1(\vec{x}, t)$ (4)

$\vec{B}$ = magnetic field = $\vec{B}_0$ (5)

e = magnitude of the electron charge = $|e|$ (6)

q_α = number of charge units and sign of charge (7)

The symbol α denotes the plasma species: debris, air, or electrons. The
particle distributions are normalized so

$$n_{\alpha 0} = \text{number density} = \int_{-\infty}^{\infty} d\vec{v}\, f_{\alpha 0} \tag{8}$$

The subscripts 0 and 1 denote zero order and first order quantities
respectively. The equations are in the CGS-Gaussian system of units.
These units are used exclusively throughout the dissertation. Note there

are actually three Vlasov equations in the ion-ion instability problem. One each is for the debris, air, and electrons. In the Vlasov equations for the ions, the magnetic field is set equal to zero. In the electron Vlasov equation, the field is retained for the cases where the electrons are magnetized. Otherwise, the field is neglected for the electrons as well because it is then insignificant. These latter cases are called the field-free cases because none of the species is influenced by the magnetic field.

The Vlasov equation, Eqn (1), is a special case of the total derivative with respect to time of the distribution in Eqn (3). This distribution is a function of the variables $\vec{x}$, $\vec{v}$, and t. The general nature of the Vlasov equation is more apparent if the reader recalls that velocity is the time derivative of distance and acceleration is the time derivative of velocity. The acceleration is written in terms of the electric and magnetic fields causing the acceleration. The total time derivative is zero because the plasma is collisionless. The distribution is written is two parts: The first part is the zero order, spatially homogeneous term which varies very slowly with time. The second part is the small, rapidly varying first order perturbation to the zero order term. The perturbation is caused by the interaction of the plasma particles with the waves, and thus, the spatial and temporal variations of this second term are of the order of the wavelength and oscillation period of a typical wave mode. Vlasov's equation must be solved simultaneously with Maxwell's equations. Because the waves are electrostatic, only Poisson's equation, Eqn (2), is needed.

Field-Free Equations. The field-free quasilinear equations are derived following Drummond and Pines (Ref 12) and Bernstein and

15

Englemann (Ref 13). Their approach is to spatially Fourier transform
Poisson's equation and the spatially averaged, linearized Vlasov's equa-
tion and then solve the results using a Green's function. The details
of this derivation are in Appendix A. An alternate derivation where
correlation theory is used can be found in Reference 14. The resulting
equations are

$$1 - \sum_{\alpha} \frac{4\pi g_{\alpha}^2 e^2}{m_{\alpha} k^2} \int_L d\vec{v} \frac{\vec{k} \cdot \frac{\partial f_{\alpha 0}(\vec{v}, t)}{\partial \vec{v}}}{[\vec{k} \cdot \vec{v} - \omega(\vec{k}, t)]} = 0 \qquad (9)$$

$$\frac{\partial f_{\alpha 0}(\vec{v}, t)}{\partial t} = \frac{\partial}{\partial \vec{v}} \cdot \left[\overleftrightarrow{D}_{\alpha}(\vec{v}, t) \cdot \frac{\partial f_{\alpha 0}(\vec{v}, t)}{\partial \vec{v}} \right] \qquad (10)$$

$$\frac{\partial \mathcal{E}(\vec{k}, t)}{\partial t} = 2 \omega_i(\vec{k}, t) \mathcal{E}(\vec{k}, t) \qquad (11)$$

$$\overleftrightarrow{D}_{\alpha}(\vec{v}, t) = 8\pi \frac{g_{\alpha}^2 e^2}{m_{\alpha}^2} \int_L d\vec{k} \frac{\mathcal{E}(\vec{k}, t) \vec{k} \vec{k} \omega_i(\vec{k}, t)}{[(\vec{k} \cdot \vec{v} - \omega_r(\vec{k}, t))^2 + \omega_i^2(\vec{k}, t)] k^2} \qquad (12)$$

where $\vec{k} = \hat{k} 2\pi / \text{wavelength}$ (13)

$\omega(\vec{k}, t) = $ complex wave
              frequency $= \omega_r(\vec{k}, t) + i \omega_i(\vec{k}, t)$ (14)

$\mathcal{E}(\vec{k}, t) = $ spectral wave
              energy (ergs) $= \lim_{V \to \infty} \frac{1}{V} \frac{E(-\vec{k}, t) E(\vec{k}, t)}{(2\pi)^3 8\pi}$ (15)

The integration procedure $\int_L$ means the integrals in Eqns (9) and (12)
are taken so the results are analytically continuous across the ω_r axis
of the complex wave frequency plane. This procedure, equivalent to
integrating along the Landau contour, is covered in Reference 15. This
reference also has an excellent alternate derivation of Eqn (9).

The four quasilinear equations, Eqns (9) to (12), form a set which

must be solved simultaneously to evolve the ion distributions. Equation
(9) is the linear dispersion relation which determines the real and
imaginary parts of the waves corresponding to a given wave $\vec{k}$. The real
part is the oscillation frequency, and the imaginary part is the growth
rate. A positive imaginary part corresponds to a growing unstable wave,
and a negative imaginary part corresponds to a damped stable mode.
Throughout the dissertation, only the fastest growing unstable mode, if
any, at each wave $\vec{k}$ is located and used. Equation (10) is a diffusion
equation in velocity space. This equation describes the slow evolution
of the species distributions due to the waves. The dyadic diffusion
coefficient which is a function of time and of the spatial variables is
given by Eqn (12). Note each of the ion species has its own separate
diffusion equation and diffusion coefficient. The diffusion equation
for the electrons is not used because they are adiabatic. The only
coupling between the species is due to the waves which are solutions of
the dispersion relation. The time rate of change of the wave energy in
each mode is given by Eqn (11).

The diffusion dyad becomes very large when

$$\vec{k} \cdot \vec{v} \approx \omega_r(\vec{k},t) \tag{16}$$

because $\qquad \omega_r(\vec{k},t) > \omega_i(\vec{k},t) \tag{17}$

The particle velocities where Eqn (16) holds define the resonant regions
of the ion distributions because

$$\vec{v}_{ph} = \text{wave phase velocity} = \frac{\omega_r}{k^2}\vec{k} \approx |\vec{v}|\cos\psi \frac{\vec{k}}{|\vec{k}|} \tag{18}$$

where ψ is the angle between $\vec{k}$ and $\vec{v}$. This resonance also dominates
the behavior of the dispersion relation. The physical significance of
this resonance between the wave phase velocity and the particle velocity

17

is covered later in the section on Landau damping/growth. Note also from Eqn (11), the wave mode energies change exponentially with time. Therefore, the diffusion coefficient has a strong time dependence via the wave energies. These strong dependences of the diffusion coefficient on position in velocity space and on time make Eqn (10) particularly difficult to solve.

The quasilinear equations conserve matter, momentum, and energy. The proof of this is done by taking the first three velocity moments of Eqn (10) as shown in Appendix B.

Equations with a Magnetic Field. Because the electrons are assumed to be adiabatic and the ions are assumed to be unmagnetized, the only quasilinear equation that changes when the magnetic field becomes important is the dispersion relation, Eqn (9). This equation is of the form:

$$1 - \sum_{\alpha} \epsilon_{\alpha} = 0 \tag{19}$$

where ϵ_{α} is the plasma dielectric for species α. The ion dielectrics are unchanged with the addition of the magnetic field and the electron dielectric becomes (Ref 16: 158-234)

$$\epsilon_{e} = \frac{\omega_{pe}^{2}}{k^{2}c_{ex}^{2}} \left\{ \frac{T_{ex}}{T_{ez}} (\lambda - 1) \frac{\omega}{k_{z}} \frac{1}{\sqrt{2}\,c_{ez}} Z'(\alpha_{0}) - \frac{T_{ex}}{T_{ez}} \right.$$

$$- \frac{\lambda}{2} \frac{1}{\sqrt{2}\,c_{ez}} \frac{1}{k_{z}} \left[\left(\frac{T_{ex}}{T_{ez}} (\omega + \Omega_{e}) - \Omega_{e} \right) Z'(\alpha_{1}) \right.$$

$$\left. + \left(-\frac{T_{ex}}{T_{ez}} (\omega - \Omega_{e}) + \Omega_{e} \right) Z'(\alpha_{-1}) \right] \right\}$$

(k_{z} not near zero)

18

or $\quad \epsilon_e = \dfrac{\omega_{pe}^2}{k^2 c_{ex}^2} \lambda \dfrac{\Omega_e^2}{\omega^2 - \Omega_e^2}$ $\qquad$ (k_z near zero) $\quad$ (20)

where $\quad \omega_{pe}$ = electron plasma
$\qquad\qquad$ frequency = $\sqrt{\dfrac{4\pi n_{eo} e^2}{m_e}}$ $\qquad\qquad$ (21)

$\quad c_{ex,z}$ = electron thermal speed
$\qquad\qquad$ in the x, z direction = $\sqrt{\dfrac{\chi T_{ex,z}}{m_e}}$ $\qquad$ (22)

$\quad \Omega_e$ = electron gyro
$\qquad\qquad$ frequency = $\dfrac{|e||\vec{B}_o|}{m_e c}$ $\qquad\qquad$ (23)

$\quad \alpha_n = \dfrac{\omega + n \Omega_e}{\sqrt{2} k_z c_{ez}}$ $\qquad\qquad n = 0, \pm 1$ $\qquad$ (24)

$\quad Z(\alpha_n)$ = plasma dispersion
$\qquad\qquad$ function = $\dfrac{1}{\sqrt{\pi}} \displaystyle\int_L \dfrac{dz\, e^{-z^2}}{z - \alpha_n}$ $\qquad$ (25)

$\quad \lambda = \dfrac{1}{2} k_x^2 \rho_{Le}^2$ $\qquad\qquad$ (26)

$\quad \rho_{Le}$ = average electron gyro
$\qquad\qquad$ (Larmor) radius = $\dfrac{\sqrt{\dfrac{2 \chi T_{ex}}{m_e}}}{\Omega_e}$ $\qquad$ (27)

Equation (20) is derived in Appendix C by averaging the electron motion in the v_x-v_y plane around the magnetic field and by assuming

$$k_y = 0 \qquad\qquad (28)$$

The derivation assumes the electrons are adiabatic so they remain in their original Maxwellian distribution. The well known plasma dispersion function tabulated by Fried and Conte (Ref 17) results from this assumption.

The magnetized dispersion relation in the form given by Eqns (9) and (20) is valid when

$$\Omega_i \ll |\omega| \ll \Omega_e \qquad\qquad (29)$$

$\quad \rho_{Li}$ = ion gyro radius = $\dfrac{V_i}{\Omega_i} \gg \dfrac{2\pi}{k_x}$, coupling length $\quad$ (30)

$$\lambda \ll 1 \qquad\qquad (31)$$

where V_i is the average streaming velocity of an ion species and Ω_i is

19

an ion gyro frequency. The reasons for the first two of these conditions were mentioned in Chapter I. Equation (31) insures the average electron gyro radius is much less than the components of the mode wavelengths in the x direction so the relatively simple form of the dielectric given in Eqn (20) can be used.

Analytical Form of the Field-Free Dielectrics. When the ions are in their original Maxwellian distributions, an analytical form of their dielectrics exists. This same form exists for field-free electrons. This form results when a coordinate rotation procedure is used to evaluate the integral in Eqn (9). The dielectrics are from Appendix D:

$$\epsilon_\alpha = \frac{\omega_{p\alpha}^2}{2\,k^2 c_{\alpha\theta}^2}\, Z'(z_\alpha) \tag{32}$$

where

$$\omega_{p\alpha} = \left[\frac{4\pi\, n_{\alpha 0}\, q_\alpha^2 e^2}{m_\alpha} \right]^{1/2} \tag{33}$$

$c_{\alpha\theta}$ = thermal speed in the wave direction = $\left[c_{\alpha x}^2 \cos^2\theta + c_{\alpha z}^2 \sin^2\theta \right]^{1/2}$ (34)

$$z_\alpha = \frac{\omega - k_N V_\alpha}{\sqrt{2}\, |k|\, c_{\alpha\theta}} \tag{35}$$

The angle θ is that between $\vec{k}$ and the x direction. The average velocity of species α is V_α, and the derivative of the plasma dispersion function defined in Eqn (25) is $Z'(z_\alpha)$.

Anomalous Transport Coefficients

The anomalous transport coefficients are obtained by taking velocity moments of the spatially averaged Vlasov equation. (See Eqn (A-9).) The standard hydrodynamic equations result from this process except that anomalous collision terms replace the normal terms due to binary collisions. The results from Appendix E are (Ref 18: 1954-1955)

$$\frac{\partial}{\partial t}\left[n_{\alpha 0} m_\alpha \vec{V}_\alpha \right] - n_{\alpha 0} q_\alpha e\, \frac{\vec{V}_\alpha \times \vec{B}_0}{c}$$

20

$$= -2 \int_{-\infty}^{\infty} d\vec{k} \ \vec{k} \ \mathcal{E}(\vec{k},t) \ \mathrm{Im}\left[\epsilon_{\alpha}(\omega,\vec{k})\right] \tag{36}$$

$$\frac{\partial}{\partial t}\left[\frac{3}{2} n_{\alpha 0} \times T_{\alpha}\right] = -2 \int_{-\infty}^{\infty} d\vec{k} \ \mathcal{E}(\vec{k},t) \left\{ \omega_i \ \mathrm{Re}\left[\epsilon_{\alpha}(\omega,\vec{k})\right] \right.$$
$$\left. + (\omega_{\lambda} - \vec{k} \cdot \vec{V}_{\alpha}) \ \mathrm{Im}\left[\epsilon_{\alpha}(\omega,\vec{k})\right]\right\} \tag{37}$$

The right hand sides of these equations are the anomalous collision
terms. These terms respectively give the momentum and energy density
transfer rates to the species α due to the spectrum of wave modes.

Physical Meaning of the Quasilinear Equations

At this time in the dissertation, a few discussions about the
physical meanings of the quasilinear equations are presented. In the
sections that follow; an analogy between velocity space and normal
diffusion is drawn, the hydrodynamic equations (sometimes called the
fluid equations) are used to explain the general behavior of waves in
the plasma, and a simple explanation of Landau damping/growth is given.
At the end of the last section, there is a quick summary of the results
from these discussions.

Diffusion Analogy. An analogy can be drawn between velocity space
and ordinary diffusion. In ordinary diffusion, a particle random walks
its way from one location to another at a rate related to the diffusion
coefficient:

$$D \sim \bar{v} l \ \frac{cm^2}{sec} \tag{38}$$

where $\bar{v}$ is the average speed of the particle and l is the mean distance
it travels between collisions (mean free path). Diffusion is a good
approximation when the mean free path is much less than the characteristic
size of the system gradients. In velocity space diffusion, a particle

21

random walks its way from one part of the distribution to another at a
rate related to the diffusion coefficient:

$$D_v \sim \bar{v}_v \, l_v \, \frac{cm^2}{sec^3} \tag{39}$$

where $\bar{v}_v$ is the average acceleration and l_v is the velocity range, Δv,
in which the acceleration takes place. Diffusion is a good approximation
when

$$\Delta v << c_{therm} \tag{40}$$

where the thermal speed, c_{therm}, is the characteristic size of the grad-
ients in velocity space.

The validity criterion given by Eqn (40) can be put in terms of an
energy criterion by assuming the change in the velocity of a particle is
caused by the absorption or emission of a quantum of wave energy. When
the wave energy is equated to the change in particle energy,

$$W_{wave} \sim \Delta W_{particle} = W_{p\,final} - W_{p\,initial}$$
$$= \frac{1}{2} m \left[(v_{initial} + \Delta v)^2 - v_{initial}^2 \right] \tag{41}$$

$$\sim m \Delta v \, v_{initial} \tag{42}$$

$$\sim m \Delta v \, c_{therm} \tag{43}$$

where $\Delta v << v_{initial}$ and $v_{initial} \sim c_{therm}$ have been assumed. The
thermal energy of the particle is

$$W_{p\,therm} \sim m c_{therm}^2 \tag{44}$$

Therefore, when Eqn (40) is multiplied by c_{therm} and Eqns (43) and (44)
are used, the criterion becomes

$$W_{wave} << W_{particle\,therm} \tag{45}$$

Equation (45) is the weak turbulence criterion of quasilinear theory
implicit in the assumption that the wave fields are first order
quantities. The term turbulence does not refer to ordinary spatial
turbulence. Rather, it refers to the turbulent random walk of a particle

22

in velocity space caused by the interaction between it and many growing unstable waves.

Waves in an Unmagnetized Plasma. The oscillation frequencies and phase velocities that result from a solution of the unmagnetized dispersion relation are characteristic of the interaction of the ions in the plasma with the electrons. The low frequency waves of interest characteristically oscillate near the ion plasma frequency and propagate near the ion acoustic speed. These properties can be seen from a simultaneous solution of the linearized hydrodynamic equations of continuity, momentum transfer, and state for each plasma species with Poisson's equation. The solution which includes a zero order streaming velocity, $\vec{V}_\alpha$, is generalized from that of Seshadri (Ref 7: 98-105). These equations for an initially homogeneous plasma are

$$\frac{\partial n_{\alpha 1}}{\partial t} + n_{\alpha o}\left[\frac{\partial}{\partial \vec{x}} \cdot \vec{v}_{\alpha 1}\right] + \vec{V}_\alpha \cdot \frac{\partial n_{\alpha 1}}{\partial \vec{x}} = 0 \qquad (46)$$

$$n_{\alpha o} m_\alpha \frac{\partial \vec{v}_{\alpha 1}}{\partial t} + n_{\alpha o} m_\alpha\left(\vec{V}_\alpha \cdot \frac{\partial}{\partial \vec{x}}\right)\vec{v}_{\alpha 1} + \frac{\partial P_{\alpha 1}}{\partial \vec{x}} - n_{\alpha o} q_\alpha e E_1 = 0 \quad (47)$$

$$\frac{P_{\alpha 1}}{m_\alpha n_{\alpha 1}} = a_\alpha^2 \qquad (48)$$

$$\frac{\partial}{\partial \vec{x}} \cdot \vec{E}_1 = 4\pi \sum_\alpha n_{\alpha 1} q_\alpha e \qquad (49)$$

where a_α = species α sound speed = $\sqrt{\dfrac{\gamma_\alpha \times T_\alpha}{m_\alpha}}$ $\qquad$ (50)

The constant γ is the ratio of the specific heat capacity for constant pressure over that for constant volume. When plane wave solutions of

the type $e^{i(\vec{k}\cdot\vec{x}-\omega t)}$ are assumed and Eqns (46) to (49) are combined, the following dispersion relation results:

$$1 - \sum_{\alpha} \frac{\omega_{p\alpha}^2}{(\omega - \vec{k}\cdot\vec{V_\alpha})^2 - k^2 a_\alpha^2} = 0 \qquad (51)$$

This is the classical multibeam dispersion relation with extra terms $k^2 a_\alpha^2$ which account for the finite temperatures of the beams.

In order to look at the characteristic interaction between a single ion species and the electrons, the existence of only one type of ions and

$$\vec{V_\alpha} = 0 \qquad (52)$$

are assumed. Therefore, Equation (51) becomes

$$1 - \frac{\omega_{pe}^2}{\omega^2 - k^2 a_e^2} - \frac{\omega_{pi}^2}{\omega^2 - k^2 a_i^2} = 0 \qquad (53)$$

The solution of this equation for the low frequencies of interest is

$$\nu_{phi} = \left[\frac{\gamma_i \times T_i}{m_i} + \frac{\gamma_e \times T_e}{m_i} \frac{q_i^2 n_i}{n_e} \right]^{1/2} \qquad (54)$$

The right hand side of Eqn (54) is the general form of the ion acoustic speed for the ion species i. Thus, the wave propagates at the ion acoustic speed. If only one ion species exists, it is singly ionized so

$$\frac{q_i^2 n_i}{n_e} = 1 \qquad (55)$$

and $T_e \gg T_i$; the often quoted expression for this speed results:

$$\nu_{ac} = \left[\frac{\gamma_e \times T_e}{m_i} \right]^{1/2} \qquad (56)$$

The speed is a function of the electron temperature and the ion mass and is much slower than the electron sound speed (Eqn (50) with $\alpha = e$). The phase velocity is slow because the light, rapidly moving electrons

24

generate electric fields which can only slowly transfer the electron momentum to the heavy ions. (A more rigorous explanation is in Reference 7: 102-103.) The condition $T_e \gg T_i$ assures the acoustic waves are not strongly Landau damped, a process which is described later in this chapter.

The oscillation frequency is obtained directly from Eqn (53) by assuming $\omega_{pi} \ll \omega_{pe}$ and $a_i = 0$ ($T_i \ll T_e$). The result is

$$\omega^2 = \frac{\omega_{pi}^2}{1 + \omega_{pe}^2 / h^2 a_e^2} \tag{57}$$

Note $\quad \frac{\omega_{pe}^2}{a_e^2} \sim \frac{\omega_{pe}^2}{c_e^2} = \frac{1}{\lambda_{De}^2} \tag{58}$

where λ_{De} = electron Debye length = $\dfrac{c_e}{\omega_{pe}} = \sqrt{\dfrac{\chi T_e}{4\pi n_e e^2}} \tag{59}$

Therefore, when the wavelength is less than the electron Debye length, the solution, Eqn (57), is

$$\omega \approx \omega_{pi} \tag{60}$$

When the reverse holds, the oscillation frequency is somewhat below the ion plasma frequency. These two cases respectively correspond to stationary ($v_{ph} = 0$) electrostatic ion oscillations and to the ion acoustic wave with a phase velocity given by Eqn (56). To summarize the above results for waves in an unmagnetized plasma, the characteristic wave phase velocity is near the ion acoustic speed, and the characteristic oscillation frequency is near or just below the ion plasma frequency.

Waves in a Magnetized Plasma. The general nature of waves in a magnetized plasma can be seen from fully electromagnetic magnetoionic theory (Ref 16: 9-12). Magnetoionic theory results from the simultaneous solution of the hydrodynamic equation of momentum transfer, Eqn

25

(47), with Maxwell's equations. The theory assumes a cold plasma which means that the pressure term is set equal to zero. Also, no zero order drift velocities exist. In the derivation below, the waves are assumed to propagate in the x direction perpendicular to a uniform magnetic field which is in the z direction.

The type of wave which is of interest is the transverse magnetic (TM) wave. This wave has its magnetic field parallel to the ambient magnetic field. Its electric field lies in the x-y plane as shown in Fig. 2. If the electric field is very nearly in the propagation
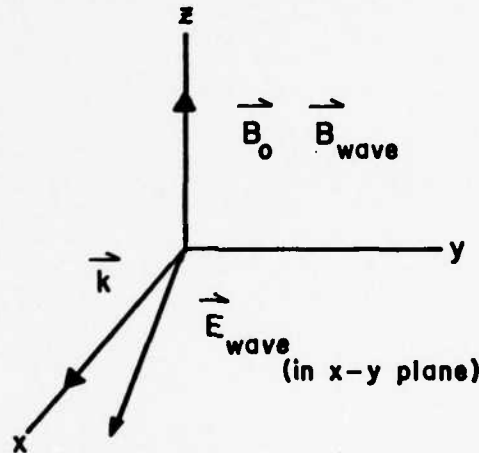
Fig. 2. Transverse Magnetic Wave.

direction, the TM mode becomes nearly electrostatic. The dispersion relation for this type of wave is (Ref 7: 328)

$$\frac{\omega}{c k_x} = \left[\frac{\mathcal{E}_1}{(\mathcal{E}_1 + \mathcal{E}_2)(\mathcal{E}_1 - \mathcal{E}_2)} \right]^{1/2} \tag{61}$$

where

$$\mathcal{E}_1 = 1 - \frac{\omega_{pe}^2}{\omega^2 - \Omega_e^2} - \frac{\omega_{pi}^2}{\omega^2 - \Omega_i^2} \tag{62}$$

$$\mathcal{E}_2 = \frac{\omega_{pe}^2 \, \Omega_e}{\omega(\omega^2 - \Omega_e^2)} - \frac{\omega_{pi}^2 \, \Omega_i}{\omega(\omega^2 - \Omega_i^2)} \tag{63}$$

Again, the existence of only one species of ions has been assumed.

26

Equation (61) can be rewritten as:

$$\frac{\omega}{c\, k_x} = \left[\frac{(\bar{\omega}^2 - \bar{\omega}_{uH}^2)(\bar{\omega}^2 - \bar{\omega}_{LH}^2)}{(\bar{\omega}^2 - \bar{\omega}_1^2)(\bar{\omega}^2 - \bar{\omega}_2^2)} \right]^{1/2} \tag{64}$$

where $\quad \bar{\omega}$ = normalized oscillation
frequency = $\dfrac{\omega}{\omega_{pe}}$ $\tag{65}$

$\bar{\omega}_1 \atop 2$ = normalized cut off
frequencies = $\mp \dfrac{\Omega_e}{2\,\omega_{pe}} + \left[\dfrac{\Omega_e^2}{4\,\omega_{pe}^2} + 1 \right]^{1/2}$ $\tag{66}$

$\bar{\omega}_{uH}$ = normalized upper hybrid
resonant frequency = $\left[1 + \dfrac{\Omega_e^2}{\omega_{pe}^2} \right]^{1/2}$ $\tag{67}$

$\bar{\omega}_{LH}$ = normalized lower hybrid
resonant frequency = $\left[\dfrac{\Omega_e^2}{\omega_{pe}^2} \dfrac{m_e}{m_i} \dfrac{1}{1 + \Omega_e^2/\omega_{pe}^2} \right]^{1/2}$ $\tag{68}$

Note the frequencies in Eqns (65) to (68) are normalized to the electron

plasma frequency. The unnormalized form of the lower hybrid frequency is

$$\omega_{LH} = \frac{\omega_{pi}}{\sqrt{1 + \omega_{pe}^2/\Omega_e^2}} \tag{69}$$

The frequency range for ion wave modes satisfies:

$$\bar{\omega}^2 << \bar{\omega}_{uH}^2, \; \bar{\omega}_1^2, \; \bar{\omega}_2^2 \tag{70}$$

so Eqn (64) becomes

$$\frac{v_{ph}}{c} = \frac{\omega}{c\, k_x} = \frac{1}{\omega_{pe}} \left[\omega_{pi}^2 \frac{\Omega_e^2}{\omega_{pe}^2} - \omega^2 \left(1 + \frac{\Omega_e^2}{\omega_{pe}^2} \right) \right]^{1/2} \tag{71}$$

This equation is valid for the frequency range:

$$0 < \omega^2 < \omega_{LH}^2 \tag{72}$$

The limit of Eqn (71) as the frequency goes to zero is

$$v_{ph} = v_{alf} \frac{n_i q_i}{n_e} \approx v_{alf} \tag{73}$$

where v_{alf} = Alfvén wave speed = $\sqrt{\dfrac{B_0^2}{4\pi\, n_i\, m_i}}$ $\tag{74}$

The ambient field is B_0. Therefore, the characteristic velocity of the

TM mode is the Alfvén speed. The mode propagates approximately at this

speed except when the frequency is almost exactly at the lower hybrid

27

frequency (Ref 7: 330).

The transverse magnetic mode is largely electrostatic when (Ref 7: 400-402)

$$\left| \frac{k_x c}{\omega} \right| \gg |\varepsilon_1| , |\varepsilon_2| \tag{75}$$

The electrostatic version of Eqn (61),

$$\varepsilon_1 = 1 - \frac{\omega_{pe}^2}{\omega^2 - \Omega_e^2} - \frac{\omega_{pi}^2}{\omega^2 - \Omega_i^2} = 0 \tag{76}$$

results when Eqn (75) is assumed. The solution of this equation in the frequency range given by Eqn (29) is

$$\omega = \frac{\omega_{pi}}{\sqrt{1 + \omega_{pe}^2 / \Omega_e^2}} = \omega_{LH} \tag{77}$$

From Eqns (72) and (77), the characteristic frequency of oscillation of the TM mode is close to but somewhat below the lower hybrid frequency.

The electrostatic criterion, Eqn (75), is approximately equivalent to the criterion:

$$\left| \frac{k_x c}{\omega_{pe}} \right| \gg \frac{\omega_{pe}}{\Omega_e} \tag{78}$$

This equation is used to test the validity of the electrostatic approximation for the waves in a magnetized plasma.

The lower hybrid frequency has an interesting physical significance. The high density limit of Eqn (69), $\Omega_e / \omega_{pe} \ll 1$, is

$$\omega_{LH} = \sqrt{\Omega_i \Omega_e \frac{g_i m_i}{n_e}} \simeq \sqrt{\Omega_i \Omega_e} \tag{79}$$

In this limit, the lower hybrid frequency is the geometric mean of the electron and ion gyro frequencies. This same result can be obtained by setting the net electron polarization drift velocity across the magnetic

field equal to the ion velocity. The electron velocity is (Ref 7: 201)

$$v_{ex} = \frac{c \frac{\partial E_x}{\partial t}}{B_0 \Omega_e} = \frac{i \omega c E_x}{B_0 \Omega_e} \qquad (\omega << \Omega_e) \quad (80)$$

where harmonic time dependence for the electric field is assumed. The ion velocity from Newton's second law,

$$m_i \frac{dv_x}{dt} = e E_x \qquad (81)$$

is

$$v_{ix} = \frac{e}{m_i} \frac{i E_x}{\omega} \qquad (82)$$

For simplicity, the ions are assumed to be singly charged. When the velocities in Eqns (80) and (82) are equated, the lower hybrid frequency in Eqn (79) results. At this frequency, the electrons and ions drift together so the plasma has no net current.

Unmagnetized vs Magnetized Waves. The usual method of determining whether the plasma is magnetized or not is by its "beta" which is the ratio of the particle pressure to the magnetic field pressure. Because only the electrons may be magnetized, the relevant beta is that for the electrons:

$$\beta_e = \frac{\text{thermal pressure}}{\text{magnetic pressure}} = \frac{\frac{3}{2} n_e m_e c_e^2}{B_0^2 / 8\pi} \qquad (83)$$

where $\qquad \beta_e << 1 \qquad$ magnetized $\qquad\qquad$ (84)

or $\qquad \beta_e >> 1 \qquad$ unmagnetized $\qquad\qquad$ (85)

The beta also relates the relative importance of the ion acoustic speed and the Alfvén wave speed:

$$\beta_e \sim 2 \frac{v_{ac}^2}{v_{alf}^2} \qquad (86)$$

where the speeds are given by Eqns (56) and (74). The range of validity

of the magnetized equation, however, is determined by the parameter
given by Eqn (26). The relationship between beta and λ is

$$\lambda \gtrsim 2(10^{17})\frac{\beta_e}{(AMU)V_R^2} \tag{87}$$

where V_R is the relative velocity in cm/sec and AMU is the debris atomic
weight in atomic mass units. In the derivation of Eqn (87), the following
were assumed:

$$V_R \gtrsim \frac{v_{ph}}{\cos\theta} \tag{88}$$

$$|v_{ph}| = \left|\frac{\omega_r}{k}\right| \gtrsim \left|\frac{\omega_{po}\cos\theta}{k_r}\right| \tag{89}$$

Equation (88) states the phase velocity is of the order of the relative
velocity. The reason for this will become apparent in the next section.
Equation (89) is true because the oscillation frequency is near the ion
plasma frequency or the lower hybrid frequency. Because the relative
velocities of interest are near 10^8 cm/sec, the magnetized equation
validity criterion, Eqn (31), approximately corresponds to Eqn (84).
Therefore, the choice of the magnetized versus the unmagnetized approach
is consistent with the use of the magnetized equations when Eqn (31)
holds and the use of the unmagnetized set when it does not.

Landau Damping/Growth. The growth rates of the modes in the un-
stable wave spectrum are mostly determined by a resonant interaction
between planes of constant wave phase and an unstable part of the ion
distributions. The unstable part for plasmas where the two ion beams
have a moderately low relative velocity is shown in Fig. 3. The figure
is a top view of the two-dimensional debris and air distributions
plotted as contours in the velocity plane. (The reference frame in this

30
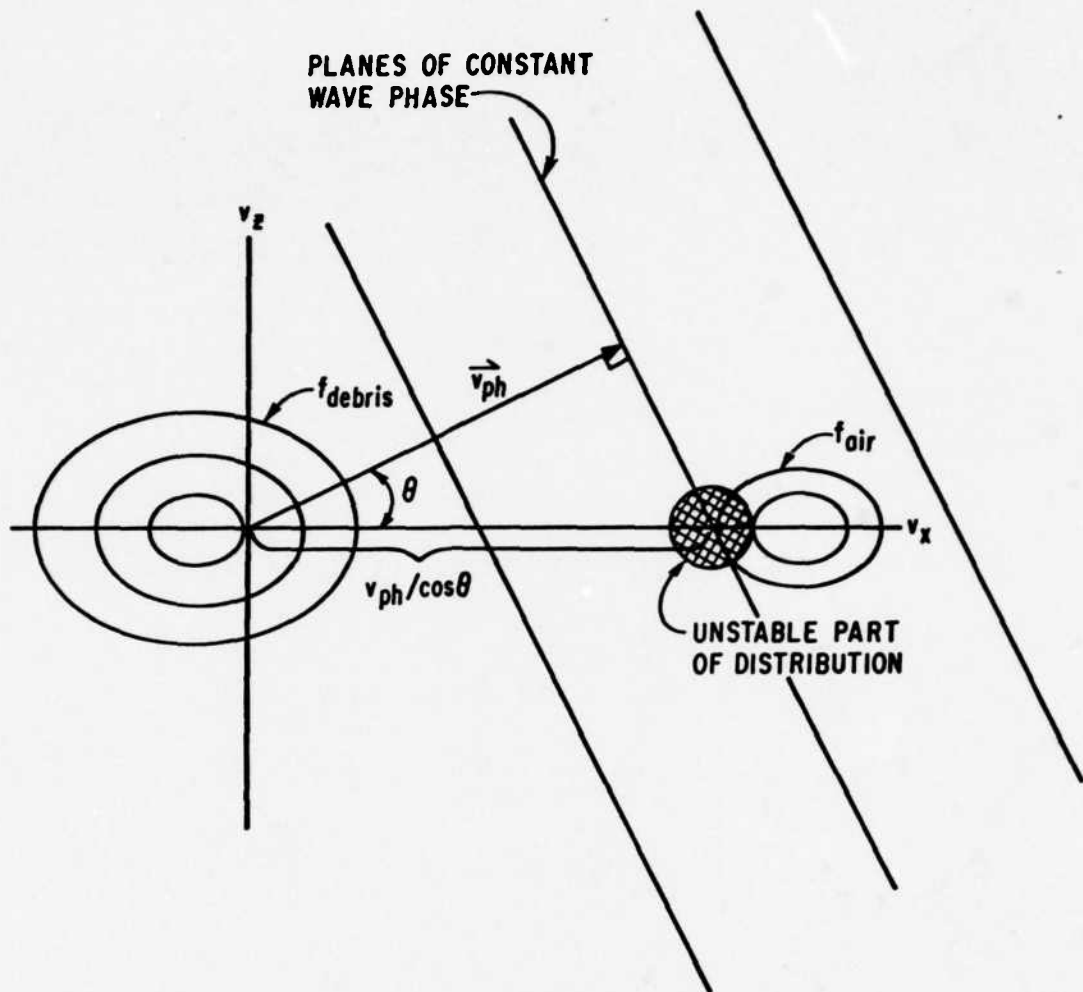
Fig. 3. Resonance Between the Unstable Region and an Unstable Wave.
figure is obtained using a procedure described in the next chapter.) The
distance between the peaks of the debris and air "mountains" is the
relative velocity between the beams (the expansion velocity). A typical
wave mode propagating in the v_x-v_z plane is shown with its phase planes
moving in step with the unstable part. This resonance between the
particles in the unstable part of the distributions and the waves is the
resonance given by Eqn (18). Therefore, the unstable part is the
resonance region of the ion distributions. Because the region is near
the v_x axis, the angles ψ and θ are approximately equal. Also, the

31

resonant particles have velocities which are approximately equal to the approximately constant relative velocity. Thus,

$$\frac{v_{ph}}{\cos\theta} \sim V_R \sim constant \tag{90}$$

The resonant region is unstable because it has a positive slope meaning that more plasma ions are at higher velocities than are at lower velocities. The preferred equilibrium state of the plasma is a single combined ion distribution with more ions at lower velocities than at higher ones. Therefore, as the plasma relaxes toward its equilibrium state, the excess particle kinetic energy must be given to the growing waves. This Landau growth effect is the opposite of the usual Landau damping process which occurs for stable plasmas (Ref 19: 383-392).

An interesting two-dimensional projection effect occurs with the unstable waves. From Eqn (90), only the phase velocity over $\cos\theta$ has to match the relative velocity. If the phase velocity is much smaller than the relative velocity, the resonance can still occur if the angle θ is close to 90 degrees. This projection effect, shown in Fig. 3, allows a wave propagating at the ion acoustic speed or the Alfvén speed to resonate with a pair of ion distributions having a much larger relative velocity. As a matter of fact, the terms "low relative velocity plasma" and "high relative velocity plasma" which are used throughout the dissertation refer to this effect. In a low velocity plasma, the relative velocity is about the same as the characteristic wave phase velocity: either the ion acoustic speed or the Alfvén speed. The unstable waves for this type of plasma propagate nearly in the streaming direction. In a high velocity plasma, the relative velocity is much larger than the characteristic wave velocity so the waves propagate at large angles to

32

the streaming direction.

The exact resonant regions for large relative velocity plasmas lie somewhat off the v_x axis as shown in Fig. 4, a close up view of the air
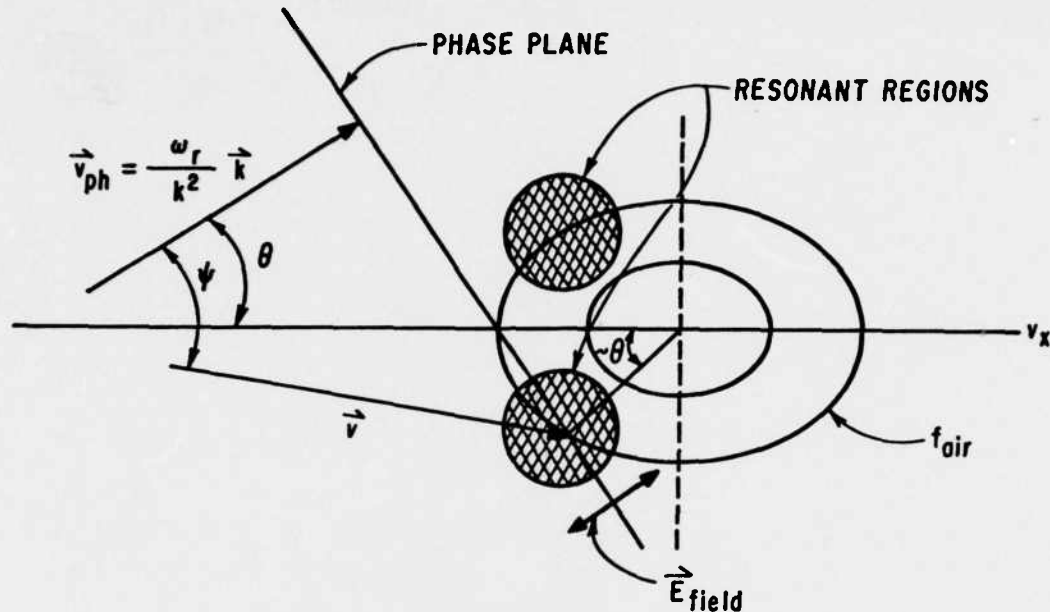
Fig. 4. Exact Resonant Regions.

distribution. The resonance between the typical wave mode and the resonant region below the v_x axis is shown. The equivalent wave mode propagating in the $-\theta$ direction resonates with the region above the axis. (The symmetries of wave modes propagating in various directions is discussed in Appendix F. See Eqns (F-39) to (F-42).) Because the wave modes are electrostatic, their oscillating electric fields can be expected to diffuse the ions primarily in the wave propagation directions. Hence, the resonant regions lie approximately at the same angle to the v_x axis as the fastest growing mode angle.

The unstable waves can only appear if the electrons do not freely move around to cancel out the electric fields generated by the ion motions. The electrons can be hindered by a high temperature or by the applied magnetic field. Hot electrons have a relatively large Debye

33

length (See Eqn (59).) so their shielding effect on the ion generated fields is reduced. Therefore, for the unmagnetized cases, unstable wave modes can be expected for plasmas where the electron Debye length is comparable to the mode wavelengths. For the magnetized cases, unstable modes propagating approximately perpendicular to the magnetic field can exist for a much colder electron distribution. This occurs because the field inhibits the electron motion perpendicular to it. The angular range of these modes around the streaming direction would be relatively small because the cold electrons can freely move along the magnetic field. The allowed free motion of the electrons along the field also explains why electromagnetic effects tend to reduce the growth rates of waves in a magnetized plasma. The wave magnetic field of an electromagnetic wave bends the ambient magnetic field allowing the electrons to move more easily along it. (See also Ref 20.)

As a summary, several general conclusions can be drawn from the discussions in the above sections. They are as follows:

(1) Equation (10) is a diffusion equation in velocity space.

(2) The wave mode oscillation frequencies are determined by the plasma parameters such as density and magnetic field strength.

(3) The mode wavelengths for a given plasma are determined by the relative velocity between the debris and the air.

(4) The growth rates of the wave modes are determined by the shape of the ion distributions and the relative mobility of the electrons.

III. The Numerical Solution Procedure

In this chapter, the general solution procedure for the quasilinear equations is described. First, the reference frame chosen for the solution is presented. Next, the procedure used to solve the equations is described. Then, the recasting of the equations into a form suitable for numerical solution--by no means a trivial process--is covered. And finally, the computer program is described. As before, many of the details are relegated to the appendices.

Before these discussions are started, an important notational distinction must be made: From this point on in the dissertation, the term "distribution" can either refer to the individual species velocity distributions as before, or it can refer to the type of plasma as a whole. The appropriate meaning will always be clear from the context. Usually, the word "distribution" (singular) will refer to the type of plasma, and the word "distributions" (plural) will refer to the plasma species.

Plasma Distribution

A typical assumed initital plasma distribution in an earth stationary reference frame is shown in Fig. 5. The figure shows the nuclear debris ions and the air ions superimposed on the hot electron background. The top half is a side view in the f_α-v_x plane, and the bottom half is the top view showing the two dimensionality of the species distributions. Again, the electrons come from both ion species and are premixed by fast processes that would be essentially complete before the ion-ion evolution begins. All three distributions are Maxwellian. The average velocity of the air is zero, and the relative velocity is the speed the debris moves through the air. The plasma distribution is spatially homogeneous

35
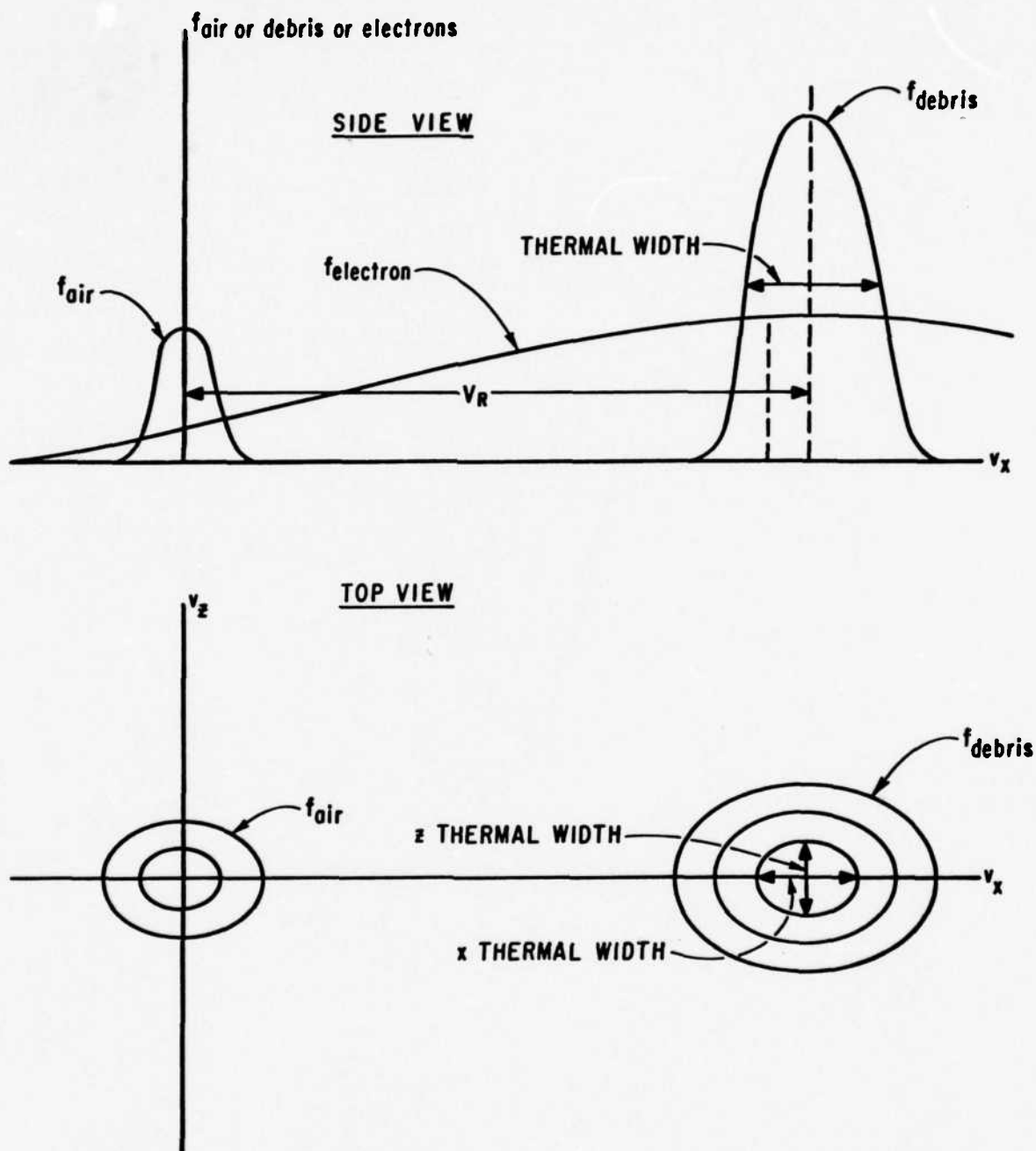
Fig. 5. Typical Plasma Distribution in an Earth Stationary
Reference Frame.

because it represents the plasma in the small volume in the debris-air mixing region shown in Fig. 1.

Figure 6 shows the same distribution in the reference frame used in the computer calculations. This figure has its v_x axis reversed from the previous figure. The average electron velocity and net current are set equal to zero. The debris plasma frequency is assumed to be greater than the air plasma frequency so the fastest growing wave modes are directed toward the right. This choice is for convenience only because the roles of the "debris" and "air" beams can be easily interchanged. The phase velocity of a typical wave mode propagating at an angle θ to the streaming direction is shown. The magnetic field is uniform and is in the z direction.

This reference frame is used in the solution of the quasilinear equations because a known, time independent, zero order solution must exist for the linearization procedures described in the previous chapter to be valid. In this frame, the electrons have no drift velocity relative to the magnetic field so there is no zero order $\vec{V} \times \vec{B}$ motion. Because the ions are unmagnetized as explained earlier, their zero order drift is purely in the x direction, and no $\vec{V} \times \vec{B}$ motion exists for them either. The ion drift velocities are arranged to assure zero order charge neutrality, to set their difference equal to the desired relative velocity, and to set the net current equal to zero. The zero current assures that there is no zero order $\vec{J} \times \vec{B}$ motion of the plasma.

An important point to note at this time is that the plasma parameters stated in the dissertation are given in this reference frame. Again, this is the frame shown in Fig. 6. Examples of such parameters are the species streaming (average) velocities and the wave phase velocities.

37
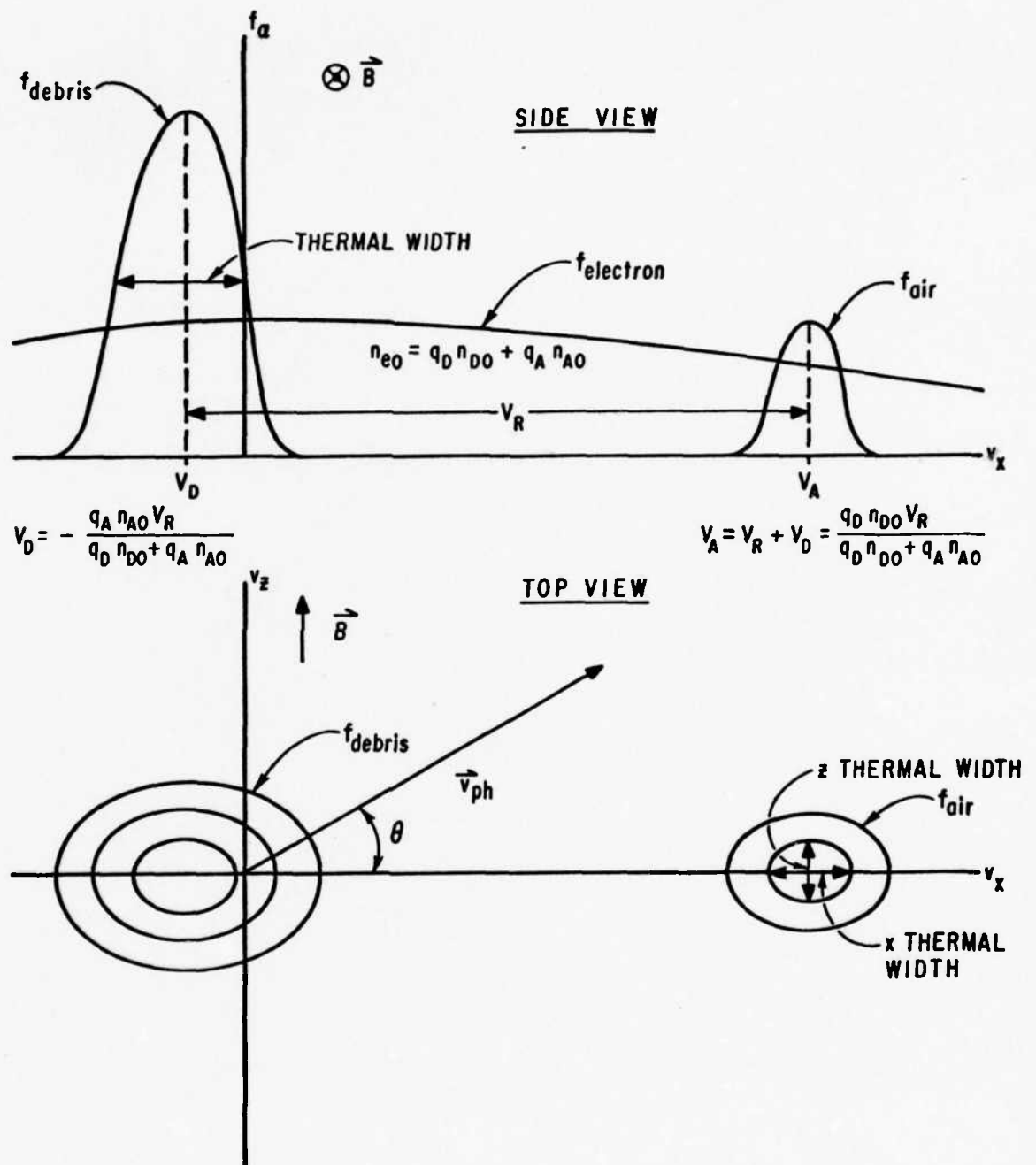
Fig. 6. Typical Plasma Distribution in the Computer Solution
Reference Frame.

Calculative Procedure

The basic calculative procedure, which was outlined in Chapter I, is to trace the evolution in time of the ion distributions as they interact with a spectrum of growing waves. This evolution is the solution of the quasilinear equations. The distributions are followed in time until the anomalous transport coefficients begin declining indicating the approach to saturation. The calculation becomes prohibitively expensive when carried beyond this point. In an evolution, the energy in each unstable mode in the wave spectrum is followed from its original thermal background value to its final value when the calculation terminates. The calculation proceeds by alternately computing the waves and evolving the ion distributions. This procedure makes use of the quasilinear assumption that the wave frequencies and growth rates change relatively slowly.

The evolution calculation is started by finding the unstable wave modes, if any, from the initial Maxwellian species distributions. These solutions of the linear problem use the analytical forms of the dispersion relation because the results can be generated more quickly and accurately. The linear problem must be solved many times because the program must locate the wavelength and propagation direction range of the unstable modes and then compute those modes which are followed during the evolution of the ions.

The ion evolution begins when the wave spectrum is allowed to act on the ion distributions causing them to change in time. This evolution is that described by the quasilinear diffusion equation. The evolution is continued until enough changes in the ion distributions have accumulated so that the wave frequency and growth rate of each mode in the spectrum must be recomputed. The growth rate, which changes faster

than the frequency, is a function of the ion distribution slopes. Thus, the program uses the slope of the faster changing, less dense air distribution to determine when to temporarily stop the evolution of the ions in order to recompute the waves. (The mode update procedure will be explained in more detail in the description of the computer program.)

Because the recomputation of the waves uses evolved ion distributions which are no longer Maxwellian, a numerical form of the dispersion relation integrals must be used. The computation of these integrals is relatively slow so the modes have to be updated as infrequently as possible. The updated modes have smaller growth rates because the general effect of the changes in the ion distributions is to stabilize. The anomalous transport coefficients are computed just after the modes are updated because the integrals for these coefficients need the current values of the frequencies and growth rates.

The calculation continues by alternately evolving the ion distributions and updating the wave modes until it is finished. Each cycle of wave mode update and ion evolution is an "evolution phase." The anomalous transport coefficients which are computed after each mode update initially grow in time as the wave energy in the spectrum increases. When the evolution begins to saturate, the coefficients peak and then begin to decline because the mode growth rates and the imaginary parts of the ion plasma dielectrics are decreasing faster than the wave energy is increasing. (See Eqns (36) and (37).)

Solution Program

The computer program written to solve the four quasilinear equations (Eqns (9) to (12)) is based on a set of routines in the GEARB package from the Lawrence Livermore Laboratory. The GEARB package solves a set

of simulaneous ordinary differential equations resulting from a finite differencing of the diffusion equation, Eqn (10), by the method of lines (Refs 21, 22, and 23). The coefficients for this set of equations include the diffusion coefficient, Eqn (12), which is recast in a suitable numerical form. The other two equations, Eqns (9) and (11), are used to calculate the wave mode frequencies, growth rates, and spectral energies which are needed in the diffusion coefficient integrals.

The computer solution takes place on three separate levels: (1) the complex frequency plane on which the solutions to the dispersion relation are found, (2) the k_x-k_z plane on which the unstable waves are located and the diffusion coefficient integrals are done, and (3) the v_x-v_z plane on which the ion distributions are evolved and the dispersion relation integrals are done. Actually, there are three separate velocity planes, one each for the debris, air, and electrons.

Recasting the Quasilinear Equations. The details of the recasting of the quasilinear equations are in Appendix F. The general recasting procedure begins with a transformation of the entire velocity plane onto a square. The spatial variables of the diffusion equation in the trans- formed coordinates are then finite differenced by the method of lines. Also, the numerical forms of the diffusion coefficient integrals and of the dispersion relation integrals are constructed. The dispersion relation integrals are analytically continued so the dispersion relation results are valid for damped ($\omega_i < 0$) modes. The analytical continuation of the diffusion coefficient integrals is not done because the evolutions are always finished when most of the modes still have positive growth rates. The programming of the analytical continuation of these integrals is a very difficult task.

Computer Program. The quasilinear equations are solved by a set of computer routines controlled by a master program, IONION. This program sets up the problem, controls the solution of the linear problem, controls the evolution of the ion distributions in the manner described earlier, and outputs the results.

Several sets of routines were obtained to perform specific tasks. The first of these, the GEARB package mentioned above, solves the coupled ordinary differential equations. The second set of routines, CONTOUR, is a complex root finder (Ref 24). This set is used to find the complex frequency solutions of the dispersion relation for the initial plasma distribution. The next routine, CROOT, is used throughout the evolution to improve dispersion relation solutions. The fourth set of routines; SINGRT, SINTRP, and XYZSPLN; does differentiations and integrations. The fifth set, DISP, is used to numerically generate the values of the plasma dispersion function and its derivative. The routines CROOT through DISP are available from the AFWL Math Library. The sixth group of routines; SAVEIT, BOSS, and SNAP; was obtained from Harry Murphy at AFWL/DYVM. These are utility routines to write restart files, time functions, and facilitate debugging. A final set of routines, available on the AFWL CDC computer system library, generates plots.

Most of the routines listed above were modified before incorporation into the solution program. A more complete explanation of these routines and of those written for the dissertation is in Appendix G. The appendix also contains a schematic diagram to show how the solution program is organized. A complete listing is available from the dissertation author at AFWL/DYCE, Kirtland AFB, New Mexico 87117. Most of the routines are written in Fortran. The total program length is about 25,000 decimal

words.

An interesting feature of the solution program is that it is also set up to evolve the ions and electrons for magnetic-field-free, electron-ion instabilities. This feature has never been tested, however.

IV. The Computational Results

In this chapter, the results from the computer runs are described. In the first few sections that follow, the tests of the linear solution and the test of the full evolution are discussed. Several test cases were done and were compared with analytical solutions to insure the program was working properly. Only the major tests of the program as a whole are described. Each subroutine was also tested before it was incorporated into the main program. Next in this chapter, a few of the results of debris-air coupling problem simulations at 200 km and 600 km are presented. Only a few highlights are given to avoid inundating the reader with data. A general discussion of these latter results is in Chapter V.

Tests of the Linear Dispersion Relation Solution

The computer results for the linear problem (the dispersion relation solutions for the initial Maxwellian distributions) were tested using three different types of plasmas for which analytical solutions are relatively easy to obtain. The analytical and computer linear solutions for each of these types are compared in the next three sections.

Equal and Opposite Cold Ion Beams. The first test case is for equally cold, equally dense debris and air distributions. The term "cold" means the thermal widths of the ion distributions are much less than the relative velocity between the beams. The ion atomic weights are also assumed to be the same so in the computer reference frame the ion beams have equal and opposite velocities. The unmagnetized electrons are assumed to be hot so unstable wave modes can exist. The relative velocity is chosen to be less than the ion acoustic velocity so the problem is essentially one dimensional. Because the problem is one

44

dimensional, unstable wave modes which propagate in the streaming direction can exist. The analytical solution, therefore, is done in one dimension and is compared with the computer generated modes where $k_x = k$ and $k_z = 0$.

The ions are cold so the wave phase velocities are well away from the bulk of their distributions:

$$\left| \frac{\omega_n}{k} - V_\alpha \right| >> c_\alpha \qquad \alpha = D, A \qquad (91)$$

Also, because the electrons are hot,

$$\left| \frac{\omega_n}{k} \right| << c_e \qquad (92)$$

Therefore, the problem is hydrodynamic, and the dispersion relation in Eqn (51) applies. In hydrodynamic problems, the effect of the distribution shapes can be ignored. This case is very similar to the equal and opposite electron beam problem frequently found in texts. (For example, see Ref 19: 222-227.)

Equation (51) after Eqns (91) and (92) are used becomes

$$1 + \frac{\omega_{pe}^2}{k^2 c_e^2} = \omega_{pi}^2 \left[\frac{1}{(\omega + kV)^2} + \frac{1}{(\omega - kV)^2} \right] \qquad (93)$$

where $\quad \omega_{pi} = \omega_{pD} = \omega_{pA} \qquad (94)$

$$V = -V_D = V_A \qquad (95)$$

$$a_\alpha = \sqrt{\gamma_\alpha}\, c_\alpha \qquad \gamma_e = 1 \;,\; \gamma_b = \gamma_A = 3 \qquad (96)$$

Note the value for γ_e from Ref 25: 189 is the value traditionally used. Equation (93) also results when a power series expansion procedure is applied directly to the non hydrodynamic dispersion relation, Eqns (19) and (32) (Ref 19: 381-392).

The solution of Eqn (93) is (Ref 26: 129-131)

45

$$\omega^2 = k^2 V^2 + \frac{\omega_{pi}^2 k^2}{(k^2 + k_{0e}^2)} \pm \left[\frac{\omega_{pi}^4 k^4}{(k^2 + k_{0e}^2)^2} + \frac{4 \omega_{pi}^2 k^2 V^2}{(k^2 + k_{0e}^2)} \right]^{1/2} \quad (97)$$

where $\quad k_{0e} = \frac{1}{\lambda_{De}}$ \hfill (98)

Unstable wave modes exist when imaginary solutions for the ω in Eqn (97) exist. Hence for instability, the minus sign must be used, and the wave k must be in the following range:

$$0 < k^2 < 2 \omega_{pi}^2 \left(\frac{1}{V^2} - \frac{1}{v_{ac}^2} \right) \quad (99)$$

where v_{ac} is given by Eqn (56). Because k is real,

$$V \overset{\text{must}}{<} v_{ac} \quad (100)$$

for instability. Equation (100) is the usual one-dimensional instability criterion. The solution of Eqn (97) for a wave k which satisfies Eqn (99) is the imaginary part of the complex frequency for the growing mode at that k. The real part is always zero.

The test calculations are done using the plasma shown in Table H-I in Appendix H. Tabulated in this appendix are all of the types of plasmas used for the dissertation calculations. The beam densities are not made exactly equal because that would cause the unstable roots to lie on the imaginary axis of the complex frequency plane. The plasma dispersion function varies many orders of magnitude across that axis so the program gives bad results due to numerical errors. The values of the ion densities are chosen to approximate those found at 200 km above the earth if the air there were completely singly ionized (Ref 27).

For the distribution in Table H-I, the unstable wave k range from Eqn (99) is

$$o < k < 9.2 \ cm^{-1} \tag{101}$$

and the complex frequency solution of Eqn (97) for $k = 6.0 \ cm^{-1}$ is

$$\omega = 0.0 + i\ 3.0\ (10^7)\ sec^{-1} \tag{102}$$

The computer solutions agree well with the results in Eqns (101) and (102). The unstable wave k range is from $2 \ cm^{-1}$ to $9 \ cm^{-1}$, and the complex frequency for $k = 6 \ cm^{-1}$ is $\omega = 8.6(10^5) + i3.0(10^7) \ sec^{-1}$. The small real part in the wave frequency is due to the slight density inequality. Unstable modes are not found for wave k's less than $2 \ cm^{-1}$ due to the following thermal effect: The phase velocity of each unstable mode must match the velocity of the distribution resonant region shown in Fig. 3. Yet, the oscillation frequency must remain near the characteristic one which, in this case, is determined by the ion plasma frequencies. From the definition of the phase velocity in Eqn (18), a small wave k implies too small of oscillation frequency so the plasma waves cannot resonate. This effect is absent in the cold plasma hydrodynamic equations because the distributions are assumed to be infinitely narrow.

An interesting note is that the computer solutions found numerous unstable wave modes which propagate at large angles to the streaming direction. Unstable modes existed at angles from zero degrees to 75 degrees. This result is not predicted by one-dimensional theory.

Bump-on-the-Tail Distribution. The next test case is the bump-on-the-tail distribution which is a weak, cold air beam passing through a warm debris plasma. Like the equal beam distribution, this one also has a commonly done electron analogy (Ref 19: 458-463). Again, the atomic weights of the air and the debris are assumed to be the same. The debris

47

beam is assumed to be warm and much denser than the air beam. The air
beam is assumed to be cool and to have a mean velocity much greater than
the thermal velocity of the debris. Again, the electrons are assumed to
be hot and unmagnetized. A side view, velocity space plot of the sum of
the debris and air distributions in the computer reference frame is
shown in Fig. 7. The initial sum (the solid line in the figure) is that
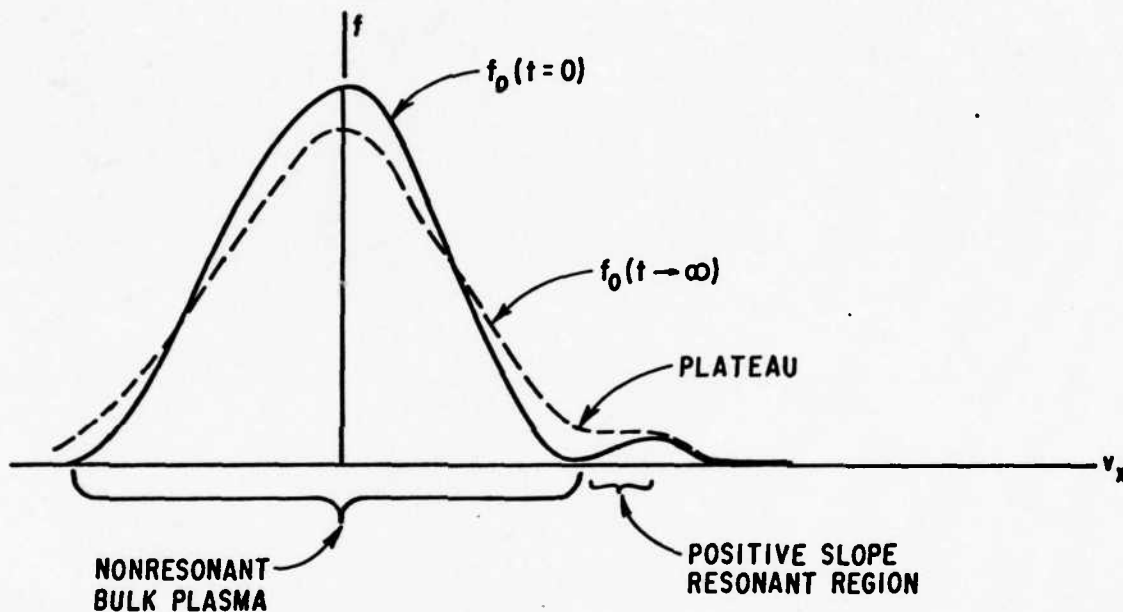
Fig. 7. Bump-on-the-Tail Distribution Before and After Evolution.

used here for the linear solutions. From the figure, the reason for the
name of this distribution is obvious because the air beam forms a small
bump on the tail of the debris distribution. In this reference frame,
the debris is almost stationary so the air velocity is the same as the
relative velocity. This velocity is again chosen to be small enough so
one-dimensional analytical theory is applicable.

The analytical solution of the dispersion relation for the real
part of the frequency by the power series method mentioned in the
previous section is

$$1 + \frac{\omega_{pe}^2}{k^2 c_e^2} = \omega_{p0}^2 \left(\frac{1}{\omega_\lambda^2} + \frac{3 c_0^2 k^2}{\omega_\lambda^4} \right) + \frac{\omega_{pA}^2}{k^2} \frac{1}{\left(\frac{\omega_\lambda}{|k|} - V_A \right)^2} \quad (103)$$

The corresponding solution for the imaginary part is

$$\omega_i = -\sqrt{\frac{\pi}{2}} \frac{\left\{ \frac{\omega_{p0}^2}{k^2 c_0^3} \frac{\omega_\lambda}{|k|} e^{-\frac{\omega_\lambda^2}{2 k^2 c_0^2}} + \frac{\omega_{pA}^2}{k^2 c_A^3} \left(\frac{\omega_\lambda}{|k|} - V_A \right) e^{-\left(\frac{\frac{\omega_\lambda}{|k|} - V_A}{2 c_A^2} \right)^2} + \frac{\omega_{pe}^2 \omega_\lambda}{k^2 c_e^3 |k|} e^{-\frac{\omega_\lambda^2}{2 k^2 c_e^2}} \right\}}{\left[\frac{2 \omega_{p0}^2}{\omega_\lambda} \left(\frac{1}{\omega_\lambda^2} + \frac{6 c_0^2 k^2}{\omega_\lambda^4} \right) + \frac{2 \omega_{pA}^2}{k^2 |k|} \frac{1}{\left(\frac{\omega_\lambda}{|k|} - V_A \right)^3} \right]} \quad (104)$$

In Eqns (103) and (104), the wave phase velocity has been assumed to be much greater than the debris thermal speed. Equation (103) is solved by iteration, and the result is inserted into Eqn (104).

The test calculations are done using the plasma distribution shown in Table H-II. Again, the air density is characteristic of that found at 200 km. The analytical solution is found for $k = 1$ cm^{-1}. For this wave k, only stable modes exist. The analytical and computer solutions for one such mode are

$$\omega = 5.7(10^7) - i \, 7.5(10^5) \text{ sec}^{-1} \quad \text{(analytical)} \quad (105)$$

$$\omega = 5.6(10^7) - i \, 6.9(10^5) \text{ sec}^{-1} \quad \text{(numerical)} \quad (106)$$

The agreement is good with the discrepancy being due to the warmth of the air beam in the computer calculation. The computer solution gives unstable modes for wave k's from 0.075 cm^{-1} to 0.75 cm^{-1} with the fastest growing mode at 0.5 cm^{-1}. The phase velocities of the growing modes are in the positive slope resonant region shown in Fig. 7. Note the real part of the frequency is just below the ion (debris) plasma frequency.

Equal Beam with Magnetized Electrons. The final linear test case is similar to the first except the electrons are cold and magnetized. The analytical solution uses the cold hydrodynamic result, Eqn (93),

49

modified to account for the electron magnetization. Because the ions are unmagnetized, the only change is to the electron dielectric. Therefore, when Eqns (53) and (76) are compared, Equation (93) becomes

$$1 + \frac{\omega_{pe}^2}{\Omega_e^2} = \omega_{pi}^2 \left[\frac{1}{(\omega + kV)^2} + \frac{1}{(\omega - kV)^2} \right] \quad (107)$$

The electron dielectric also results directly from Eqn (20) when Eqns (22), (26), (27), and (29) are used. Equation (107) can be rewritten using the definition of the lower hybrid frequency, Eqn (69):

$$1 = \omega_{LH}^2 \left[\frac{1}{(\omega + kV)^2} + \frac{1}{(\omega - kV)^2} \right] \quad (108)$$

The solution of Eqn (108) follows that of Eqn (93):

$$\omega^2 = k^2 V^2 + \omega_{LH}^2 \pm \left[\omega_{LH}^4 + 4 \omega_{LH}^2 k^2 V^2 \right]^{1/2} \quad (109)$$

Analogous to Eqn (99), the unstable wave k range is

$$0 < k^2 < \frac{2 \omega_{LH}^2}{V^2} \quad (110)$$

The test plasma is shown in Table H-III. For this case, the unstable k range is

$$0 < k < 6.6 \ cm^{-1} \quad (111)$$

and the complex frequency from Eqn (109) for k = 4.8 cm^{-1} is

$$\omega = 0.0 + i \ 2.2 (10^7) \ sec^{-1} \quad (112)$$

The computer solutions corresponding to Eqns (111) and (112) are

$$3.5 < k < 6.7 \ cm^{-1} \quad (113)$$

$$\omega = 6.8 (10^5) + i \ 2.2 (10^7) \ sec^{-1} \quad (114)$$

The agreement, again, is quite good with the discrepancy in the lower end of the wave k range being due to the resonant effect described earlier.

50

The computer solutions for this test case have two very interesting features. First, the unstable modes are all *found in the extremely* small angular range: $0 \lesssim \theta \lesssim 5$ degrees. The cold electrons freely move along the magnetic field stabilizing the waves with even small components of motion parallel to the field. And second, the wave oscillation frequencies quickly increase as the propagation direction moves away from being exactly perpendicular to the field. As θ increases, the wave type changes from an ion-ion wave to a modified two-stream wave. The relationship between the ion-ion and modified two-stream wave types is described later in this chapter.

Test of the Evolution

The test of the computer evolution of the ion distributions is done for the bump-on-the-tail plasma distribution described earlier. Only an unmagnetized test case needs to be done because the ion diffusion equations are unchanged when the electrons become magnetized. In fact, the only place the effect of electron magnetization appears in the quasilinear equations is in the electron dielectric term of the dispersion relation. (The magnetized dispersion relation was tested in the previous section.) In the test evolution, the relative velocity is chosen to be far enough below the debris acoustic velocity so the fastest growing wave modes are in the streaming direction. Thus, the computer evolution should be approximately one dimensional.

A one-dimensional analytical solution of the quasilinear equations follows Davidson (Ref 14: 174-182) and is in Appendix I. This solution gives the time asymptotic behavior of the ion distributions after quasilinear saturation has occurred. A plot showing qualitatively the nature of the asymptotic solution is included in Fig. 7. The figure shows the

51

formation of a plateau in the resonant region and a slight heating of the debris ions. No further changes in the distributions from the configuration shown is possible according to quasilinear theory.

The test evolution is done using the distribution in Table H-IV. Unstable wave modes exist for

$$1.1 \leq k_x \leq 3.7 \quad cm^{-1} \tag{115}$$

with the fastest growing mode:

$$\omega = 8.1(10^7) + i\ 6.3(10^6)\ sec^{-1} \tag{116}$$

at
$$k_x = 3.2\ cm^{-1} \tag{117}$$

$$k_z = 0.0\ cm^{-1} \tag{118}$$

A complete listing of all of the wave modes used in the test evolution is in Table J-I in Appendix J. Tabulated in this appendix are all of the wave modes used to begin each of the dissertation evolution calculations. These modes are derived from solutions of the linear dispersion relation using the initial plasma distributions.

The possible appearances of new unstable wave modes late in the evolution calculations are ignored in this and all other evolutions in the dissertation. The initial modes must accumulate spectral energies several orders of magnitude above the initial thermal values before the distributions begin to change. This large head start insures the insignificance of any late appearing modes in modifying the plasma. Even among the initially growing modes, the fastest growing mode quickly dominates by accumulating a spectral energy much larger than all of the rest.

As can be seen from Table J-I, all of the growing modes propagate within 40 degrees of the streaming direction (the x direction) so the computer quasilinear solution starting with these modes is essentially

one dimensional. The phase velocities over $\cos\theta$ of these modes lie in the range:

$$2.5\,(10^7) \le \frac{v_{ph}}{\cos\theta} \le 2.8\,(10^7)\ cm/sec \qquad (119)$$

which corresponds to the positive slope of the combined distribution shown in Fig. 7. This range is in the resonant region which changes the most rapidly during the quasilinear evolution.

The evolution results are shown in Figs. 8 and 9. In these figures and in all such figures; the debris distribution, the air distribution, and their sum are plotted in a three-dimensional perspective view. The electrons are not plotted as they always remain in their initial Maxwellian distribution. The plane is the positive u_z half of the square which represents the positive v_z half of the velocity plane as is described in Appendix F. (The plane in the figure is the computer velocity mesh.) The point of view is above the positive v_z axis looking downward and in the negative v_z direction. The front and back edges of the plane represent $v_z = \infty$ and $v_z = 0$ respectively. The left and right edges represent $v_x = \infty$ and $v_x = -\infty$ respectively. The heights of the distributions are normalized to the original Maxwellian heights. This normalization is held constant throughout an evolution so a change in apparent height is real. Because in this type of plot appearance of the initial individual debris and air Maxwellians is the same for any type of plasma, the initial ion distribution plots corresponding to Fig. 8a and 8b are omitted for the remainder of the dissertation. The computer program constructs these three types of plots and lists the distribution values over the velocity mesh at the end of each phase of the evolution. These plots and listings, which are available from the author, are used

53

8a. Debris

8b. Air
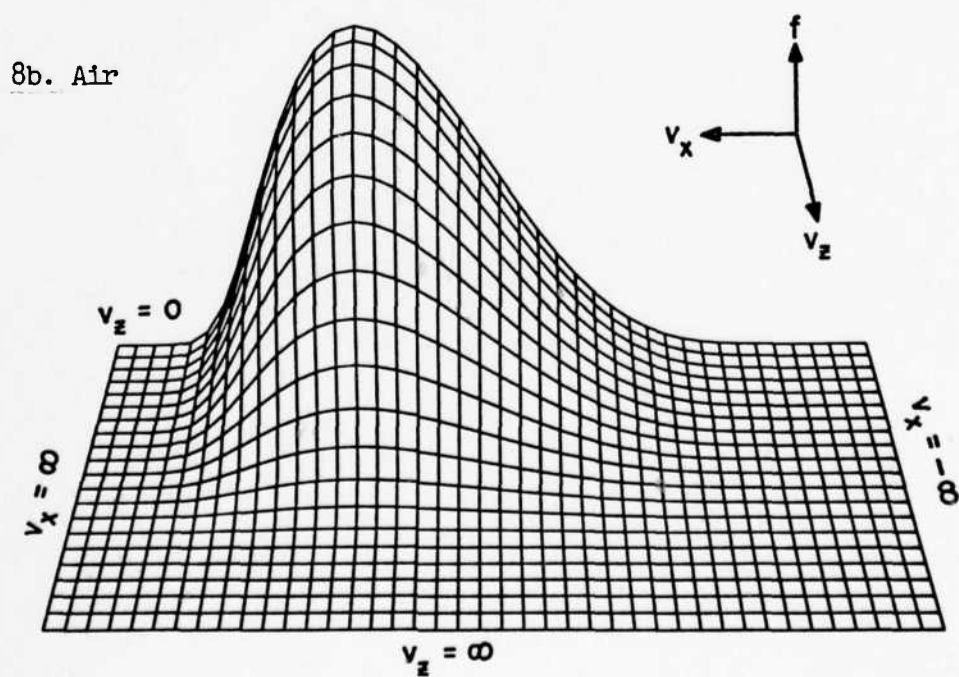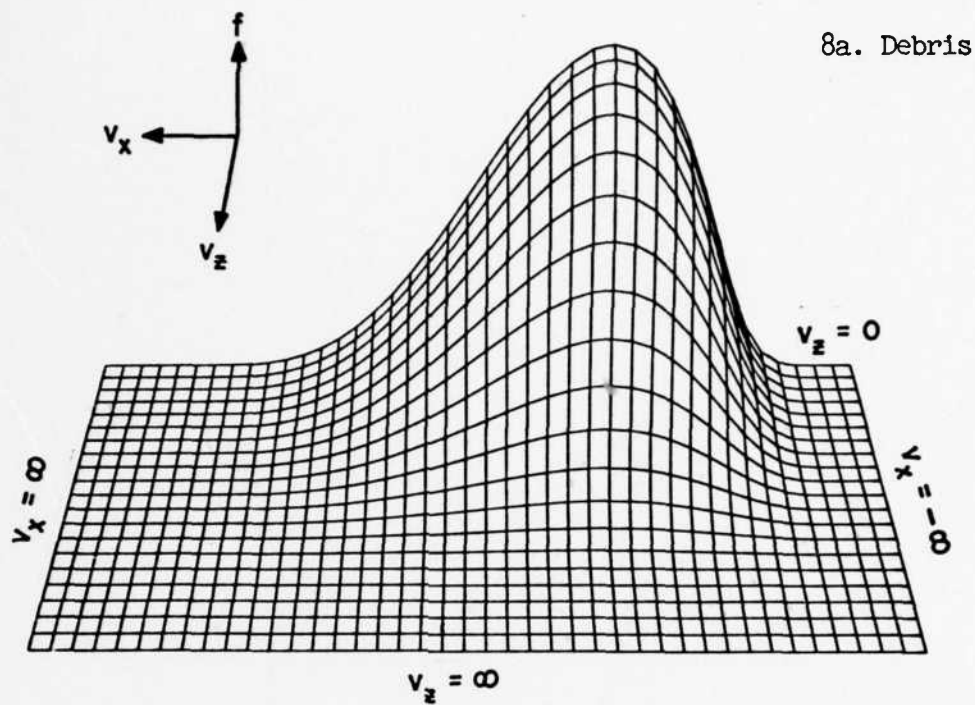
Fig. 8. Initial Distributions for the Bump-on-the-Tail Test Evolution.

8c. Ions

9a. Debris
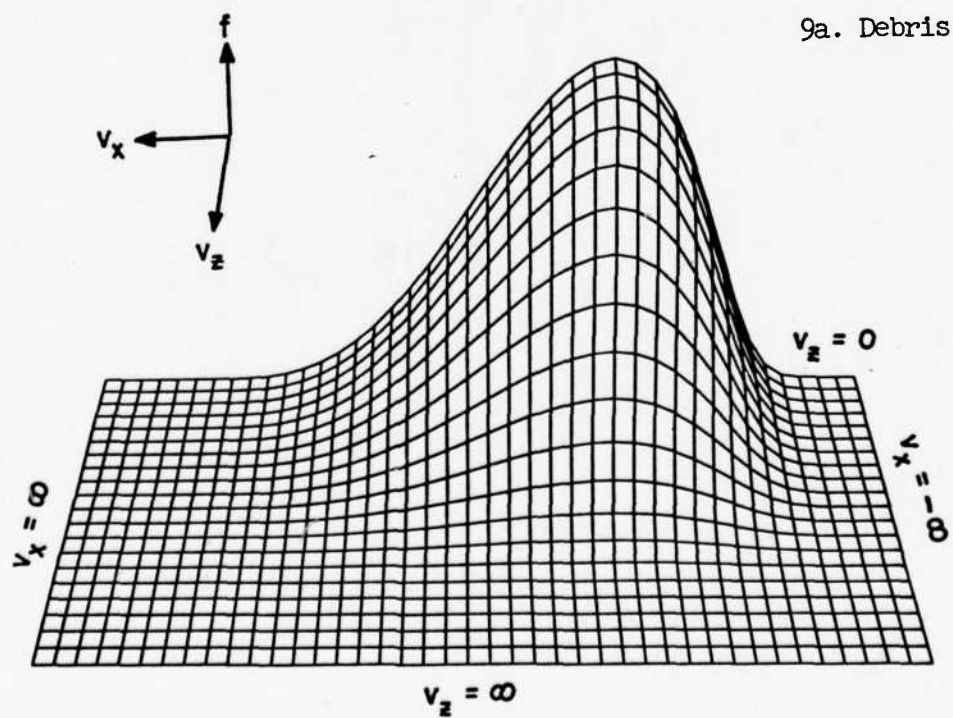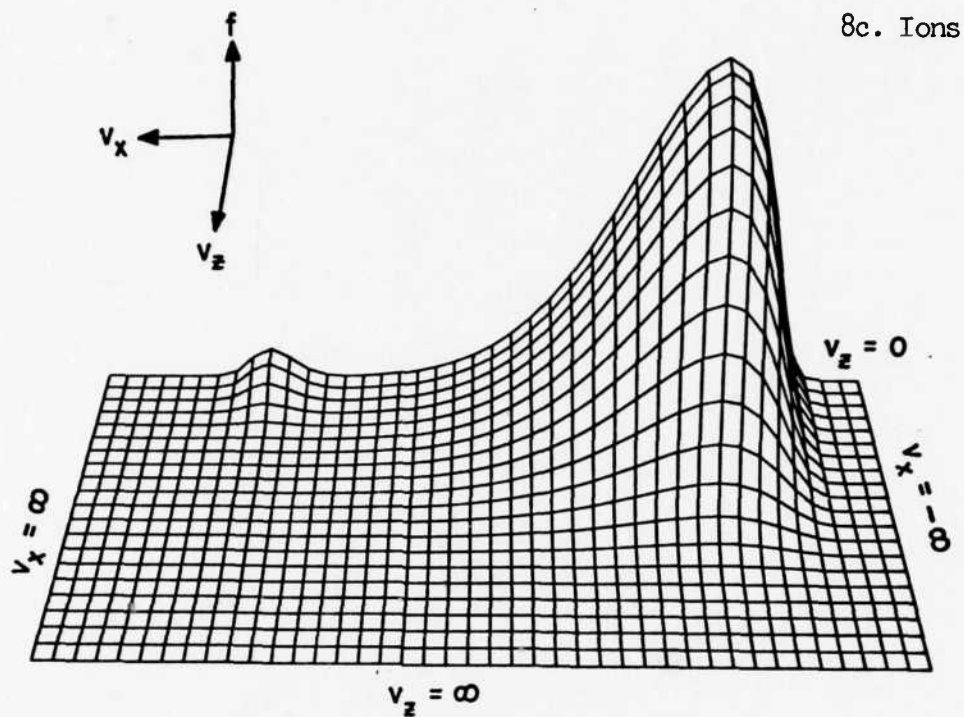
Fig. 9. Final Distributions for the Bump-on-the-Tail Test
Evolution.

9b. Air

9c. Ions

AFIT/DS/PH/78-1
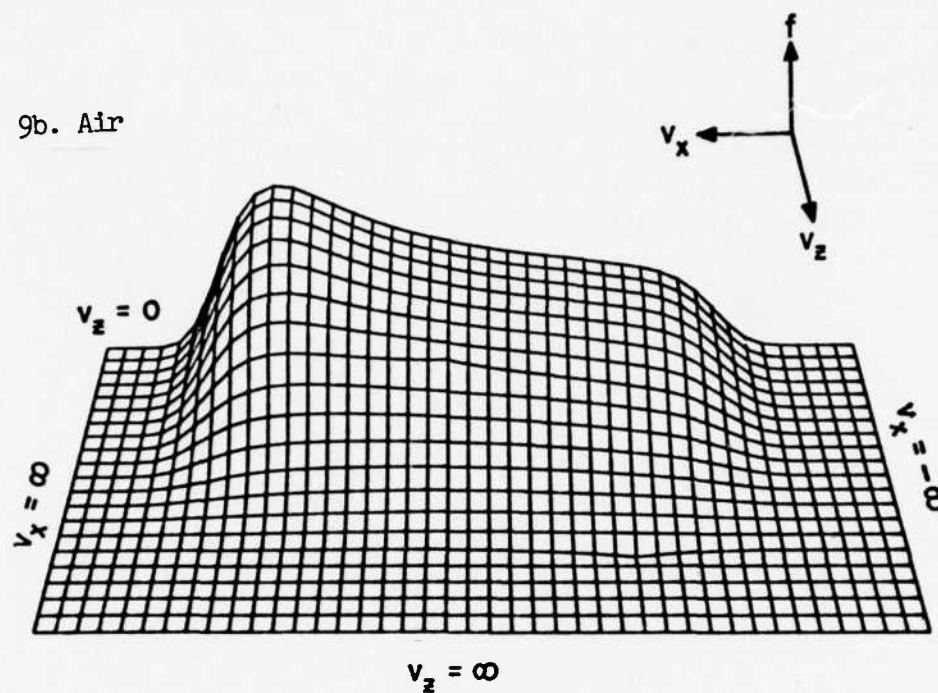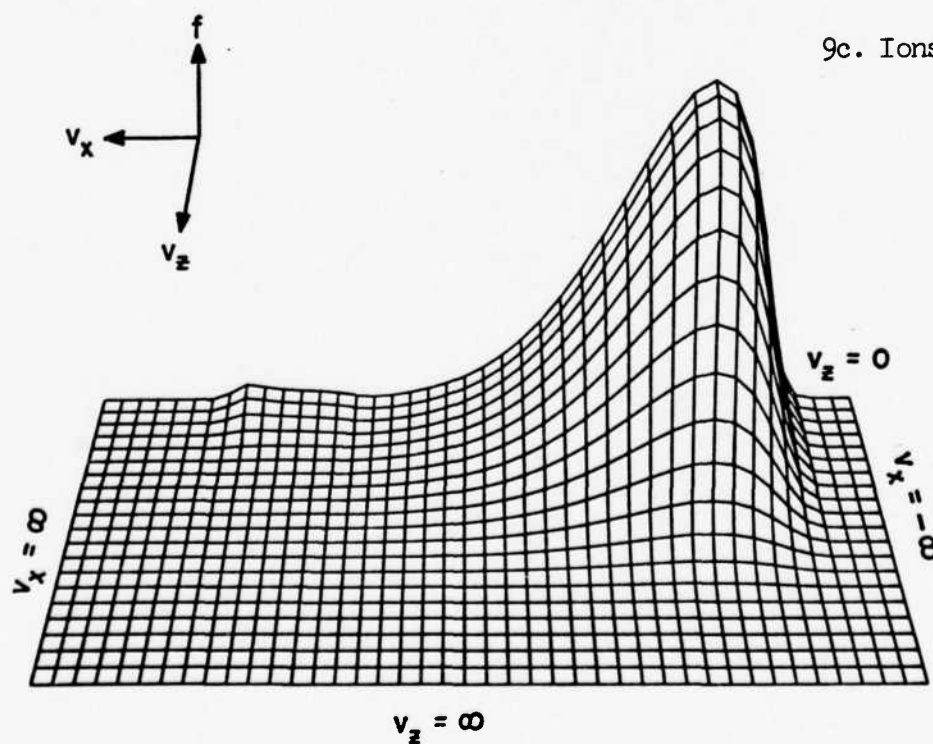
to check on the general progress of the evolutions. Because the plots
are intended to show the qualitative changes to the ion distributions
during the evolutions, the numerical values of the plotted points are not
important, and hence, are omitted.

In Figs. 8 and 9, the initial distributions and the final distribu-
tions calculated are respectively shown. The final distributions are
those at normalized time = 120 where the normalized time is in units of
the debris plasma oscillation time,

$$\mathcal{T}_{norm} = \omega_{p\delta}^{-1} \tag{120}$$

(This time normalization is used frequently throughout the remainder of
the dissertation.) At that time, the wave modes were rapidly changing
from growing modes into damped modes, and the anomalous transport
coefficients were declining. Therefore, Figure 9 shows the distributions
close to saturation.

The computer evolution results shown in Fig. 9 agree well both with
the analytical solution results shown in Fig. 7 and with the assumptions
used in the dissertation calculations. A plateau does form in the reso-
nant region. The temperature of the debris increases 0.4 percent which
approximately agrees with the result, 0.2 percent, from Eqns (I-32) and
(I-34). This change in the nonresonant particle energy is of the order
of the wave energy as predicted by Eqn (I-36). (The discrepancy is
mostly due to the large amount of heating in the tail of the debris
distribution. The tail is in the resonant region, but the computer
temperature calculation includes the tail with the nonresonant particles.
In fact, the change in the resonant particle energy is not computed
because it involves velocity moments of parts of the debris and air
distributions.)

57

The evolution is complete in about 10^{-6} seconds after the ion beams have moved 40 cm relative to each other. This distance (the coupling length) is much smaller than a typical debris bubble mixing region size of a few kilometers so the homogeneous approximation is a good one. The evolution time is much less than the 10^{+1} seconds needed for collisions to alter the distributions significantly (Ref 28: 133), yet it is greater than the time from Eqn (A-31) needed for the neglected free streaming terms to damp away.

The total wave energy throughout the entire evolution is less than the debris and air thermal energies so Eqn (45) holds. (Incidentally, most of the total particle energy is in the electrons.) Therefore, the assumption that the electric fields are first order quantities so the higher order mode coupling terms in Eqn (A-17) can be ignored is reasonable. The wave energy normalized to the initial total ion energy is plotted versus time in Fig. 10. As can be seen from the figure, most of the evolution consists of an approximately linear phase where the wave energy grows exponentially. Late in the evolution, the calculation becomes nonlinear as the changing distributions slow the wave energy growth rate. This behavior is typical of the general nature of all of the evolutions where nothing much happens for most of the time, and then suddenly, a lot begins to happen very quickly.

Because late in the evolution the total wave energy approaches the air thermal energy, the possibility of particle trapping should be investigated. Particle trapping occurs when an ion is trapped by a single wave and is carried along with it. Trapping is a highly nonlinear process so the quasilinear equations break down when it occurs. The time needed for a singly ionized air ion to be trapped is (Ref 14: 54-56)

58
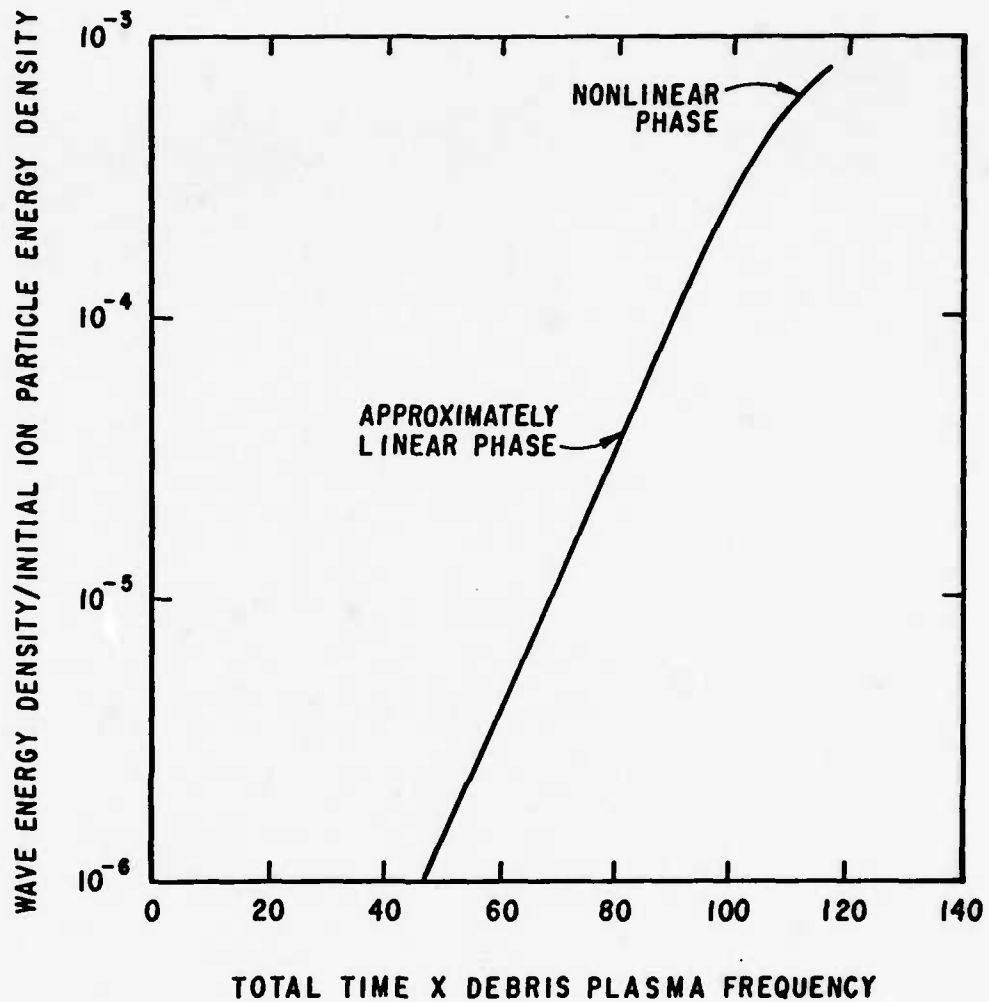
Fig. 10. Normalized Total Wave Energy Density for the Bump-on-the-Tail Test Evolution.

$$\tau_{trapping} \sim 2\pi \sqrt{\frac{m_A}{q_A \ell \, k \sqrt{8\pi \, W_{wave}}}} \qquad (121)$$

$$\sim 1(10^{-6}) \; sec \qquad (122)$$

where W_{wave} is the average electric field energy density in the few fastest growing wave modes. (Most of the total wave energy is in these

59

modes.) The field energy is taken at its maximum value (the worst case). The time in Eqn (122) is about the same as the evolution completion time so particle trapping cannot begin to occur until the evolution is essentially complete.

The maximum momentum transport coefficient is 0.17 $\frac{momentum}{vol-sec}$. This coefficient corresponds to the effective anomalous collision frequency:

$$\nu_c \approx \frac{\frac{\partial mom/vol}{\partial t}\Big|_{anom}}{m_A \, n_A \, (V_A - V_D)} \qquad (123)$$

$$\approx 2(10^5) \; sec^{-1} \qquad (124)$$

where the numerator is obtained from Eqn (36) and the computer results. This collision frequency is about 0.2 percent of the debris plasma frequency. (Note throughout the remainder of this chapter, the anomalous transport coefficient results will always be quoted in terms of an effective momentum transfer collision frequency for air normalized to the debris plasma frequency.) The collision time, which is the reciprocal of Eqn (124), is much less than the collisional relaxation time mentioned above. Therefore, the instability modifies the plasma much faster than binary collisions in agreement with the collisionless assumption of Vlasov theory.

The temporal behavior of the normalized anomalous collision frequency shown in Fig. 11. The exponential growth early in the evolution is clear as well as the fall off late in the evolution as the distributions begin to saturate. The fall off is due to the rapid decline of both the mode growth rates and imaginary parts of their ion dielectrics. The average air velocity normalized to the debris acoustic speed is also shown in the figure. The decrease in the air velocity is the main energy

60
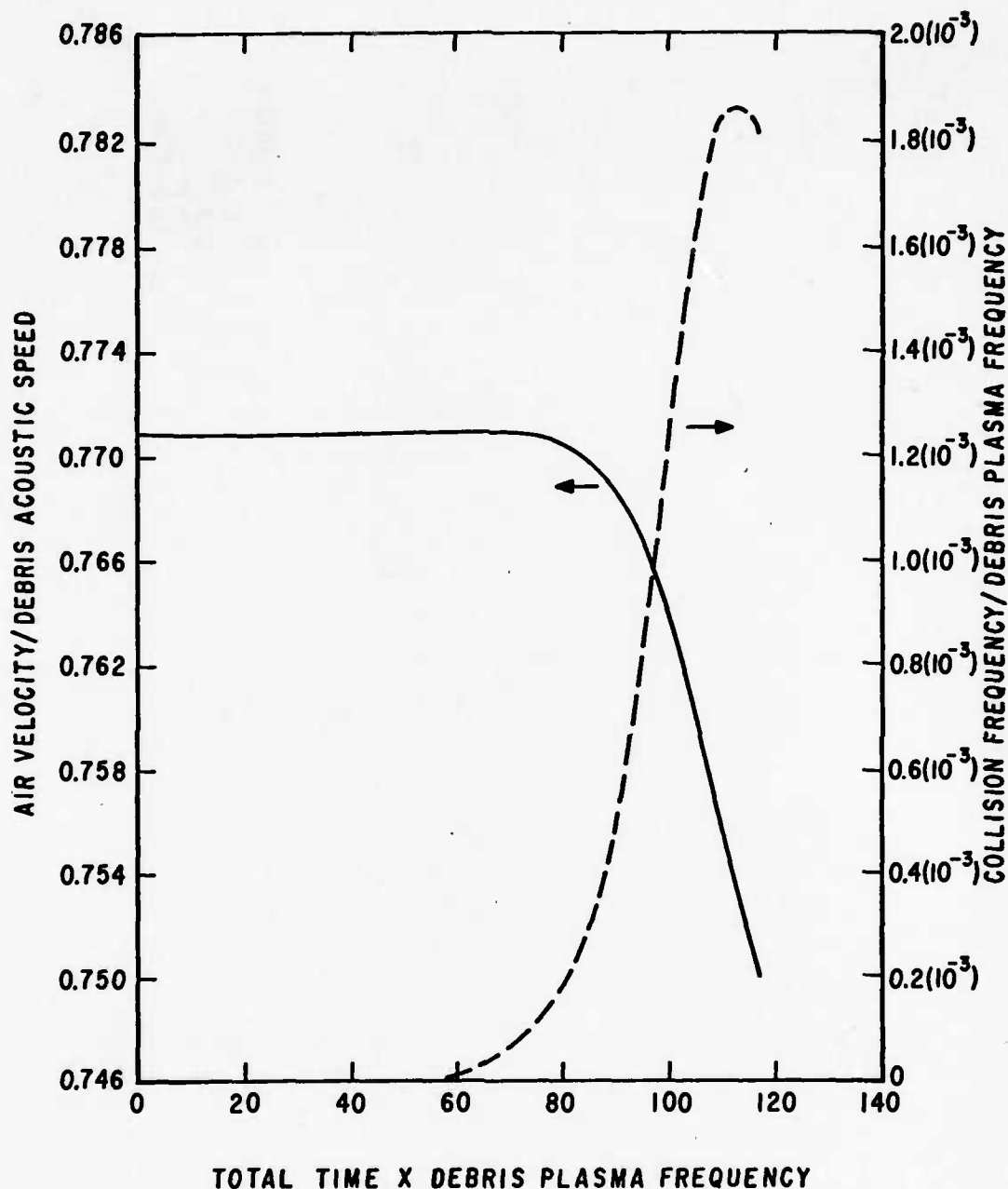
Fig. 11. Anomalous Collision Frequency and Average Air Velocity
for the Bump-on-the-Tail Test Evolution.

source driving the instability.

The temporal behavior of the initially fastest growing mode is shown in Fig. 12. The real and imaginary parts of its frequency normalized to the debris plasma frequency are shown. Again, the approximately

61
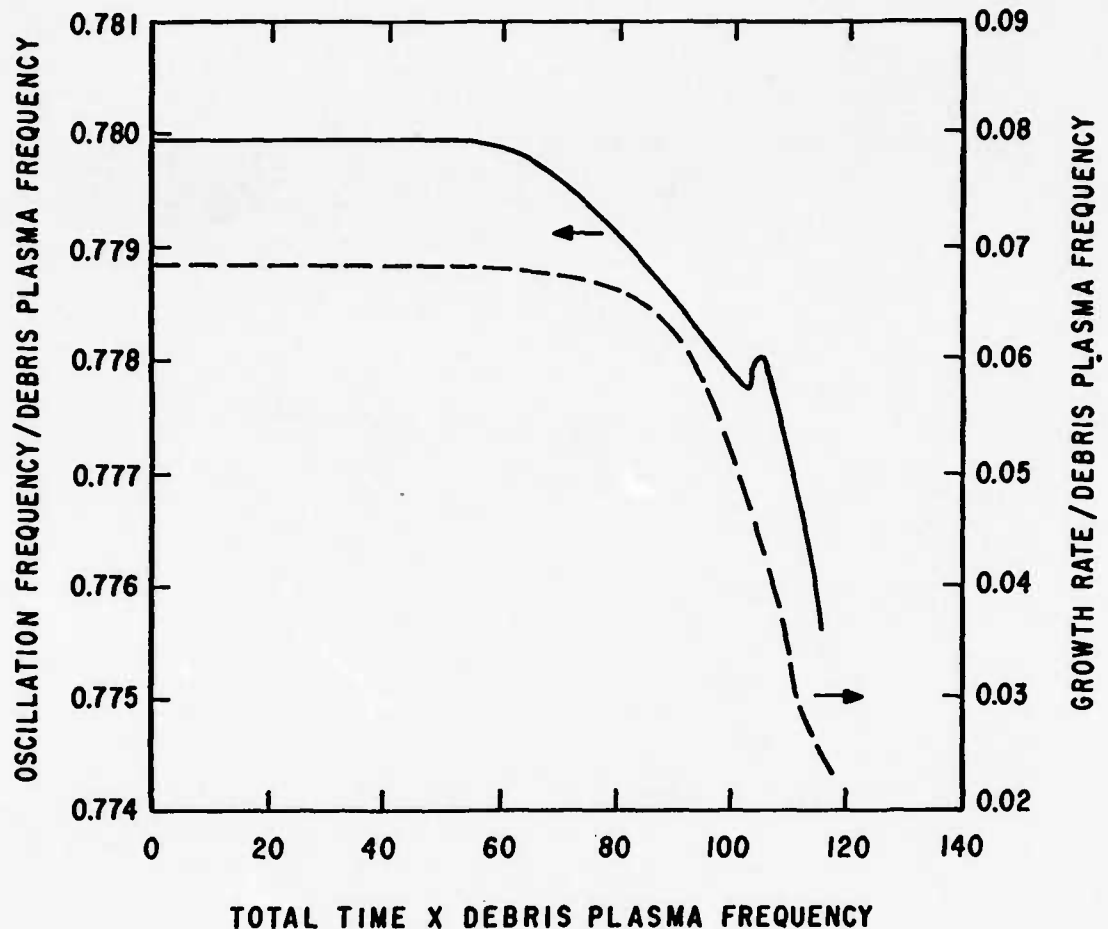
Fig. 12. Temporal Behavior of the Initially Fastest Growing Mode
for the Bump-on-the-Tail Test Evolution.

linear phase followed by the nonlinear phase is evident. The growth rate

falls because the changes in the distributions tend toward stabilization.

The decrease in the real part reflects the decrease in the resonant

region velocity as the air heats and slows down. The real part of the

frequency decreases to maintain the resonance given by Eqn (18). The

small oscillation in this curve is caused by a small inflection in the

air distribution slope passing the velocity resonant with this mode.

The sudden change in the slope of the curve for the imaginary part

near time = 110 in Fig. 12 is due to the calculation beginning to break

down. The wave modes very late in the evolution were not updated often

62

enough. The development of a method of determining the frequency of mode update during an evolution is not a trivial task. Several iterations were required to get a suitable method. The method must update infrequently early in the evolution when the energies in the wave modes are small and update frequently late in the evolution when the distributions are changing rapidly. The distributions in a calculation which breaks down develop oscillations essentially between plus and minus infinity within a few hundreths of an e-folding time. The update control used in the trial evolution was an earlier attempt at the control algorithm. Fortunately, a small degree of breakdown has little effect in the maximum anomalous transport coefficients.

In conclusion, the computer evolution appears physically sound and agrees with an analytical solution. The results also seem to be relatively accurate and consistent. The anomalous momentum transfer coefficients for the debris and air should be equal and opposite. They are to two significant figures. The electron transport coefficients are much smaller than those for the ions so the adiabatic electron assumption is a good one. The numerical version of the dispersion relation applied to the initial Maxwellian distributions gives results which agree with the analytical dispersion relation results. The oscillation frequencies are the same to two or three places, and the growth rates usually agree to about one or two places. Occasionally, however, discrepancies of up to a factor of two appear in the growth rates. Particle, momentum, and energy densities checked by CONSERV are conserved to within one percent. The fast integration routine for the diffusion coefficients, COEFINT, is not very accurate compared to SINGRT. Yet, the net diffusion is the same with the maximum anomalous transport

63

coefficients from an evolution using each routine agreeing to two places. Evidently, because so many diffusion coefficient integrals are done, the inaccurate COEFINT results average out to those of SINGRT. In general, the computer evolution results seem to be accurate to at least within a factor of two.

Debris-Air Evolution Results

The debris-air evolutions are divided into two categories according to whether or not the electrons are magnetized. The reasons for these two categories and the criteria for placing a given debris-air problem into one of them are covered in Chapters I and II. The evolutions using air densities typical of altitudes of 200 km fall into the unmagnetized category because the resulting electron distribution can be expected to overpower any magnetic fields which are present. For air densities typical of 600 km, the reverse holds so such evolutions fall into the magnetized category. Also, at 600 km the electrostatic criterion, Eqn (78), holds quite well for reasonable magnetic field strengths. The evolution results from sample problems in each of these categories are described below.

Unmagnetized Evolution Results. The first sample unmagnetized debris-air problem is the same bump-on-the-tail distribution used above except with a relative velocity greater than the ion acoustic speed. The species distributions and relevant parameters are shown in Table H-V. This distribution is chosen so that two-dimensional effects are emphasized and so the results can be compared to and contrasted with the largely one-dimensional test case. The neglect of the magnetic field is a good assumption because a reasonable 25-gauss field and a typical electron temperature of $3(10^4)$ eV give an electron β_e of $2(10^2)$. The

linear solutions for the unstable modes are shown in Table J-II.

The results of this evolution are shown in Figs. 13 and 14. The distributions shown are respectively the initial one for the ions and those at the time of the maximum momentum transfer rate. The fastest growing mode initially propagates at a 73-degree angle. The heating of the air at approximately that angle to the negative v_x direction is apparent in Fig. 14. The plateau shown in Fig. 7 does not form. When the evolution is finished, the angle of maximum growth decreases to 69 degrees but the large accumulated wave energy in the initially fastest growing mode still dominates the evolution.

The maximum value of the momentum transfer rate is $0.078 \frac{momentum}{vol-sec}$ which is less than half of that for the one-dimensional evolution even though the initial wave growth rates are nearly the same. The momentum transfer rate in terms of the normalized collision frequency is plotted in Fig. 15. The normalized average air velocity is also shown. The dotted line extension to the collision frequency curve is the result from an earlier attempt at the evolution which began to break down just before the peak was reached. This result clearly shows the relative insensitivity of the collision frequency on the exact details of an evolution. This breakdown is also shown in the next figure, Fig. 16. This figure also reveals that the real part of the wave mode frequency increases with time. This is true for most of the evolutions, but the reason for this is not clear. Of course, the imaginary part always decreases with time.

Because the unstable waves for this distribution (where V_R/v_{Dac} = 2.6) propagate nearly perpendicular to the streaming direction, the distribution temperature in the v_z direction increases dramatically. The
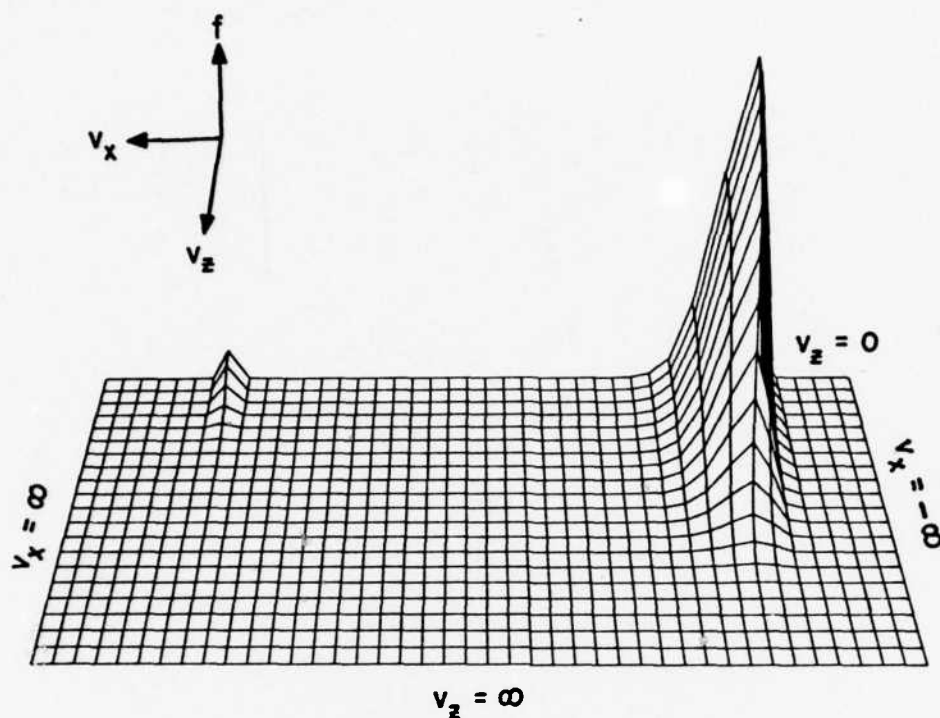
Fig. 13. Initial Bump-on-the-Tail Ion Distribution with a High Relative Velocity.

14a. Debris
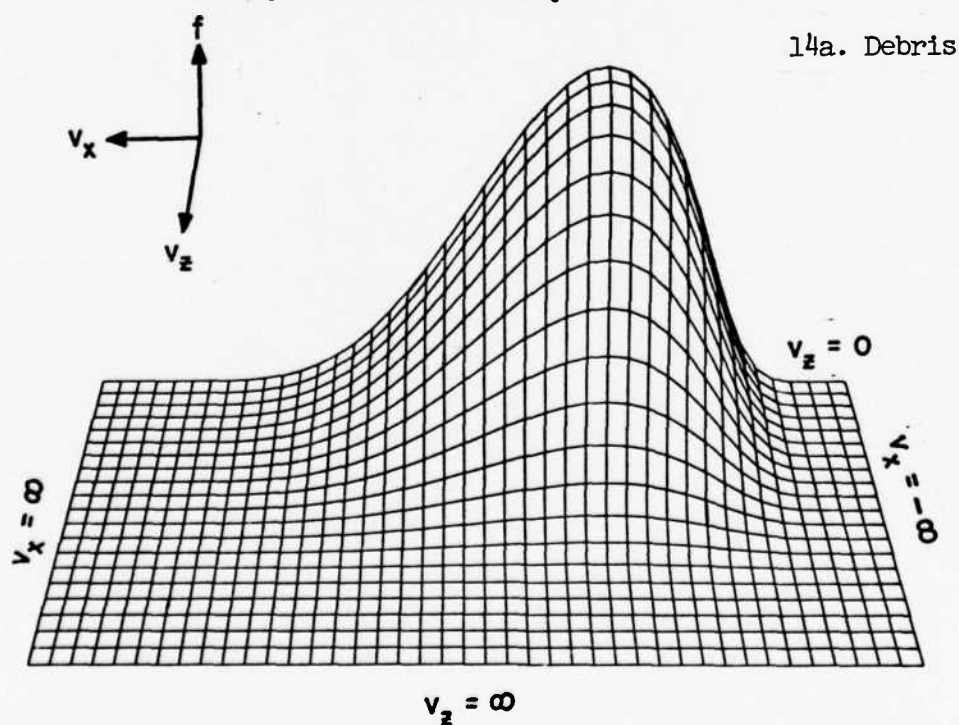
Fig. 14. Peak ν_c Bump-on-the-Tail Distributions with a High Relative Velocity.

66

14b. Air
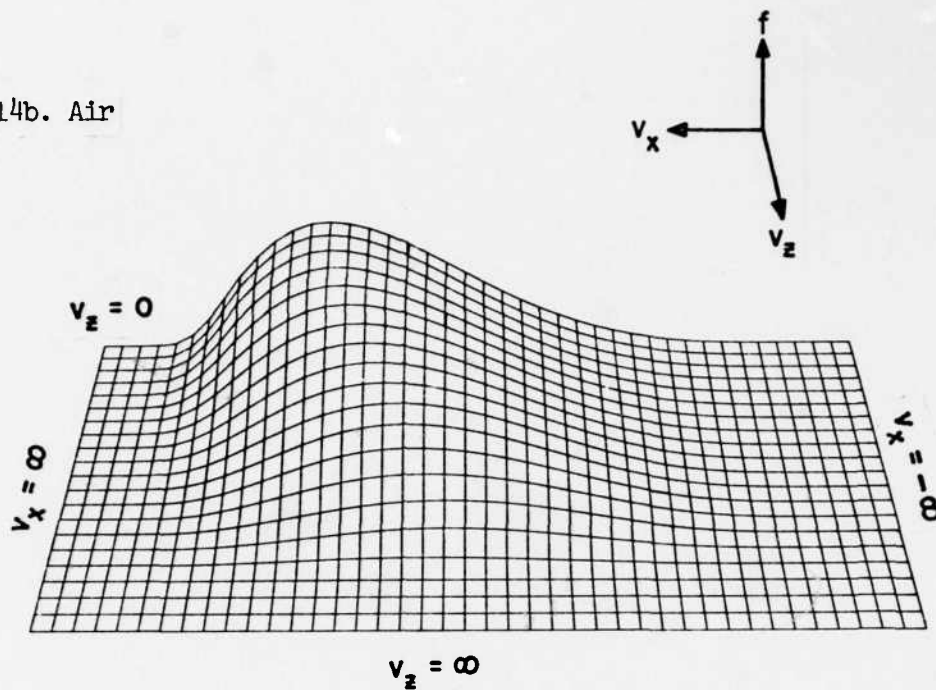
14c. Ions
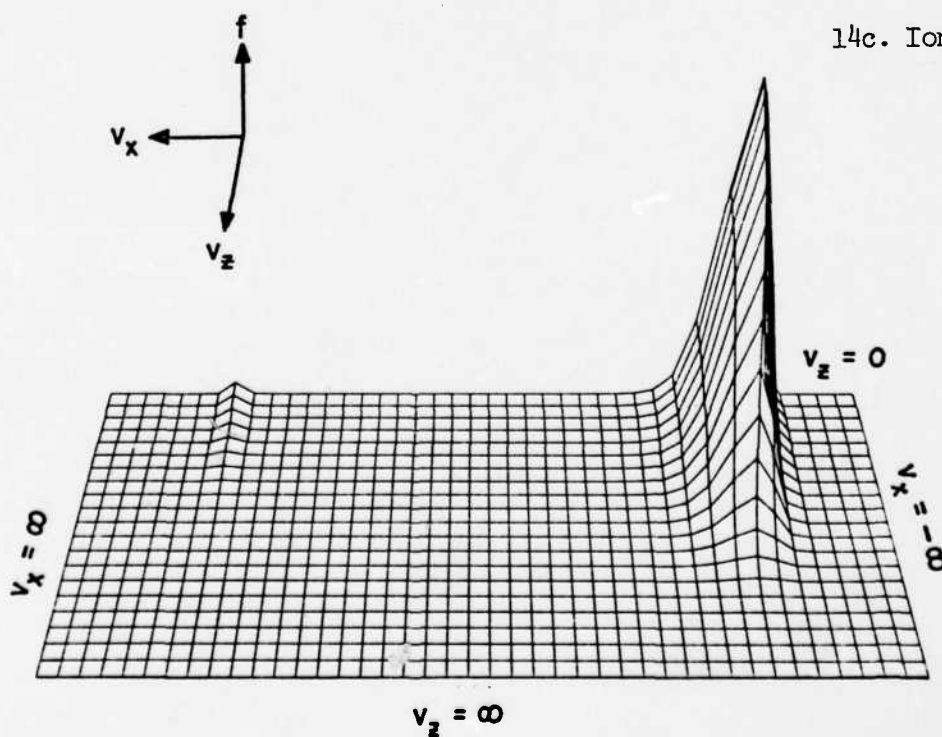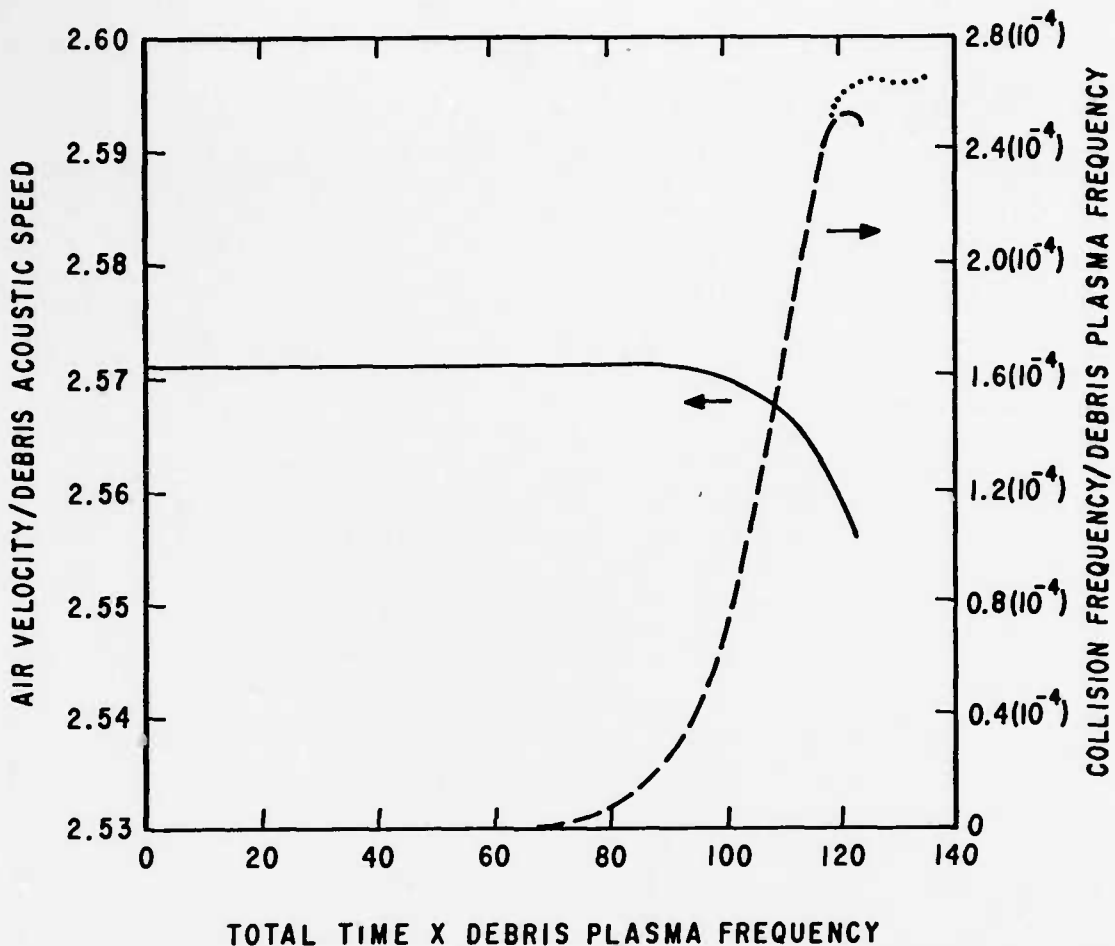
Fig. 15. Anomalous Collision Frequency and Average Air Velocity
for the Large Relative Velocity Bump-on-the-Tail
Evolution.

debris and air v_z temperatures by the time the maximum momentum transfer
rate is reached respectively increase 0.35 percent and 110 percent. The
v_x temperatures actually decrease 0.02 percent and 11 percent respec-
tively These results contrast with the strong v_x heating in the one-
dimensional (V_R/v_{Dac} = 0.78) evolution. The corresponding values to
those above for the v_z temperature increases are 0.01 percent and -5.1
percent, and those for v_x are 0.35 percent and 91 percent. The one-
dimensional anomalous heating rates are somewhat less than those for the
two-dimensional evolution. These observations indicate that at the
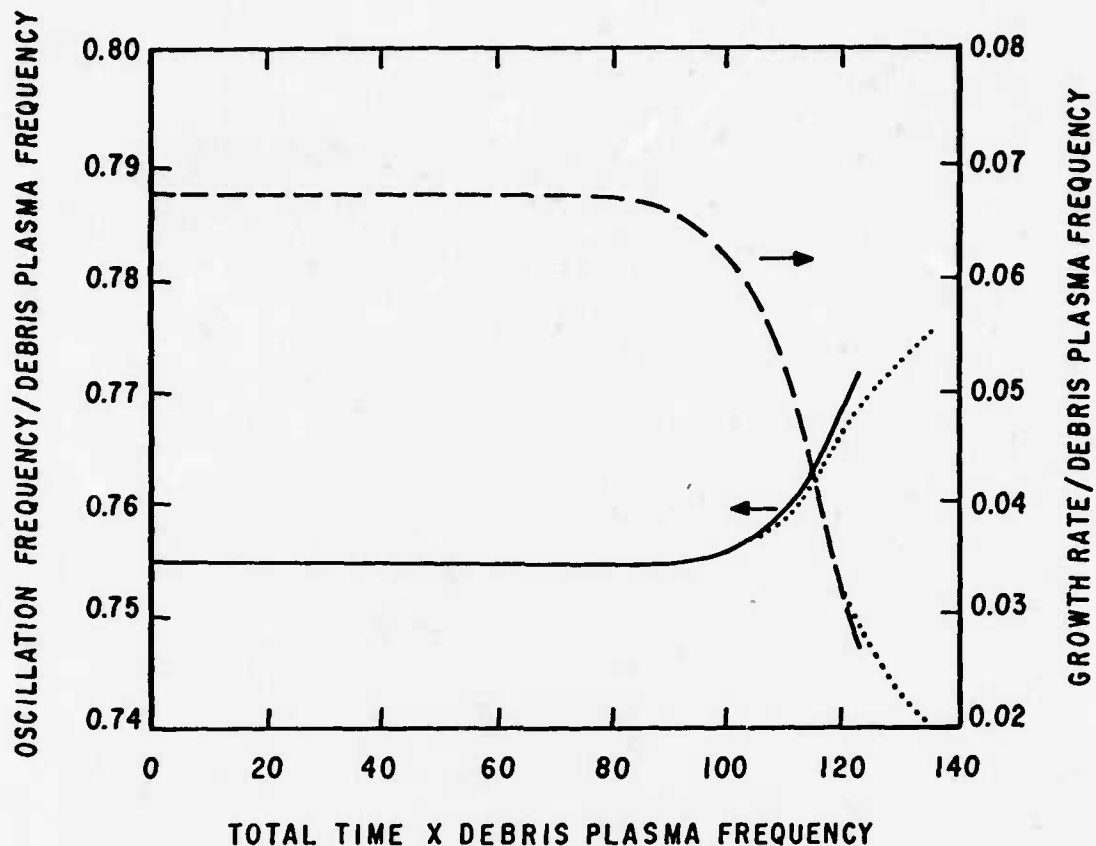
Fig. 16. Temporal Behavior of the Initially Fastest Growing
Mode for the Large Relative Velocity Bump-on-the-
Tail Evolution.

higher relative velocities more of the wave energy heats the distribu-
tions at large angles to the streaming direction but less momentum
transfer occurs. The importance of the use of two dimensionality in the
evolutions is apparent.

The coupling length for the two-dimensional evolution is 130 cm
which is still much smaller than the debris-air mixing region. The ratio
of the total wave energy at the time of the peak momentum transfer rate
to the initial thermal wave energy is $6.3(10^3)$. The evolution took 50
min of computer time while the one-dimensional evolution took 2 1/4 hrs.
The difference is mostly due to the relatively large number of wave
modes followed in the one-dimensional case.

The next two evolutions are the 2C0-km simulations which are done
for low and high relative velocities. The low velocity distribution
parameters are shown in Table H-VI, and those for the high velocity run
are in Table H-VII. The corresponding linear solutions are in Tables
J-III and J-IV. Before these distributions were evolved, the possible
existence of the ion acoustic instability between the electrons and
either of the ion beams was examined (Ref 19: 476-478). The ion acoustic
modes do not exist, however, because the warm temperatures of the ion
beams shut off the instability. (The ion acoustic instability will
occur only if the ions are cold and have a large velocity relative to
the electrons so the ion Landau damping does not overwhelm the weak
Landau growth from the electrons.)

The results of these evolutions are shown in Figs. 17 through 20.
Again, the figures show the initial combined ion distributions only and
the debris, air, and combined ion distributions at the time of the
maximum momentum transfer rate. The results in the figures again show
the one dimensionality of the low relative velocity $(V_R/v_{Dac} = 1.2)$
evolution and the two dimensionality of the high velocity $(V_R/v_{Dac} = 3.8)$
evolution. The low velocity results in Fig. 18 show predominately one-
dimensional heating. This occurs because the initially fastest growing
mode propagates at zero degrees. Both the debris and air ions experience
resonant heating with the flattened areas of their distributions cor-
responding to the phase velocities of the growing modes. The one-
dimensional heating is reflected in the changes in the debris and air
temperatures. The changes in the v_x direction are 8.6 percent and 18
percent, and the changes in the v_z direction are -0.45 percent and -2.7
percent. The relative velocity decreases 1.5 percent providing the
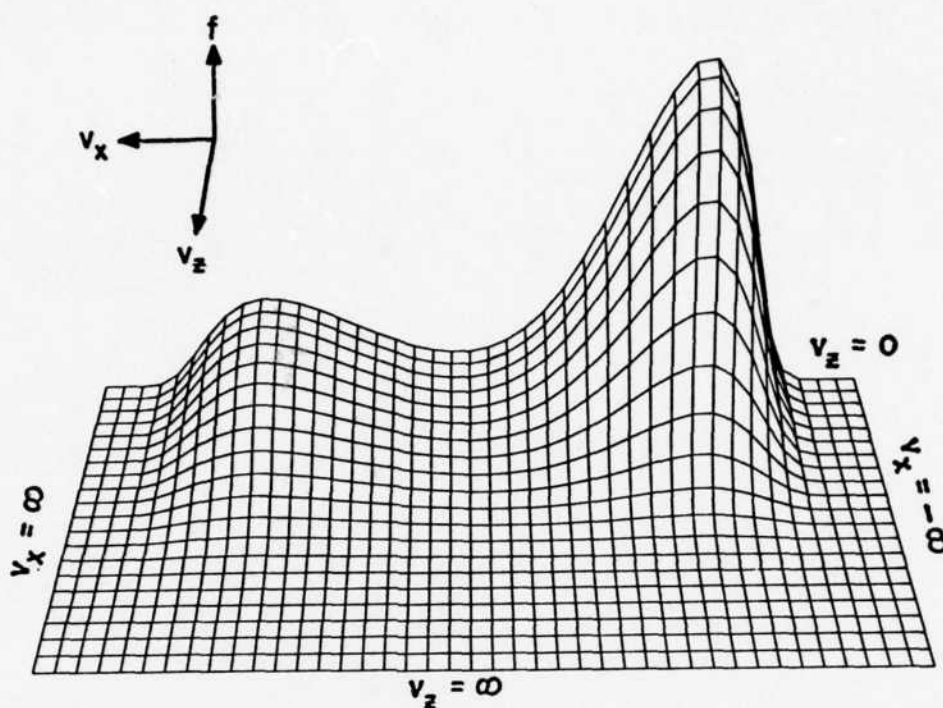
Fig. 17. Initial Ion Distribution for the 200-km Simulation with a Low Relative Velocity.
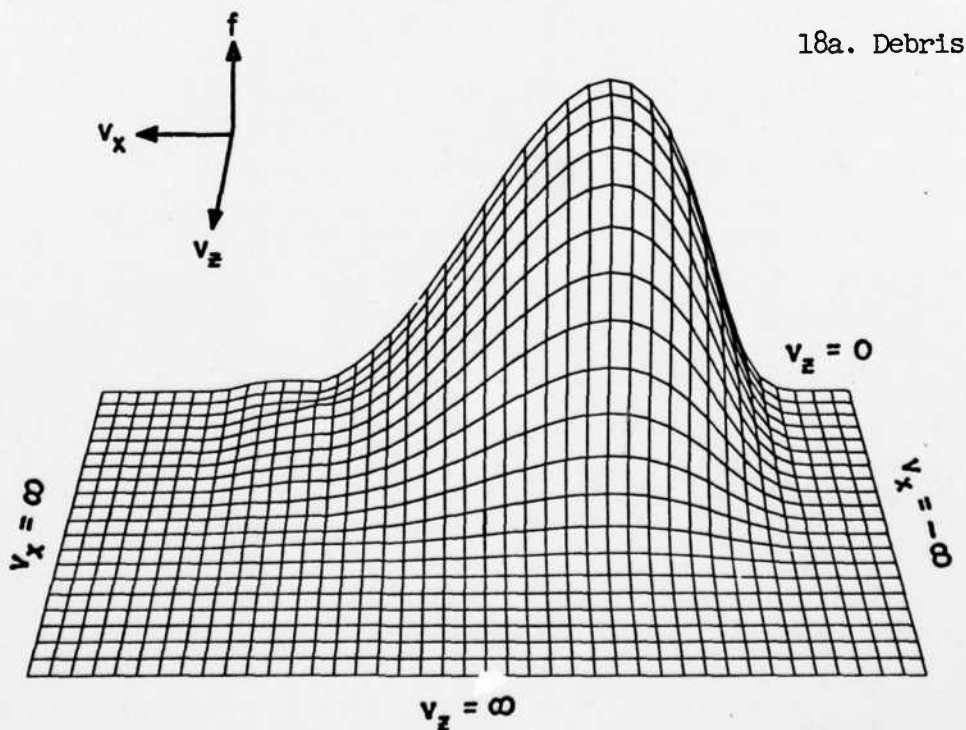
18a. Debris

Fig. 18. Peak ν_c Distributions for the 200-km Simulation with a Low Relative Velocity.

18b. Air
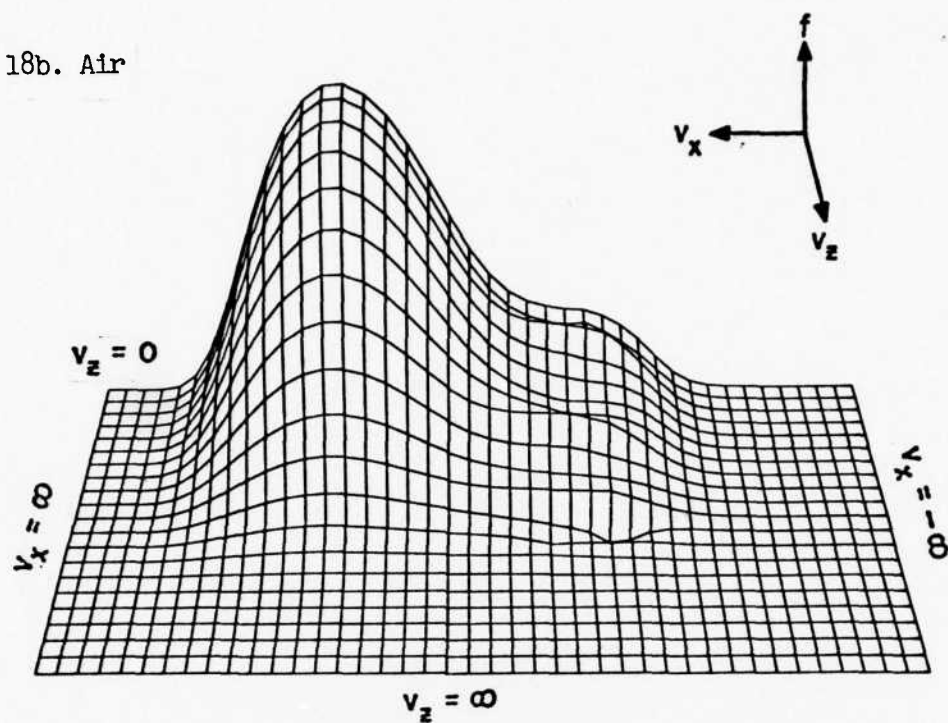
18c. Ions
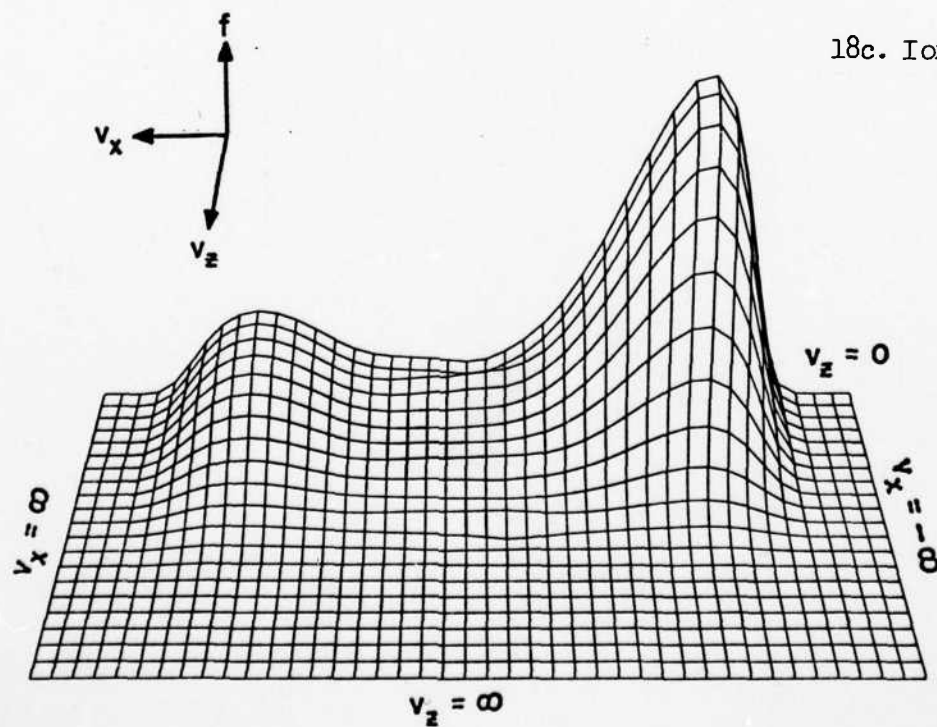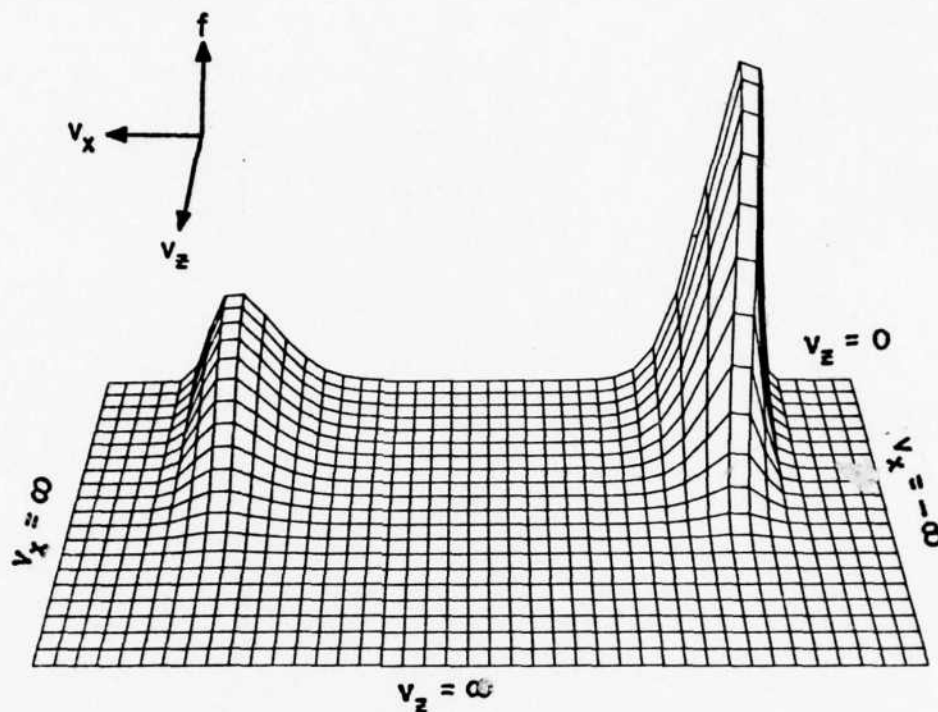
Fig. 19. Initial Ion Distribution for the 200-km Simulation with a High Relative Velocity.

20a. Debris
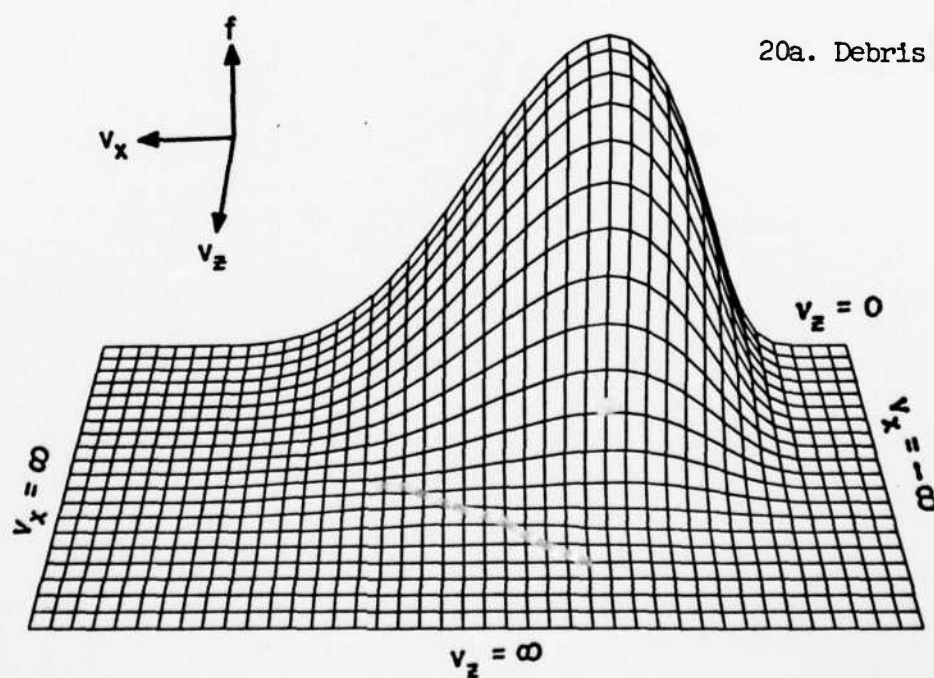
Fig. 20. Peak ν_c Distributions for the 200-km Simulation with a High Relative Velocity.

20b. Air

20c. Ions

74
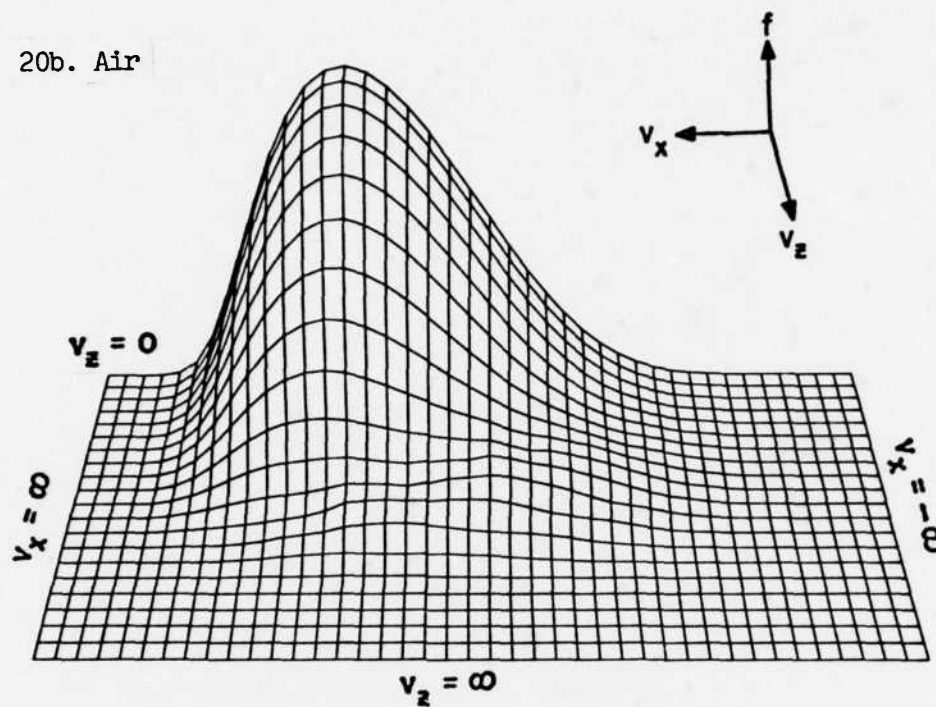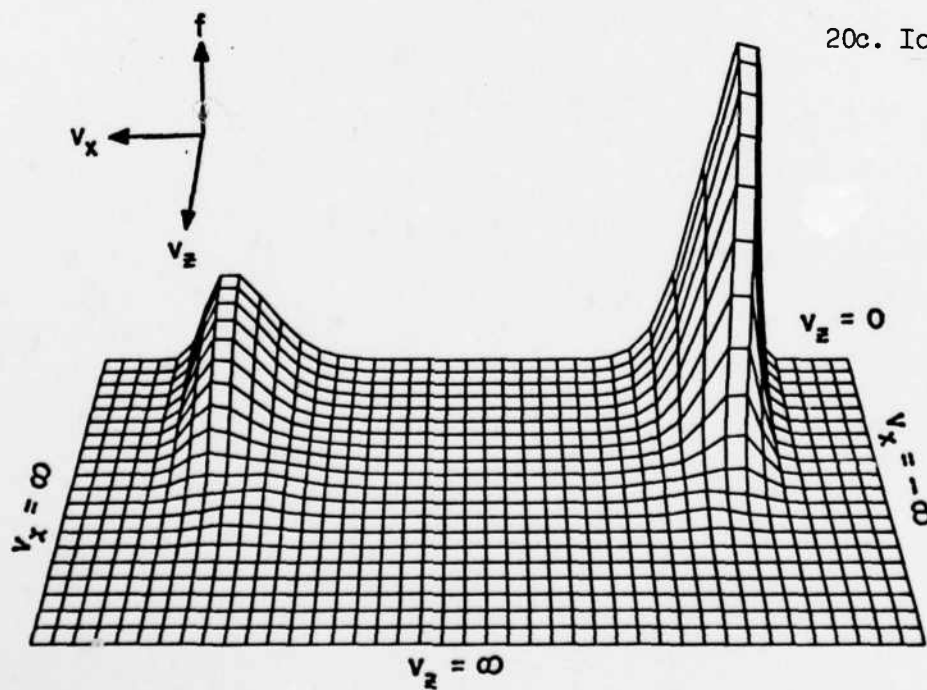
energy to drive the instability. The high velocity results in Fig. 20 show heating at large angles to the streaming direction because the fastest growing modes propagate approximately between 55 and 70 degrees. The flattened area on the air distribution corresponds to one of the resonant regions shown in Fig. 4. No resonant heating of the debris occurs. The changes in the debris and air temperatures in the v_x direction are 1.3 percent and 3.5 percent, and the changes in the v_z direction are 5.3 percent and 12 percent. The relative velocity decreases 0.39 percent.

The normalized anomalous collision frequencies for both of the 200-km simulations are graphed in Fig. 21. The maximum anomalous collision frequency for the low velocity simulation is roughly an order of magnitude higher than that for the high velocity run. The maximum for the low velocity also occurs in about one half of the time of the other. This result is also reflected in the larger difference in coupling lengths than can be accounted for by the difference in relative velocities. The lengths for the low and high velocity runs are 31 and 160 cm. The anomalous energy transport rates for the high velocity run are about a factor of two higher than the low velocity results.

The imaginary parts of the initially fastest growing modes in the two simulations are shown in Fig. 22. Even though the low velocity run ends in half the time and has an order of magnitude larger anomalous collision frequency, its initial growth rate is only a third larger. The ratios of the total wave energies at the end of the two simulations to those at their beginnings are $1.6(10^4)$ and $3.2(10^4)$ respectively for the low and high velocity runs. The respective computer running times were 2.4 and 1.3 hrs.
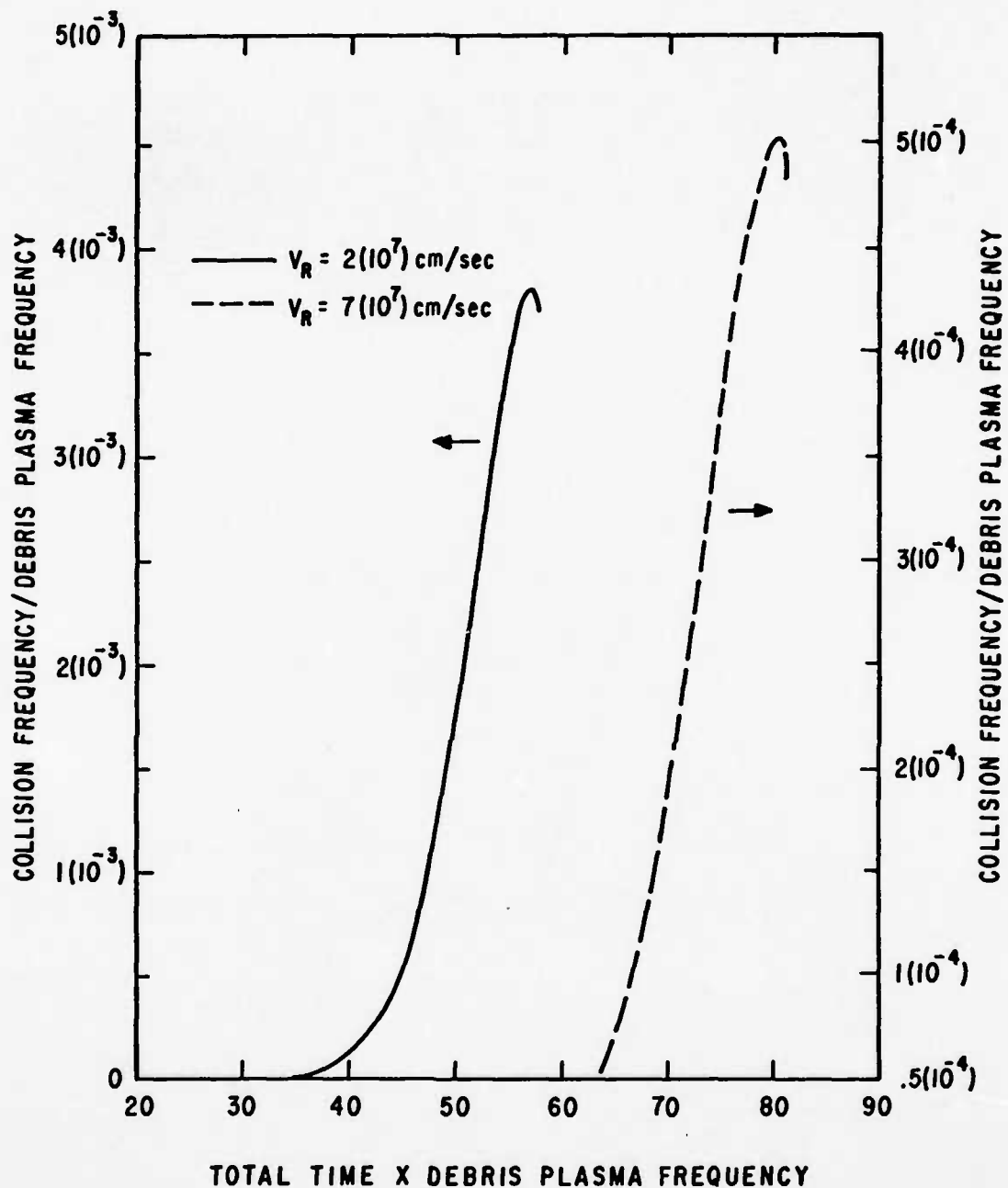
Fig. 21. Anomalous Collision Frequencies for the 200-km Simulations.

Magnetized Evolution Results. The magnetized cases simulating the 600-km problem are somewhat more complicated to evolve for several reasons. First, the modified two-stream instability often competes with the ion-ion instability (Refs 3: 53-56 and 29). Fortunately, only the

76
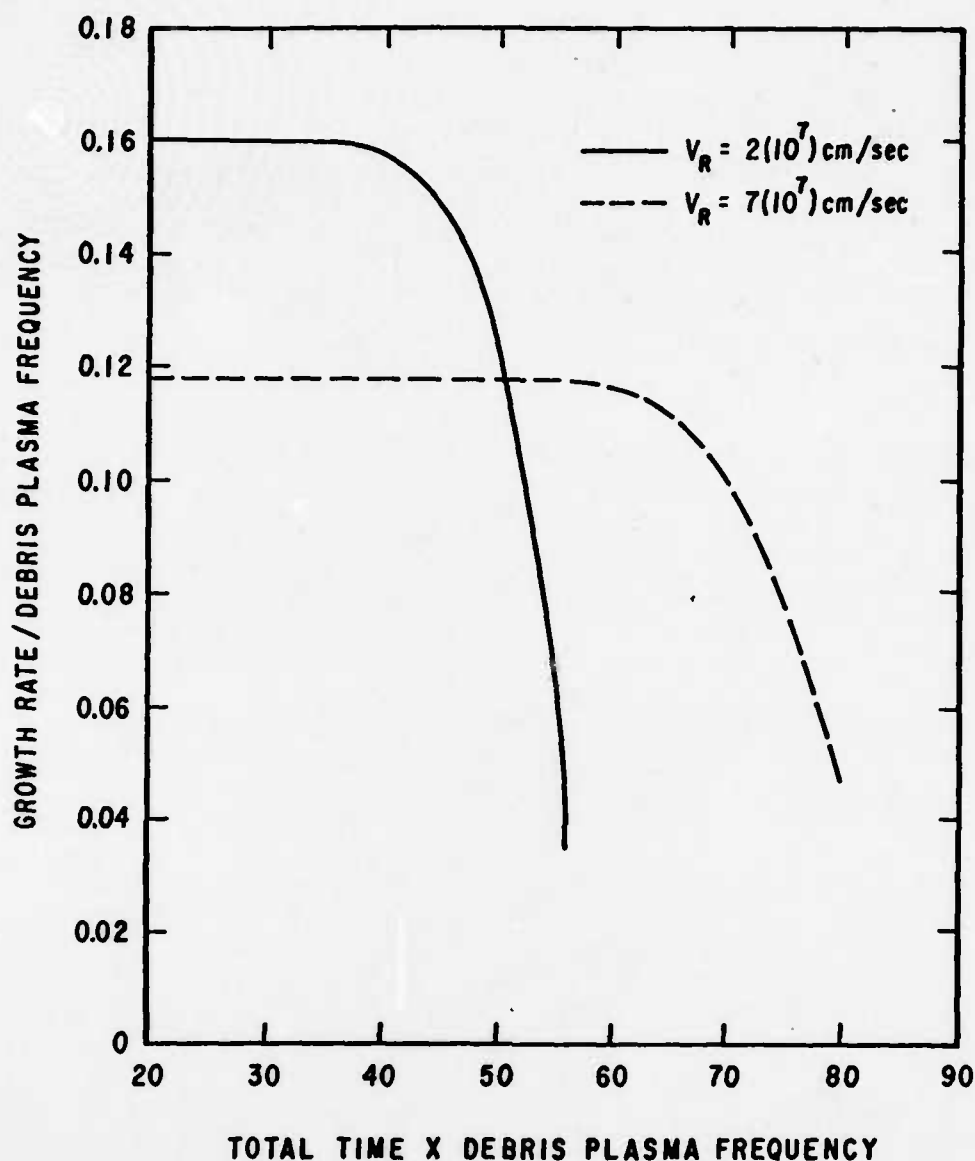
Fig. 22. Temporal Behavior of the Initially Fastest Growing
Modes for the 200-km Simulations.

ion-ion instability operates for the high electron temperatures used in

the simulations. Next, the electrostatic criterion also has to be

satisfied. This requires some juggling of the relative velocities, the

magnetic field strength, and the ion densities (the simulation altitude)

to insure that the criterion is rigorously satisfied for the evolutions

used in the dissertation. Finally, the magnetized evolutions use more

77

computer time because the dispersion relation is more complicated and the evolutions take longer to reach the peak momentum transfer rate.

The mixture of modified two-stream and ion-ion modes which appears when the electron temperature is reduced is shown in Table J-V. This table shows the linear solutions for the distribution shown in Table H-VIII except the electron temperature in the v_z direction is an order of magnitude lower than the tabulated value. The type of mode is determined by the relative magnitudes of the imaginary parts of the dielectrics. For example, the mode at $k_x = 0.1064$ cm^{-1} and $k_z = 0.0$ cm^{-1} is ion-ion because the imaginary part of the electron dielectric is much less than those of the ion dielectrics. Conversely, the mode at $k_x = 0.1064$ cm^{-1} and $k_z = 3.125(10^{-4})$ cm^{-1} is a modified two-stream mode between the air and the electrons. Note also, the extremely small angular range of the unstable modes.

The distributions evolved are in Tables H-VIII and H-IX respectively for low and high relative velocities. The corresponding linear solutions are in Tables J-VI and J-VII. All of the wave modes shown are clearly ion-ion. Before the distributions were evolved, the possible existence of modified two-stream modes propagating to the "left" (See Fig. 6) was also checked. No such modes were found so all of the unstable modes for the distribution are ion-ion, and therefore, the electrons are adiabatic.

The evolution results are shown in Figs. 23 through 26. The low relative velocity ($V_R/v_{Dalf} = 0.042$) evolution results are very similar to those of the low velocity evolution for 200 km. The heating is one dimensional, and the phase velocities of the unstable modes and the resonant areas of the distributions are the same as those in the 200-km low velocity case. The changes in the debris and air temperatures in

78
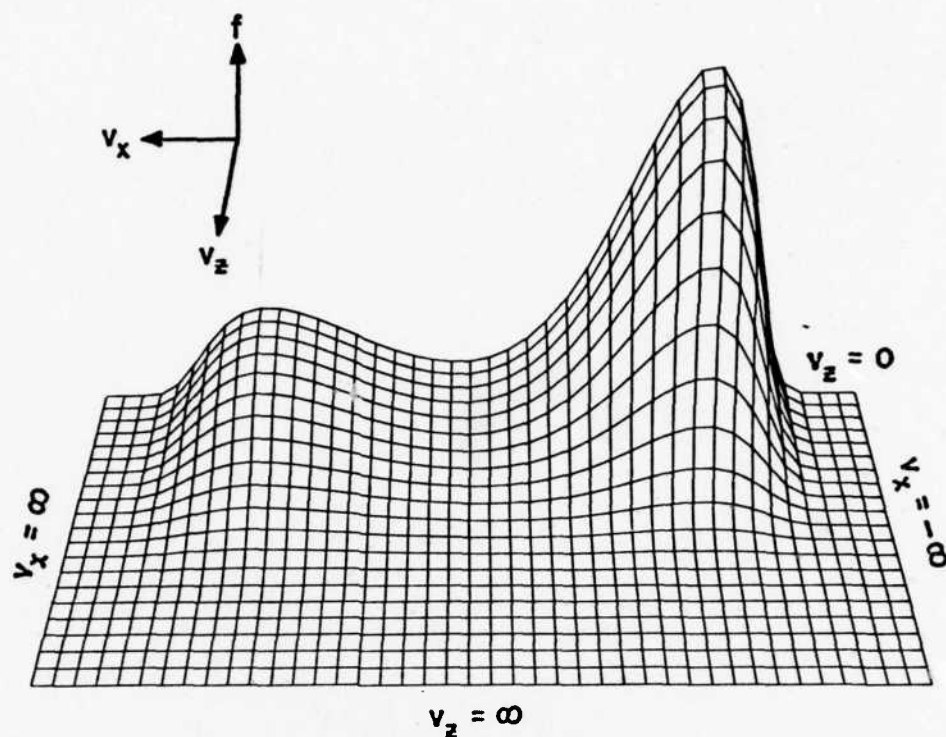
Fig. 23. Initial Ion Distribution for the 600-km Simulation with a Low Relative Velocity.
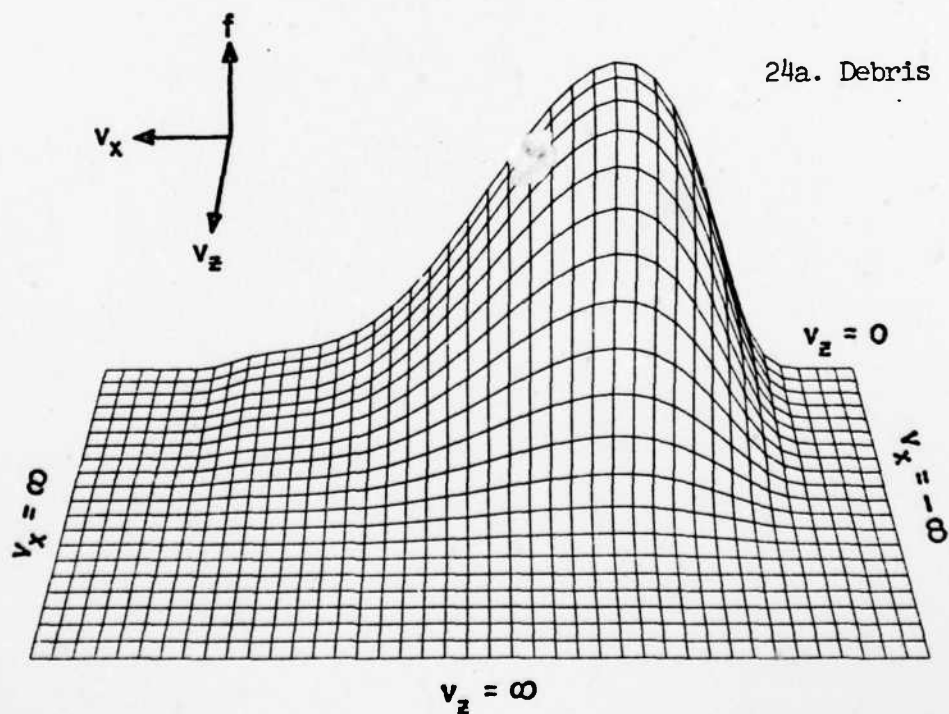
24a. Debris

Fig. 24. Peak γ_c Distributions for the 600-km Simulation with a Low Relative Velocity.

24b. Air

24c. Ions

80
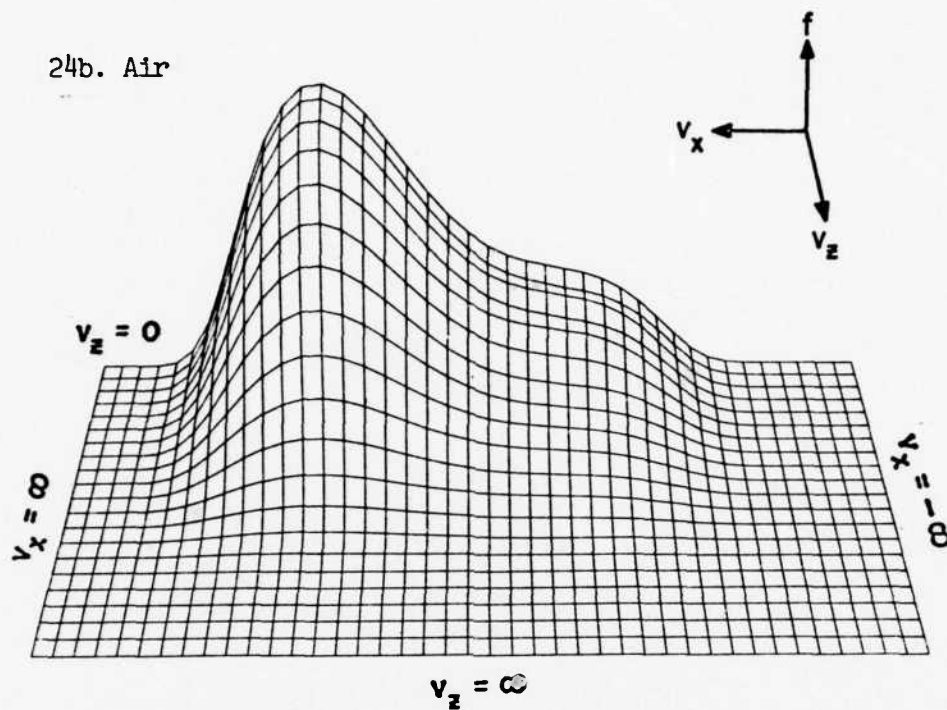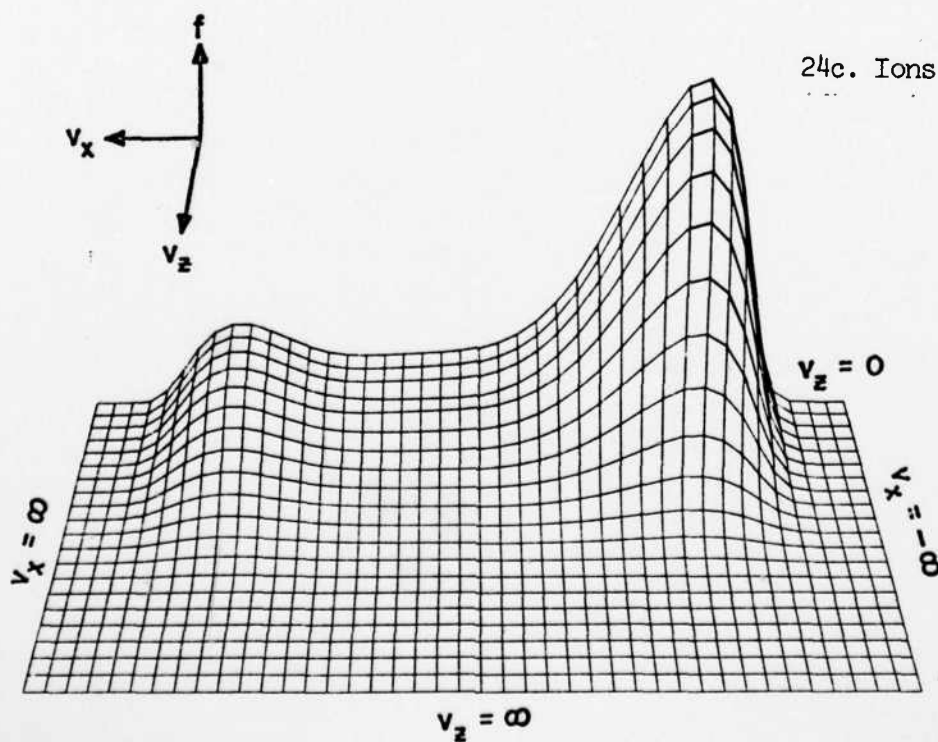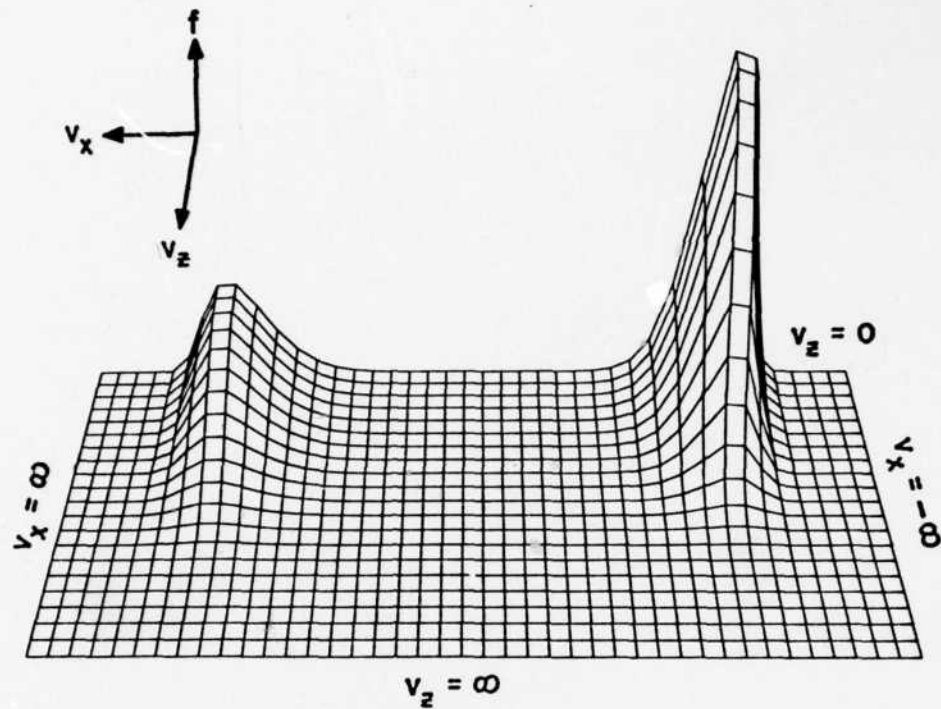
Fig. 25. Initial Ion Distribution for the 600-km Simulation with a High Relative Velocity.
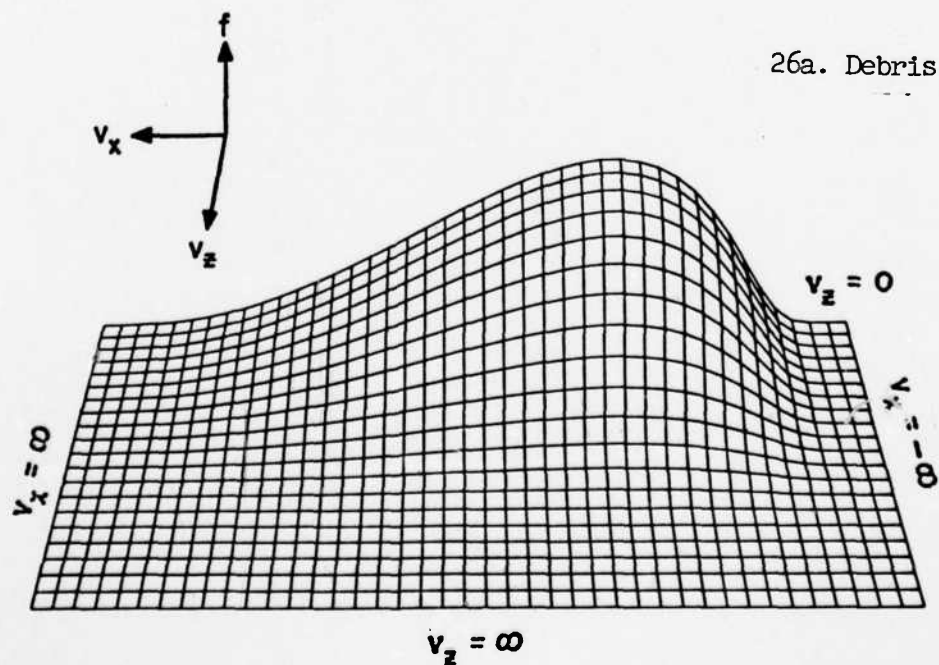
26a. Debris

Fig. 26. Peak ν_c Distributions for the 600-km Simulation with a High Relative Velocity.

81

26b. Air
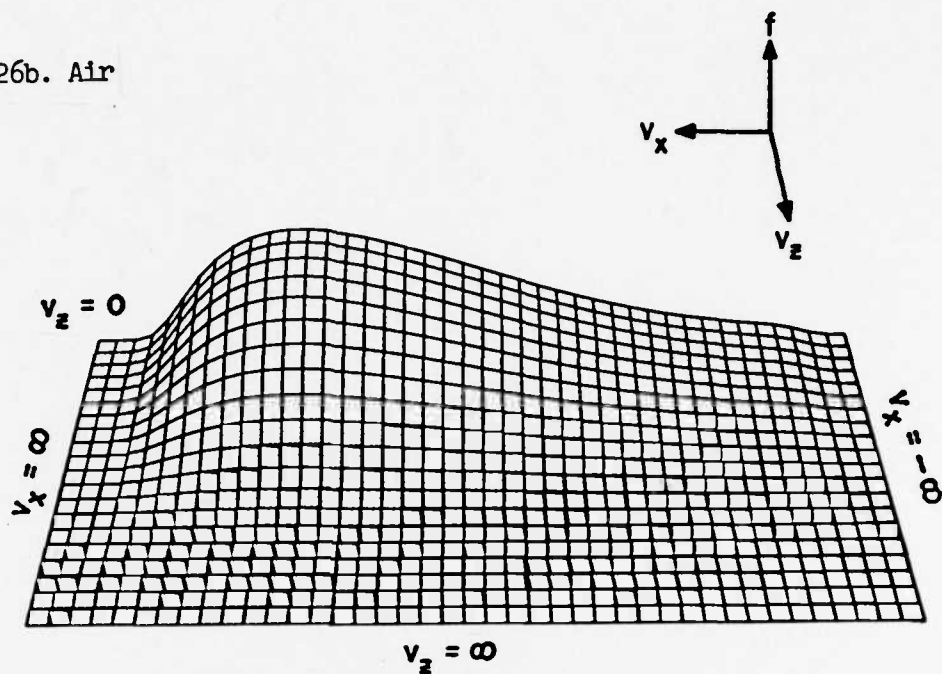
26c. Ions
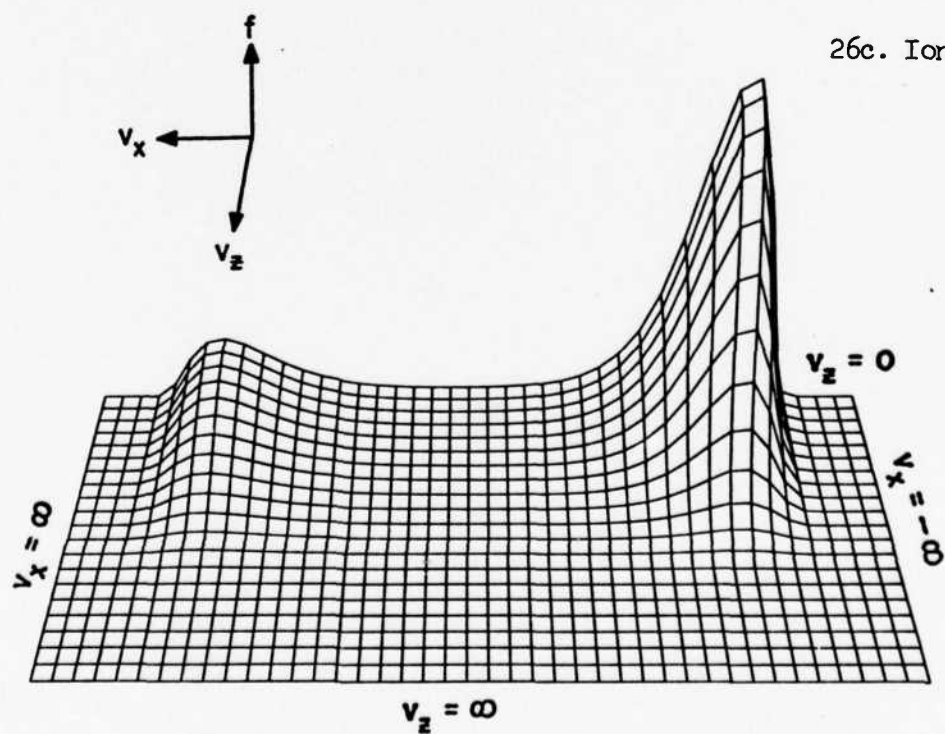
the v_x direction are 20 percent and 35 percent, and the changes in the v_z direction are -1.8 percent and -5.5 percent. These changes are much larger than the 200-km results. The relative velocity decreases 3.3 percent.

The high velocity results are quite different from the corresponding 200-km case. The relative velocity used is between the debris Alfven and acoustic speeds $(V_R/V_{Dalf} = 0.15$ and $V_R/V_{Dac} = 4.5)$ so one-dimensional magnetized modes and two-dimensional unmagnetized modes both exist. This division is shown in Table J-VII, the linear solutions. The magnetized modes propagate in the streaming direction, and the unmagnetized modes propagate in an angular range near 60 degrees. The unmagnetized modes are very similar to the wave modes for the high velocity, 200-km case. Because the magnetized modes have the larger growth rates, the heating is predominately in the v_x direction as shown in Fig. 26. The changes in the debris and air temperatures in the v_x direction are 110 percent and 190 percent, and the changes in the v_z direction are -18 percent and -36 percent. The heating of the distributions is fairly uniform with little resonant heating being observed. The relative velocity decreases 2.7 percent.

The normalized anomalous collision frequencies for these simulations are shown in Fig. 27. The peak collision frequency for the high velocity run is about four times as large as that for the low velocity run. The next figure, Fig. 28, shows the growth rates of the initially fastest growing modes. The initial growth rate for the high velocity distribution is twice that of the other. The ratios of the total wave energies at the end of the simulations to those at their beginnings are $5.7(10^5)$ and $4.0(10^7)$.

83
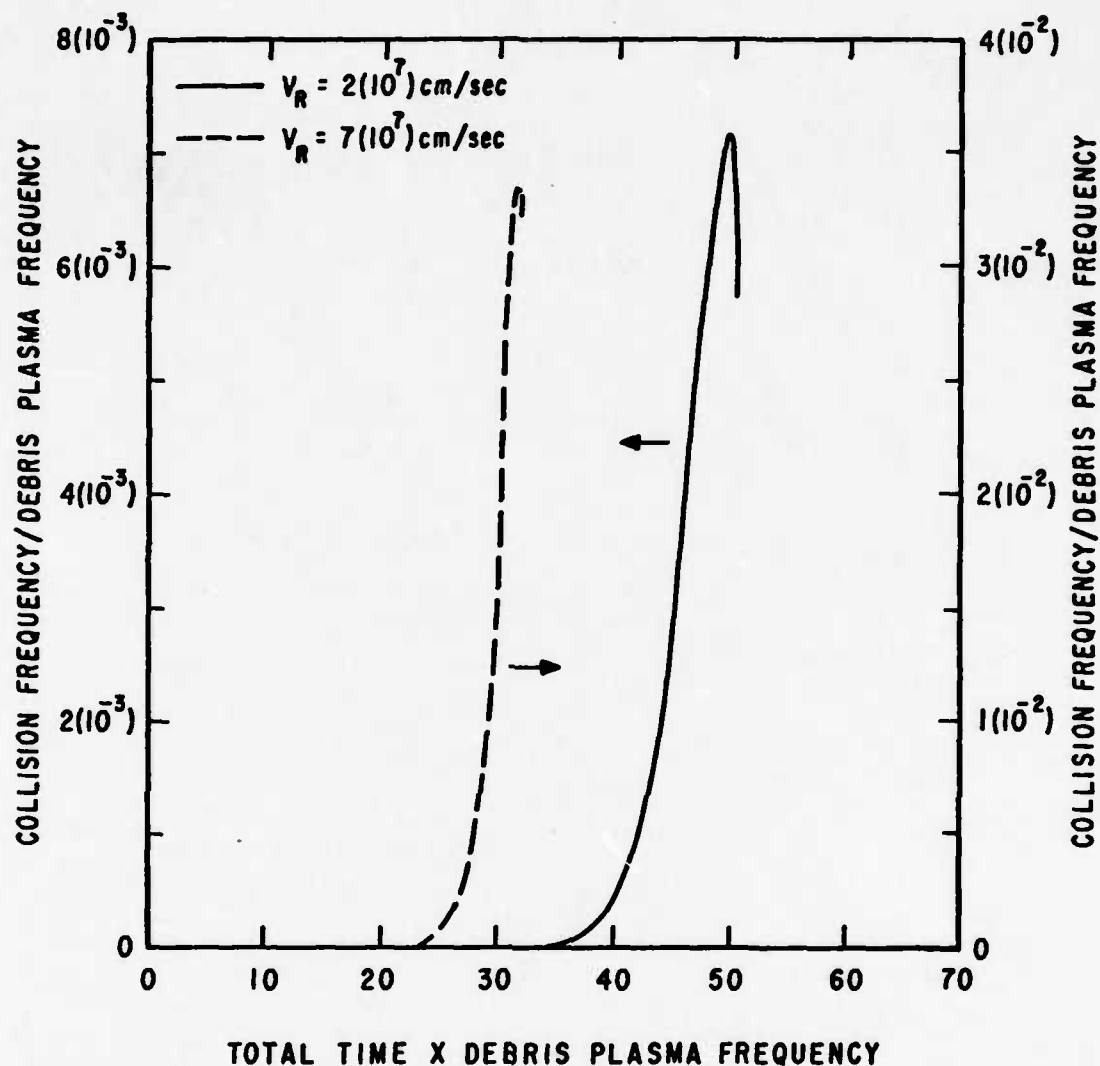
Fig. 27. Anomalous Collision Frequencies for the 600-km
Simulations.

The coupling lengths for the low and high velocity runs are 880 and
1900 cm. These lengths are much larger than an ion gyro radius so the
assumption that the ions are field free breaks down. In the debris-air
coupling problem, this breakdown means that a mechanism based on curving
ion paths causing the coupling (Ref 30) is more likely.

The computer running times for these evolutions were 2.7 and 3.8
hrs. The long times were partly due to the use of an earlier inefficient
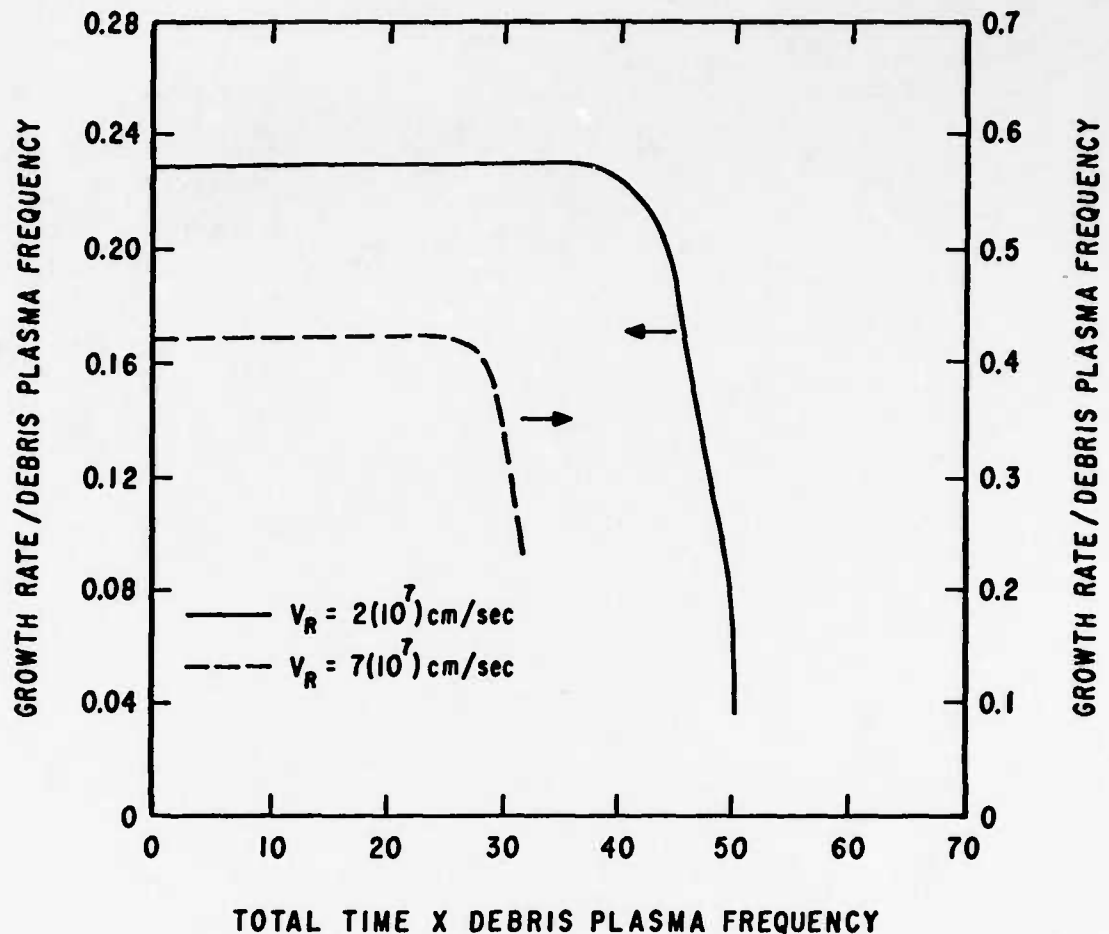
Fig. 28. Temporal Behavior of the Initially Fastest Growing
Modes for the 600-km Simulations.

control on the mode updates.

The above discussion on the 600-km simulation results completes the presentation of the dissertation evolution calculations. In the first few sections of this chapter, the testing of the computer program written to do the evolutions was described. Included in that description was an evaluation as to how well the computer results satisfy the assumptions of quasilinear theory. In the remaining sections of the chapter, the results of the simulation calculations were presented. These results are summarized and evaluated in the next chapter.

V. Discussion and Recommendations

First in this chapter, the results of the evolutions done for the dissertation are summarized. Next, the results are checked for consistency both with the assumptions made in Chapter I and with the assumptions of quasilinear theory. And finally in the chapter, some recommendations for further study are made.

Summary of Evolution Results

Several general features of the evolutions are apparent. First, the nature of the evolutions changes dramatically as time progresses. At early times, nothing much happens because the wave energies are still small. At late times, the ion distributions begin to change rapidly, and the growing wave modes rapidly begin to drop out becoming damped modes. The bulk of the computer time is spent in the latter phases of the evolutions.

The next general feature of the evolutions is that the maximum anomalous transport rates occur before saturation. Although these rates are proportional to the wave energy, they also depend on the distribution slopes through the wave growth rates and plasma dielectrics. (See Eqns (36) and (37).) These slopes decrease rapidly late in the evolution calculations causing the transport rates to peak and then decline.

The evolutions verify the characteristic frequencies and velocities derived in Chapter II. The unmagnetized waves do tend to oscillate near the ion plasma frequency. This tendency is apparent when one compares the initial wave oscillation frequencies for the bump-on-the-tail cases in Tables J-I and J-II with the debris plasma frequency in Table H-IV. This tendency is less apparent when the ion beams are of comparable densities because the interactions of the debris-electron oscillations

with the air-electron oscillations reduce the resulting wave frequencies. In fact, when the ion beams are equal and opposite ($\omega_{pD} = \omega_{pA}$), the wave frequencies go to zero. Similarly, the magetized waves do tend to oscillate at the lower hybrid frequency. Note these results confirm the reasonableness of the time normalization in Eqn (120). The characteristic velocity for the unmagnetized waves is the ion acoustic speed because the wave phase velocities do tend to be near this speed. The actual phase velocities are somewhat less than the ion acoustic speed, however, due to the wave interaction effect described above. (Also, see Eqn (18).) Because the waves cannot move faster than the ion acoustic speed, the unstable wave modes for plasma distributions with high relative velocities must propagate at large angles to the streaming direction. Their phase planes can then keep up with the resonant areas as shown in Fig. 4. The characteristic velocity for the magnetized waves seems to be the Alfvén speed. This is most apparent in the high velocity, 600-km evolution. In that evolution, the initial magnetized waves propagate faster than the ion acoustic speed, but they still are in the streaming direction because the relative velocity is less than the Alfvén speed. In general, the relationship between the characteristic velocity and relative velocity of a given plasma type determines whether the evolutions will be one dimensional or two dimensional.

The next feature of the evolutions is that they are definitely ion-ion. The transfer of momentum and energy from the ions to the electrons is negligible compared to the transfers between the two ion species.

Another feature is that the peak transport rates are attained in about ten e-folding times where an e-folding time is the reciprocal of the largest initial wave growth rate. This result is quite different

from the usual "back-of-the-envelope" time to quasilinear saturation of
one e-folding time. This time to attain the peak transport rates also
corresponds to the time when the wave energy begins to become comparable
to the ion thermal energy.

The evolutions are characterized by strong diffusion in the
regions of the distributions resonant with the waves and by weak dif-
fusion in the nonresonant regions. The flattened areas on the distribu-
tions in the figures in the previous chapter are the result of the strong
diffusion. The weak diffusion cannot be seen in the figures, but it is
apparent in the numerical printouts of the distributions. In general,
the effect of the nonresonant diffusion is a slight heating of the ion
distributions similar to that shown in Fig. 7.

The evolutions appear to be numerically stable. Occasionally, a
small dip at a single mesh point in an ion distribution suddenly
appeared during an evolution calculation probably due to an error in the
GEARB solution. This dip quickly filled in during the next few phases
of the evolution thereby proving the inherent stability of the solution.
Yet, if the wave modes were not updated often enough, an evolution would
quickly become unstable with rapidly growing oscillations in the particle
distributions. Clearly, the most important factor on numerical stability
is the frequency of mode update.

The final general feature of the dissertation results is that more
momentum transfer and less particle heating occurs in the low relative
velocity evolutions than in the high velocity ones. This phenomenon is
reasonable because the predominately z direction diffusion in the high
velocity runs is symmetric as shown in Fig. 4. A momentum transfer in
the positive z direction in the upper resonant region is canceled out

by a momentum transfer in the negative z direction in the lower region.
The net effect, therefore, is a spreading of the distribution which
increases the z temperature. The low velocity diffusion, on the other
hand, is predominately in the x direction as shown in Fig. 3. This
diffusion is not symmetric so a net transfer of momentum does occur. The
phenomenon can be seen in Table I which is a summary of the dissertation
evolution results. The tabular entries are in a suitable form for
insertion into a CGS set of hydrodynamic equations. The implication of
these results for the exospheric nuclear explosion coupling problem is
that the ion-ion instability is not effective in coupling the air to the
debris when their relative velocity is high.

Validity of Approximations

The assumptions used in the dissertation quasilinear calculations
hold fairly well in most cases. The electric field energy in the unstable
waves does remain smaller than the particle thermal energy in accordance
with the weak turbulence criterion, Eqn (45). The wave electric fields,
therefore, are of first order, and the perturbation approach used to
derive the quasilinear equations is valid. The electrostatic approxima-
tion criterion, Eqn (78), holds for the magnetized distributions used.
(The criterion is not pertinent for the unmagnetized cases because
coupling between the electrostatic waves and possible electromagnetic
waves does not occur.) The wave oscillation frequencies for the
magnetized cases do fall in the range defined by Eqn (29). The average
electron gyro radii are small so Equation (31) is satisfied. The ion
radii, however, are large compared to the mode wavelength as required
in part of Eqn (30), but they are small compared to the coupling length
violating the other part of that equation. This violation means the

89

Table I

Summary of the Maximum Anomalous Transport Coefficients

	Momentum (mom/cm^3-sec)		Energy (ergs/cm^3-sec)	
	Debris	Air	Debris	Air
Low Velocity Bump on the Tail	$1.7(10^{-1})$	$-1.7(10^{-1})$	$3.5(10^6)$	$6.1(10^5)$
High Velocity Bump on the Tail	$7.7(10^{-2})$	$-7.8(10^{-2})$	$4.6(10^6)$	$1.1(10^6)$
Low Velocity 200-km Simulation	$7.4(10^{-1})$	$-7.4(10^{-1})$	$7.1(10^6)$	$6.4(10^6)$
High Velocity 200-km Simulation	$3.4(10^{-1})$	$-3.4(10^{-1})$	$1.0(10^7)$	$1.0(10^7)$
Low Velocity 600-km Simulation	$4.2(10^{-5})$	$-4.2(10^{-5})$	$4.2(10^2)$	$3.3(10^2)$
High Velocity 600-km Simulation	$6.9(10^{-4})$	$-6.9(10^{-4})$	$1.8(10^4)$	$1.8(10^4)$

magnetized ion-ion instability does not reach saturation before the plasma is altered by the ion gyro motions around the magnetic field lines. The coupling lengths and unstable mode wavelengths are always less than a few meters so the homogeneous approximation is a good one. (Recall the mixing region thickness is of the order of a few kilometers.) The anomalous collision frequencies are always much larger than the binary collision frequencies so the Vlasov approach is valid. The phase mixing times for the free-streaming terms are always much less than the evolution times (the times to reach the maximum transport rates) so the free-streaming terms can be neglected. The trapping times are of the order of the evolution times, however.

In general, the unmagnetized quasilinear evolutions done for the dissertation seem to be valid up to about the time the transport coefficients peak and then begin to decline. After that time, the wave energy begins to become too large, particle trapping begins to occur, and the mode growth rates begin to change rapidly. These factors combine to make evolution calculations at times much beyond the peaks invalid and prohibitively expensive. These problems result from the fundamental limitation of quasilinear theory: It is a weak turbulence theory, and therefore, it cannot handle wave-wave or strong wave-particle interactions. Yet, by the time the evolution calculations become invalid, their main objective, which is a reasonably accurate set of maximum anomalous transport coefficients, has been attained.

The magnetized evolutions appear to be limited by the ion gyration times (Ω_i^{-1}) which are much less than the evolution times. A simple solution to this problem is not readily apparent within the scope of the theory in the dissertation. Yet, in these cases too, quasilinear

91

theory has served a useful purpose because the calculated transport coefficients are reasonable estimates of the actual ones.

Recommendations for Further Study

Two of the more obvious immediate extensions of the dissertation effort are (1) to run more evolutions to determine how the results scale and (2) to generalize the computer program so it can do instability evolutions with nonadiabatic electrons. A few aspects of scaling are fairly straightforward and would require only an evolution or two to verify. For example, if the temperatures of the species, the ion relative velocity, and the ratio of the debris plasma frequency to that of the air are all held constant while the debris density varies; the change in wave mode growth rates will match the change in debris plasma frequency. Also, the spectrum of unstable modes will always propagate in the same angular range. This behavior can already be seen in the unmagnetized modes for the high relative velocity 200-km and 600-km runs in Tables J-IV and J-VII. The ratios of the growth rates of corresponding modes are all the same and are equal to the ratio of the debris plasma frequencies. Therefore, the maximum transport cofficients should scale as (See Eqn (11).)

$$\frac{coef_{new}}{coef_{old}} \sim \frac{E_{thermal\ new}}{E_{thermal\ old}}\ \ell^{2\omega_{iold}\left(\frac{\omega_{pnew}}{\omega_{pold}} - 1\right)} \tag{125}$$

The computer program has already been generalized enough so it can handle unmagnetized electron-ion instabilities. In this generalization, the electron dielectric is computed numerically using the same procedures described in Appendices F and G for the always unmagnetized ions. This numerical computation is necessary because the electrons are not always adiabatic in electron-ion evolutions. More importantly, however, the

92

program needs to be generalized enough so it can evolve the modified
two-stream instability because the wave k's for this instability lie
close to those for the ion-ion instability. (See Table J-V.) To do
this, the routines which calculate the magnetized electron dielectric
have to be modified to accommodate a non Maxwellian electron distribution.

Another relatively straightforward extension of the dissertation
effort is a further optimization of the program so it uses less computer
time. The bulk of the program execution time is spent in updating the
wave modes so the best way to save time is to reduce the number of wave
modes followed during an evolution calculation and to reduce the
frequency of mode update. The evolution results indicate the feasibility
of these reductions because only the few fastest growing modes really
influence the ion distributions and because the evolutions can tolerate
a small degree of breakdown without much loss in the accuracy of the
transport coefficients.

There seems to be no convenient way to extend the program to
include electromagnetic effects. It would have to be modified extensive-
ly unless, somehow, the ions could be assumed to be electrostatic. This
extension would allow the evolution of magnetized distributions with
very high relative velocities. The electrostatic criterion, Eqn (78),
is violated at these high velocities because, in accordance with Eqn (18),
the wave k becomes too small. The desirability of such an extension is
not clear, however, because the ease of the electron motions along the
magnetic field lines would probably preclude any unstable modes which
propagate at large angles to the streaming direction. Therefore, one-
dimensional hydrodynamic theory, which already has been done, would
suffice.

To conclude this chapter, a quick summary of the entire dissertation is as follows: In Chapter I, the connection was made between the dissertation time evolutions of plasmas with three particle species and the debris-air coupling problem. In Chapter II, the quasilinear equations were presented, and some physical discussions were made regarding these equations. In Chapter III, the solution procedure for the equations was explained. The solution of the equations describes the slow time evolution of the ion distributions which is caused by a spectrum of weak electrostatic waves. In Chapter IV, the results of the evolutions were presented. And finally, in this chapter, the results were summarized. The general conclusion is that a fair amount of momentum transfer between the debris and the air occurs for the low relative velocity plasmas but little occurs for the high velocity ones.

As a final note, recall that the dissertation program can be applied to other areas than the high altitude nuclear burst problem. Such other areas include the bow shock of the terrestrial magnetosphere, the magnetotail, and the controlled thermonuclear reaction problem. In fact, the dissertation techniques are often applicable for a general physical problem which includes two low density warm ion beams and a single electron distribution.

Bibliography

1. Cladis, J.B., et. al., The Trapped Radiation Handbook. Defense
   Nuclear Agency (DNA) Report 2524H, Revision 5, 1977.

2. Hollars, D.R., private communication.

3. Lampe, M., et. al., "Anomalous Transport Coefficients for HANE
   Applications Due to Plasma Micro-Instabilities." Naval Research
   Laboratory (NRL) Report 3076, 1975.

4. Crevier, W.F. and R. Clark, private communications.

5. Davidson, R.C., et. al., "Electron Heating by Electron-Ion Beam
   Instabilities." Physical Review Letters, 24: 579-582, 1970.

6. Lampe, M., et. al., "Two-Dimensional Study of Electron-Ion Streaming
   Instabilities." The Physics of Fluids, 17: 428-439, 1974.

7. Seshadri, S.R., Fundamentals of Plasma Physics. New York: American
   Elsevier Publishing Company, 1973.

8. Papadopoulos, K., et. al., "Heating of Counterstreaming Ion Beams in
   an External Magnetic Field." The Physics of Fluids, 14: 849-857, 1971.

9. Forslund, D.W. and C.R. Shonk, "Numerical Simulation of Electrostatic
   Counterstreaming Instabilities in Ion Beams." Physical Review
   Letters, 25: 281-284, 1970.

10. Doveil F. and D. Gresillion, "Space-Time Structure of Ion Beam-
    Plasma Turbulence." The Physics of Fluids, 18: 1756-1761, 1975.

11. Uman, M.A., Introduction to Plasma Physics. New York: McGraw-Hill
    Book Company, 1964.

12. Drummond, W.E. and D. Pines, "Nonlinear Plasma Oscillations." Annals
    of Physics, 28: 478-499, 1964.

13. Bernstein, I.B. and F. Engelmann, "Quasilinear Theory of Plasma
    Waves." The Physics of Fluids, 9: 937-952, 1966.

14. Davidson, R.C., Methods in Nonlinear Plasma Theory. New York:
    Academic Press, 1972.

15. Jackson, J.D., "Longitudinal Plasma Oscillations." Journal of
    Nuclear Energy Part C: Plasma Physics, 1: 171-189, 1960.

16. Stix, T.H., The Theory of Plasma Waves. New York: McGraw-Hill Book
    Company, 1962.

17. Fried, B.D. and S.D. Conte, The Plasma Dispersion Function. New York:
    Academic Press, 1961.

18. Liewer, P.C. and N.A. Krall, "Self-Consistent Approach to Anomalous Resistivity Applied to Theta Pinch Experiments." The Physics of Fluids, 16: 1953-1963, 1973.

19. Krall, N.A. and A.W. Trivelpiece, Principles of Plasma Physics. New York: McGraw-Hill Book Company, 1973.

20. Auer, P.L., et. al., "Thermalization in the Earth's Bow Shock." Journal of Geophysical Research, 76: 2927-2939, 1971.

21. Liskovets, O.A., "The Method of Lines (Review)." Differential Equations, 1: 1308-1323, 1965.

22. Hindmarsh, A.C., "GEARB: Solution of Ordinary Differential Equations Having Banded Jacobian." Lawrence Livermore Laboratory Report UCID-30059, Revision 2, 1977.

23. Sincovec, R.F. and N.K. Madsen, "Software of Nonlinear Partial Differential Equations." ACM Transactions on Mathematical Software, 1: 232-263, 1975.

24. Giri, D.V. and C.E. Baum, "Further Development in the Application of Contour Integration to the Evaluation of the Zeros of Analytic Functions and Relevant Computer Programs." AFWL Math Note 42, 1976.

25. Cap, F.F., Handbook on Plasma Instabilities. New York: Academic Press, 1976.

26. Tidman, D.A. and N.A. Krall, Shock Waves in Collisionless Plasmas. New York: Wiley-Interscience, 1971.

27. U.S. Standard Atmosphere, 1962. National Aeronautics and Space Administration, 1962.

28. Spitzer, L., Physics of Fully Ionized Gases. New York: Interscience Publishers, 1962.

29. McBride, J.B., et. al., "Theory and Simulation of Turbulent Heating by the Modified Two-Stream Instability." The Physics of Fluids, 15: 2367-2383, 1972.

30. Longmire, C.L., "Notes on Debris-Air-Magnetic Interaction." Rand Corporation Memorandum RM-3386-PR, 1963.

Appendix A

The Derivation of the Magnetic-Field-Free

Quasilinear Equations

The derivation of the field-free quasilinear equations for electrostatic waves starts with these nonlinear Vlasov-Maxwell equations:

$$\frac{\partial f_\alpha}{\partial t} + \vec{v} \cdot \frac{\partial f_\alpha}{\partial \vec{x}} + \frac{q_\alpha e}{m_\alpha} \vec{E} \cdot \frac{\partial f_\alpha}{\partial \vec{v}} = 0 \tag{A-1}$$

$$\frac{\partial}{\partial \vec{x}} \cdot \vec{E} = 4\pi \sum_\alpha q_\alpha e \int_{-\infty}^{\infty} d\vec{v}\, f_{\alpha 1} \tag{A-2}$$

where $f_\alpha(\vec{x}, \vec{v}, t) = f_{\alpha 0}(\vec{v}, t) + f_{\alpha 1}(\vec{x}, \vec{v}, t)$ (A-3)

$$B_0 = E_0 = 0 \tag{A-4}$$

$$n_{\alpha 0} = \text{number density} = \int_{-\infty}^{\infty} d\vec{v}\, f_{\alpha 0}(\vec{v}) \tag{A-5}$$

$$\vec{E} = \vec{E}_1(\vec{x}, t) \tag{A-6}$$

$$e = |e| \tag{A-7}$$

and α denotes plasma species (debris, air, or electrons), $q_\alpha e$ denotes the charge of the species, and m_α denotes mass. The initial density is assumed to be uniform. The Vlasov equation is spatially averaged with the average defined as

$$\langle g(\vec{x}) \rangle = \lim_{V \to \infty} \frac{1}{V} \int_{-\infty}^{\infty} d\vec{x}\, g(\vec{x}) \tag{A-8}$$

to give because $\langle f_{\alpha 1} \rangle = \langle \vec{E} \rangle = 0$:

$$\frac{\partial f_{\alpha 0}}{\partial t} = - \frac{q_\alpha e}{m_\alpha} \frac{\partial}{\partial \vec{v}} \cdot \langle \vec{E} f_{\alpha 1} \rangle \tag{A-9}$$

Note the quantity $\langle \vec{E} f_{\alpha 1} \rangle$ is of second order. Hence, the time rate of

97

change of $f_{\alpha 0}$ is of that order. When Eqn (A-9) is subtracted from Eqn (A-1),

$$\frac{\partial f_{\alpha 1}}{\partial t} + \vec{v} \cdot \frac{\partial f_{\alpha 1}}{\partial \vec{x}} + \frac{q_\alpha e}{m_\alpha} \vec{E} \cdot \frac{\partial f_{\alpha 0}}{\partial \vec{v}}$$

$$= - \frac{q_\alpha e}{m_\alpha} \frac{\partial}{\partial \vec{v}} \cdot \left[\vec{E} f_{\alpha 1} - \langle \vec{E} f_{\alpha 1} \rangle \right] \tag{A-10}$$

With the spatial Fourier transforms defined as

$$\begin{Bmatrix} f_{\alpha 1}(\vec{v}, \vec{k}, t) \\ \vec{E}(\vec{k}, t) \end{Bmatrix} = \int_{-\infty}^{\infty} d\vec{x}\, e^{-i\vec{k}\cdot\vec{x}} \begin{Bmatrix} f_{\alpha 1}(\vec{v}, \vec{x}, t) \\ \vec{E}(\vec{x}, t) \end{Bmatrix} \tag{A-11}$$

$$\begin{Bmatrix} f_{\alpha 1}(\vec{v}, \vec{x}, t) \\ \vec{E}(\vec{x}, t) \end{Bmatrix} = \frac{1}{(2\pi)^3} \int_{-\infty}^{\infty} d\vec{k}\, e^{i\vec{k}\cdot\vec{x}} \begin{Bmatrix} f_{\alpha 1}(\vec{v}, \vec{k}, t) \\ \vec{E}(\vec{k}, t) \end{Bmatrix} \tag{A-12}$$

the transforms of Eqns (A-9) and (A-10) are

$$\frac{\partial f_{\alpha 0}}{\partial t} = - \frac{q_\alpha e}{m_\alpha} \frac{\partial}{\partial \vec{v}} \cdot \left[\lim_{V \to \infty} \frac{1}{V} \frac{1}{(2\pi)^3} \int_{-\infty}^{\infty} d\vec{k}\, \vec{E}(-\vec{k}, t) \cdot f_{\alpha 1}(\vec{k}, \vec{v}, t) \right] \tag{A-13}$$

$$\frac{\partial f_{\alpha 1}(\vec{k}, \vec{v}, t)}{\partial t} + i\vec{k}\cdot\vec{v}\, f_{\alpha 1}(\vec{k}, \vec{v}, t) = - \frac{q_\alpha e}{m_\alpha} \vec{E}(\vec{k}, t) \cdot \frac{\partial f_{\alpha 0}}{\partial \vec{v}}$$

$$- \frac{q_\alpha e}{m_\alpha} \frac{1}{(2\pi)^3} \int_{-\infty}^{\infty} d\vec{k}'\, \vec{E}(\vec{k}-\vec{k}', t) \cdot \frac{\partial f_{\alpha 1}(\vec{k}', \vec{v}, t)}{\partial \vec{v}} \tag{A-14}$$

The Green's function for the operator on the left side of Eqn (A-14) is

$$G(\vec{k}, t) = e^{-i\vec{k}\cdot\vec{v}\,t} \tag{A-15}$$

so the integral equation equivalent to Eqn (A-14) is

$$f_{\alpha 1}(\vec{k}, \vec{v}, t) = f_{\alpha 1}(\vec{k}, \vec{v}, t=0)\, e^{-i\vec{k}\cdot\vec{v}\,t}$$

$$- \frac{q_\alpha e}{m_\alpha} e^{-i\vec{k}\cdot\vec{v}\,t} \int_0^t dt'\, e^{i\vec{k}\cdot\vec{v}\,t'} \left\{ \vec{E}(\vec{k}, t') \frac{\partial f_{\alpha 0}(\vec{v}, t)}{\partial \vec{v}} \right.$$

$$\left. + \frac{1}{(2\pi)^3} \int_{-\infty}^{\infty} d\vec{k}'\, \vec{E}(\vec{k}-\vec{k}', t') \cdot \frac{\partial f_{\alpha 1}(\vec{k}', \vec{v}, t')}{\partial \vec{v}} \right\} \tag{A-16}$$

When Eqn (A-16) is substituted into itself to iterate, the first few terms of the result are

$$f_{a_1}(\vec{h}, \vec{v}, t) = f_{a_1}(\vec{h}, \vec{v}, t=0) \, e^{-i\vec{h}\cdot\vec{v}t}$$

$$- \frac{q_a e}{m_a} \, e^{-i\vec{h}\cdot\vec{v}t} \int^t dt' \, e^{i\vec{h}\cdot\vec{v}t'} \vec{E}(\vec{h}, t') \cdot \frac{\partial f_{a_0}(\vec{v}, t')}{\partial \vec{v}}$$

$$- \frac{q_a e}{m_a} \frac{1}{(2\pi)^3} \, e^{-i\vec{h}\cdot\vec{v}t} \int_0^t dt' \, e^{i\vec{h}\cdot\vec{v}t'} \int_{-\infty}^{\vec{\infty}} d\vec{h}' \, \vec{E}(\vec{h}-\vec{h}', t')$$

$$\cdot \frac{\partial}{\partial \vec{v}} \left[f_{a_1}(\vec{h}', \vec{v}, t=0) \, e^{-i\vec{h}'\cdot\vec{v}t'} \right] \qquad \text{(A-17)}$$

The first term on the right hand side of Eqn (A-17) is the free-streaming term based on the initial disturbance to the distribution. The last term describes the effect of coupling of energy from one wave mode at a given $\vec{k}$ into another. This term is ignored as each wave mode is assumed to proceed independently from all of the rest. This assumption is good when the wave amplitudes are small, first order quantities. The meaning of "small" is described in the Diffusion Analogy section of Chapter II.

The electric field is assumed to be in the form:

$$E(\vec{h}, t) = E(\vec{h}, t=0) \, e^{-i\Delta(\vec{h}, t)} \qquad \text{(A-18)}$$

where $\quad \vec{E}(\vec{h}, t) = \frac{\vec{h}}{|\vec{h}|} \, E(\vec{h}, t) \qquad$ (A-19)

because $\quad \frac{\partial}{\partial \vec{x}} \times \vec{E}(\vec{h}, t) = 0 \qquad$ (A-20)

The variable $s(\vec{k}, t)$ is defined so

$$\frac{\partial \Delta(\vec{h}, t)}{\partial t} = \omega(\vec{h}, t) \qquad \text{(A-21)}$$

or $\quad \Delta(\vec{h}, t) = \int_0^t dt' \, \omega(\vec{h}, t') \qquad$ (A-22)

99

The time variation of ω is assumed to be slow compared with ω_r^{-1} where $\omega = \omega_r + i\omega_i$. In fact, when $\omega \neq \omega(t)$, Eqn (A-18) reduces to

$$E(\vec{h},t) = E(\vec{h},t=0)\, e^{-i\omega(\vec{h})t} \tag{A-23}$$

From the condition that $E(\vec{x},t)$ must be real so $E^*(\vec{x},t) = E(\vec{x},t)$ and from the definition of the Fourier transform,

$$E^*(-\vec{h},t) = E(\vec{h},t) \tag{A-24}$$

When Eqn (A-18) is solved for $s(\vec{k},t)$ and Eqn (A-24) is used,

$$s(-\vec{h},t) = -s^*(\vec{h},t) \tag{A-25}$$

and

$$\omega(-\vec{h},t) = -\omega^*(\vec{h},t) \tag{A-26}$$

The inversion property of $\omega(\vec{k},t)$ in Eqn (A-26) is often very useful.

The second term on the right hand side of Eqn (A-17) is changed by using

$$e^{i\vec{h}\cdot\vec{v}t'}E(\vec{h},t) = \frac{\dfrac{\partial}{\partial t'}\left[e^{i(\vec{h}\cdot\vec{v}t' - s(\vec{h},t'))} - 1\right]}{i[\vec{h}\cdot\vec{v} - \omega(\vec{h},t')]}E(\vec{h},t=0) \tag{A-27}$$

and by integrating by parts. The integrated part is saved, and the integral is neglected because it is of third order. Eqn (A-17) then becomes after the mode coupling term is dropped:

$$f_{\alpha 1}(\vec{h},\vec{v},t) = f_{\alpha 1}(\vec{h},\vec{v},t=0)\, e^{-i\vec{h}\cdot\vec{v}t}$$

$$-\frac{q_\alpha e}{m_\alpha}\,\frac{\vec{E}(\vec{h},t) - e^{-i\vec{h}\cdot\vec{v}t}\vec{E}(\vec{h},t=0)}{i[\vec{h}\cdot\vec{v} - \omega(\vec{h},t)]} \cdot \frac{\partial f_{\alpha 0}(\vec{v},t)}{\partial \vec{v}} \tag{A-28}$$

Equation (A-2), Fourier transformed, is

$$i h E(\vec{h},t) = 4\pi \sum_\alpha q_\alpha e \int_{-\infty}^{\infty} d\vec{v}\, f_{\alpha 1}(\vec{h},\vec{v},t) \tag{A-29}$$

where Eqn (A-20) is used again. When Eqn (A-28) is inserted into Eqn (A-29),

$$1 - \sum_{\alpha} \frac{4\pi q_{\alpha}^2 e^2}{m_{\alpha} k^2} \int_L d\vec{v} \; \frac{\vec{k} \cdot \frac{\partial f_{\alpha 0}(\vec{v},t)}{\partial \vec{v}}}{[\vec{k} \cdot \vec{v} - \omega(\vec{k},t)]}$$

$$= \sum_{\alpha} \frac{4\pi q_{\alpha} e \; e^{i s(\vec{k},t)}}{i k \; E(\vec{k},t=0)} \int_{-\infty}^{\infty} d\vec{v} \; f_{\alpha 1}(\vec{k},\vec{v},t=0) e^{-i\vec{k}\cdot\vec{v}t}$$

$$- \sum_{\alpha} \frac{4\pi q_{\alpha}^2 e^2}{m_{\alpha} k^2} \int_L d\vec{v} \; \frac{\vec{k} \cdot \frac{\partial f_{\alpha 0}(\vec{v},t)}{\partial \vec{v}}}{[\vec{k} \cdot \vec{v} - \omega(\vec{k},t)]} e^{i s(\vec{k},t) - i\vec{k}\cdot\vec{v}t} \qquad \text{(A-30)}$$

where, as necessary, the integrals are taken below the singularity in the denominators to insure the results are analytic across the real axis in the complex frequency plane. The integration symbol $\int_L$ denotes this process because the process is equivalent to integrating along the Landau contour. The first and second terms on the right hand side of Eqn (A-30) are the free-streaming terms. These terms are not associated with growing or decaying waves and phase mix to zero in times of the of

$$(k \Delta v)^{-1} \qquad \text{(A-31)}$$

where Δv is the width of $f_{\alpha 1}(\vec{k},\vec{v},t=0)$ for the first term and is the width of $f_{\alpha 0}(\vec{v},t)$ for the second term. These are the times necessary for the particle free streaming to smooth out initial spatial inhomogeneities. The time asymptotic form of Eqn (A-30) is, therefore,

$$1 - \sum_{\alpha} \frac{4\pi q_{\alpha}^2 e^2}{m_{\alpha} k^2} \int_L d\vec{v} \; \frac{\vec{k} \cdot \frac{\partial f_{\alpha 0}(\vec{v},t)}{\partial \vec{v}}}{[\vec{k} \cdot \vec{v} - \omega(\vec{k},t)]} = 0 \qquad \text{(A-32)}$$

which is the linear dispersion relation for $\omega = \omega(\vec{k},t)$. This equation is valid for both damped and growing wave modes. Note however, the waves cannot be too strongly damped because then the waves will die out before the free-streaming terms go away. The damping time which is approximately ω_i^{-1} must be greater than the time given by Eqn (A-31).

101

The quasilinear equation for the time rate of change of the distribution results when Eqn (A-28) is inserted into Eqn (A-13):

$$\frac{\partial f_{\alpha o}(\vec{v},t)}{\partial t} = - \frac{q_{\alpha} e}{m_{\alpha}} \frac{\partial}{\partial \vec{v}} \cdot$$

$$\left\{ \lim_{V \to \infty} \frac{1}{V} \frac{1}{(2\pi)^3} \int_{-\infty}^{\infty} d\vec{k} \; \vec{E}(-\vec{k},t) \left[f_{\alpha 1}(\vec{k},\vec{v},t=0) e^{-i\vec{k}\cdot\vec{v}t} \right. \right.$$

$$\left. \left. - \frac{q_{\alpha} e}{m_{\alpha}} \frac{\vec{E}(\vec{k},t) - e^{-i\vec{k}\cdot\vec{v}t} \vec{E}(\vec{k},t=0)}{i[\vec{k}\cdot\vec{v} - \omega(\vec{k},t)]} \cdot \frac{\partial f_{\alpha o}(\vec{v},t)}{\partial \vec{v}} \right] \right\} \quad \text{(A-33)}$$

When the free-streaming terms are neglected and the integral is taken below the singularity,

$$\frac{\partial f_{\alpha o}(\vec{v},t)}{\partial t} = \frac{q_{\alpha}^2 e^2}{m_{\alpha}^2} \frac{\partial}{\partial \vec{v}} \int_L d\vec{k} \left\{ \lim_{V \to \infty} \frac{1}{V} \frac{1}{(2\pi)^3} E(-\vec{k},t) E(\vec{k},t) \right.$$

$$\left. \cdot \frac{\vec{k}\vec{k}}{k^2} \cdot \frac{\frac{\partial f_{\alpha o}(\vec{v},t)}{\partial \vec{v}}}{i[\vec{k}\cdot\vec{v} - \omega(\vec{k},t)]} \right\} \quad \text{(A-34)}$$

The free-streaming terms can be neglected for times greater than $(\Delta kv)^{-1}$ where Δk is the width of the wave spectrum and v is a typical particle velocity. This criterion is similar to Eqn (A-31).

The spectral wave energy, $\mathcal{E}(\vec{k},t)$, and the quasilinear diffusion coefficient for species α, $\overleftrightarrow{D}_{\alpha}(\vec{v},t)$, are respectively defined as

$$\mathcal{E}(\vec{k},t) = \lim_{V \to \infty} \frac{1}{V} \frac{E(-\vec{k},t)E(\vec{k},t)}{(2\pi)^3 \, 8\pi} \quad \text{(ergs) (A-35)}$$

$$\overleftrightarrow{D}_{\alpha}(\vec{v},t) = 8\pi \frac{q_{\alpha}^2 e^2}{m_{\alpha}^2} \int_L d\vec{k} \frac{\mathcal{E}(\vec{k},t) \, \vec{k}\vec{k}}{i[\vec{k}\cdot\vec{v} - \omega(\vec{k},t)] \, k^2} \quad \text{(A-36)}$$

Therefore, Eqn (A-34) becomes

$$\frac{\partial f_{\alpha o}(\vec{v},t)}{\partial t} = \frac{\partial}{\partial \vec{v}} \cdot \left[\overleftrightarrow{D}_{\alpha}(\vec{v},t) \cdot \frac{\partial f_{\alpha o}(\vec{v},t)}{\partial \vec{v}} \right] \quad \text{(A-37)}$$

The time dependence of the spectral wave energy from Eqns (A-18), (A-24),

(A-25), and (A-35) is

$$\mathcal{E}(\vec{h}, t) = \mathcal{E}(\vec{h}, t=0)\, e^{2\,Im[\Delta(\vec{h}, t)]} \qquad \text{(A-38)}$$

When Eqn (A-38) is differentiated and Eqn (A-21) is used,

$$\frac{\partial \mathcal{E}(\vec{h}, t)}{\partial t} = 2\,\omega_i(\vec{h}, t)\, \mathcal{E}(\vec{h}, t) \qquad \text{(A-39)}$$

A more convenient form of the diffusion coefficient results when Eqn (A-36) is broken into its real and imaginary parts and Eqn (A-26) is used:

$$\overset{\leftrightarrow}{D}_\alpha(\vec{v}, t) = 8\pi\, \frac{q_\alpha^2 e^2}{m_\alpha^2} \int_L d\vec{h}\, \frac{\mathcal{E}(\vec{h}, t)\, \vec{h}\,\vec{h}\,\omega_i(\vec{h}, t)}{[(\vec{h}\cdot\vec{v} - \omega_\lambda(\vec{h}, t))^2 + \omega_i^2(\vec{h}, t)]\, h^2} \qquad \text{(A-40)}$$

where $\quad \mathcal{E}(-\vec{h}, t=0) = \mathcal{E}(\vec{h}, t=0) \qquad$ (A-41)

has been assumed.

Equations (A-32), (A-37), (A-39), and (A-40) are the simultaneous set of quasilinear equations for wave-particle interactions.

Appendix B

Conservation in Quasilinear Theory

The equations of quasilinear theory conserve matter, momentum, and energy as can be seen by taking the first three velocity moments of Eqn (10). The first moment is

$$\int_{-\infty}^{\infty} d\vec{v}\, \frac{\partial f_{\alpha 0}(\vec{v},t)}{\partial t} = \int_{-\infty}^{\infty} d\vec{v}\, \frac{\partial}{\partial \vec{v}} \cdot \left[\overleftrightarrow{D}_{\alpha}(\vec{v},t) \cdot \frac{\partial f_{\alpha 0}(\vec{v},t)}{\partial \vec{v}} \right] \quad \text{(B-1)}$$

$$\frac{\partial}{\partial t} \int_{-\infty}^{\infty} d\vec{v}\, f_{\alpha 0} = \oint d\vec{S} \cdot \left[\overleftrightarrow{D}_{\alpha} \cdot \frac{\partial f_{\alpha 0}}{\partial \vec{v}} \right] \quad \text{(B-2)}$$

$$\frac{\partial n_{\alpha 0}}{\partial t} = 0 \quad \text{(B-3)}$$

The surface integral is at infinity because the velocity integral is over all space. Equation (B-3) shows that the species density is a constant so particles are conserved. The next moment is

$$\int_{-\infty}^{\infty} d\vec{v}\, m_{\alpha} \vec{v}\, \frac{\partial f_{\alpha 0}}{\partial t} = \int_{-\infty}^{\infty} d\vec{v}\, m_{\alpha} \vec{v}\, \frac{\partial}{\partial \vec{v}} \cdot \left[\overleftrightarrow{D}_{\alpha} \cdot \frac{\partial f_{\alpha 0}}{\partial \vec{v}} \right] \quad \text{(B-4)}$$

$$\frac{\partial}{\partial t} \int_{-\infty}^{\infty} d\vec{v}\, m_{\alpha} \vec{v}\, f_{\alpha 0} = -m_{\alpha} \int_{-\infty}^{\infty} d\vec{v}\, \overleftrightarrow{D}_{\alpha} \cdot \frac{\partial f_{\alpha 0}}{\partial \vec{v}} \quad \text{(B-5)}$$

where the chain rule and the divergence theorem have been used. When Eqns (9) and (A-36) and the sum of Eqn (B-5) over all of the species are all combined,

$$\frac{\partial}{\partial t}\left[\begin{matrix} total \\ momentum/vol \end{matrix} \right] = -\frac{2}{i} \int_{L} d\vec{k}\, \mathcal{E}(\vec{k},t)\, \vec{k} \cdot 1 \quad \text{(B-6)}$$

$$= 0 \quad \text{(B-7)}$$

Equation (B-7) follows because the integrand is odd. Therefore, momentum is conserved. The third moment is

$$\frac{1}{2} m_\alpha \int_{-\infty}^{\infty} d\vec{v} \, v^2 \, \frac{\partial f_{\alpha 0}}{\partial t} = \frac{1}{2} m_\alpha \int_{-\infty}^{\infty} d\vec{v} \, v^2 \, \frac{\partial}{\partial \vec{v}} \cdot \left[\bar{\bar{D}}_\alpha \cdot \frac{\partial f_{\alpha 0}}{\partial \vec{v}} \right] \quad \text{(B-8)}$$

$$\frac{\partial}{\partial t} \left[\begin{array}{c} species \, \alpha \\ particle \\ energy \\ vol \end{array} \right] = -\frac{2}{i} \frac{4\pi q_\alpha^2 e^2}{m_\alpha} \int_L d\vec{k} \, \mathcal{E} \int_{-\infty}^{\infty} d\vec{v} \, \vec{v} \cdot \vec{k} \, \frac{\vec{k} \cdot \frac{\partial f_{\alpha 0}}{\partial \vec{v}}}{[\vec{k} \cdot \vec{v} - \omega] k^2} \quad \text{(B-9)}$$

where as before Eqn (A-36) is used. Equation (B-9) is broken into two separate integrals one of which is odd by letting

$$\vec{k} \cdot \vec{v} = \vec{k} \cdot \vec{v} - \omega + \omega \quad \text{(B-10)}$$

The symmetry property of ω, Eqn (A-26), and Eqn (9) are also used.

Therefore, after the sum of Eqn (B-9) over all of the species is taken,

$$\frac{\partial}{\partial t} \left[\begin{array}{c} total \\ particle \\ energy \\ vol \end{array} \right] = -2 \int_{-\infty}^{\infty} d\vec{k} \, \omega_i \, \mathcal{E} \quad \text{(B-11)}$$

$$= -\int_{-\infty}^{\infty} d\vec{k} \, \frac{\partial \mathcal{E}}{\partial t} \quad \text{(B-12)}$$

$$= -\frac{\partial}{\partial t} \left[\frac{wave}{energy} \frac{}{vol} \right] \quad \text{(B-13)}$$

A loss in particle energy is balanced by a gain in wave energy so total energy is conserved.

Appendix C

Electron Dielectric for a Nonzero Magnetic Field

The dielectric is derived from the first order perturbation of the electron distribution function calculated in the Lagrangian coordinate system. The Lagrangian system follows the zero order trajectories of the electrons. The derivation is very long and tedious so only the highlights are presented. For further details, see Ref 16.

The rate of change of the distribution along the trajectory $\vec{x} = \vec{x}(t)$ is

$$\frac{df_e}{dt} = \frac{\partial f_e}{\partial t} + \frac{\partial f_e}{\partial \vec{x}} \cdot \frac{d\vec{x}}{dt} + \frac{\partial f_e}{\partial \vec{v}} \cdot \frac{d\vec{v}}{dt} \tag{C-1}$$

The change along the zero order trajectory is given by

$$\left(\frac{df_e}{dt}\right)_0 = \frac{\partial f_e}{\partial t} + \vec{v} \cdot \frac{\partial f_e}{\partial \vec{x}} - \frac{e}{m_e} \frac{\vec{v} \times \vec{B}_0}{c} \cdot \frac{\partial f_e}{\partial \vec{v}} \tag{C-2}$$

where $\quad \vec{E}_0 = 0 \tag{C-3}$

$$\left(\frac{df_{eo}}{dt}\right)_0 = \text{zero order solution} = 0 \tag{C-4}$$

$$f_e(\vec{v}, \vec{x}, t) = f_{eo}(\vec{v}) + f_{e1}(\vec{v}, \vec{x}, t) \tag{C-5}$$

$$e = |e| \tag{C-6}$$

Equation (C-4) describes the helical motion of a charged particle in a uniform magnetic field. Vlasov's equation, Eqn (1), after linearization is

$$\left[\frac{\partial}{\partial t} + \vec{v} \cdot \frac{\partial}{\partial \vec{x}} - \frac{e}{m_e} \frac{\vec{v} \times \vec{B}_0}{c} \cdot \frac{\partial}{\partial \vec{v}}\right] f_{e1} = \frac{e}{m_e}\left(\vec{E}_1 + \frac{\vec{v} \times \vec{B}_0}{c}\right) \cdot \frac{\partial f_{eo}}{\partial \vec{v}} \tag{C-7}$$

The result when Eqns (C-2) and (C-7) are compared is

$$\left(\frac{df_{e1}}{dt}\right)_0 = \begin{bmatrix} \text{rate of change of} \\ f_{e1} \text{ along the zero} \\ \text{order trajectory} \end{bmatrix} = \frac{e}{m_e}\left(\vec{E}_1 + \frac{\vec{v} \times \vec{B}_1}{c}\right) \cdot \frac{\partial f_{eo}}{\partial \vec{v}} \quad (C\text{-}8)$$

where Eqns (C-4) and (C-5) have been used to eliminate $(\vec{v} \times \vec{B}_o) \cdot \frac{\partial f_{eo}}{\partial \vec{v}}$.

The solution of Eqn (C-8) for growing wave modes is (The solution for damped modes is done by analytic continuation.)

$$f_{e1}(\vec{v}, \vec{x}, t) = \frac{e}{m_e} \int_{-\infty}^{t} dt' \left[\vec{E}_1(\vec{x}', t') + \frac{\vec{v}' \times \vec{B}_1(\vec{x}', t')}{c}\right] \cdot \frac{\partial f_{eo}(\vec{v}')}{\partial \vec{v}'} \quad (C\text{-}9)$$

where the integration is done along the zero order trajectory. Equation (C-9) is rewritten using Maxwell's equations assuming plane wave solutions:

$$f_{e1}(\vec{v}, \vec{x}, t) = \frac{e}{m_e} \int_{-\infty}^{t} dt' \, e^{i \vec{h} \cdot \vec{x}' - i \omega t'} \vec{E}(\vec{x}', t')$$

$$\left[1 + \frac{\vec{v}' \vec{h}}{\omega} - \frac{\vec{v}' \cdot \vec{h}}{\omega}\right] \cdot \frac{\partial f_{eo}(\vec{v}')}{\partial \vec{v}'} \quad (C\text{-}10)$$

This equation in the Eulerian (fixed) coordinates $\vec{v}$, $\vec{x}$, and t is

$$f_{e1}(\vec{v}, \vec{x}, t) = \frac{e}{m_e} \int_{0}^{\infty} d\tau \, \exp\left\{i \vec{h} \cdot \vec{x} - i\omega t + \left[\frac{i v_x}{\Omega_e}\right.\right.$$

$$\cdot (-h_x \sin\Omega_e \tau + h_y(1 - \cos\Omega_e \tau)) + \frac{i v_y}{\Omega_e}(-h_y \sin\Omega_e \tau$$

$$-h_x(1 - \cos\Omega_e \tau)) + i v_z(-h_z \tau) + i \omega \tau\bigg]\bigg\}$$

$$\cdot \left\{E_x(v_x \cos\Omega_e \tau + v_y \sin\Omega_e \tau)\left[f_{eo\perp} + \frac{h_z}{\omega}\left(f_{eo z}\right.\right.\right.$$

$$-v_z f_{eo\perp})\bigg] + E_y(-v_x \sin\Omega_e \tau + v_y \cos\Omega_e \tau)$$

$$\cdot \left[f_{eo\perp} + \frac{h_z}{\omega}(f_{eo z} - v_z f_{eo\perp})\right] + E_z\left[\frac{v_x}{\omega}(-h_x \cos\Omega_e \tau\right.$$

$$+ k_y \sin \Omega_e \tau) + \frac{v_z}{\omega}(-k_x \sin \Omega_e \tau - k_y \cos \Omega_e \tau) \Big]$$

$$\cdot (f_{eo2} - v_z f_{eo\perp}) + E_z f_{eo2} \Big\} \tag{C-11}$$

where $\quad \tau = t - t'$ $\tag{C-12}$

Ω_e = electron gyro frequency = $\dfrac{|e||\vec{B}_o|}{m_e c}$ $\tag{C-13}$

$$\vec{B}_o = B_o \hat{z} \tag{C-14}$$

$$f_{eo\perp} = \frac{1}{v_x} \frac{\partial f_{eo}}{\partial v_x} = \frac{1}{v_y} \frac{\partial f_{eo}}{\partial v_y} \tag{C-15}$$

$$f_{eo2} = \frac{\partial f_{eo}}{\partial v_z} \tag{C-16}$$

The last two equations follow from the azimuthally symmetric form of the zero order distribution:

$$f_{eo} = f_{eo}\left(\frac{v_\perp^2}{2}, v_z \right) \tag{C-17}$$

where $\quad v_\perp^2 = v_x^2 + v_y^2$ $\tag{C-18}$

Note Equation (C-11) is of the form:

$$f_{e1}(\vec{v}, \vec{x}, t) = e^{i\vec{k}\cdot\vec{x} - i\omega t} \, f_{e1}(\vec{v}, \vec{k}, \omega) \tag{C-19}$$

The remaining equations will only deal with the Fourier amplitude, $f_{e1}(\vec{v}, \vec{k}, \omega)$. The phase factor is dropped.

The spatial average of $f_{e1}(\vec{v}, \vec{k}, \omega)$ in the direction perpendicular to the ambient magnetic field is defined as

$$\langle f_{e1} \rangle_\perp = \int\!\!\int_{-\infty}^{\infty} dv_x \, dv_y \, f_{e1} \tag{C-20}$$

The zero order distribution is assumed to be a Maxwellian in the perpen-

dicular direction so

$$f_{eo}\left(\frac{v_\perp^2}{2}, v_z\right) = \frac{n_{eo} m_e}{2\pi X T_{e\perp}} g_{eo}(v_z) e^{-\frac{m_e(v_x^2 + v_y^2)}{2 X T_{e\perp}}} \tag{C-21}$$

where the distribution in the parallel direction has yet to be specified. The spatial average of Eqn (C-11) in terms of rotating coordinates is

$$\langle f_{e1} \rangle_\perp = \frac{e}{m_e} e^{-\lambda} \sum_{n=-\infty}^{\infty} \int_0^T d\tau\, e^{i(n\Omega_e + \omega - k_z v_z)\tau}$$

$$\cdot \left[\frac{k_- \xi_+ X T_{e\perp}}{2\Omega_e m_e}(I_{n+1} - I_n) + \frac{k_+ \xi_- X T_{e\perp}}{2\Omega_e m_e}(I_n - I_{n-1}) + \xi_z I_n \right] \tag{C-22}$$

where
$$\lambda = \frac{1}{2} k_\perp^2 \rho_{Le}^2 \tag{C-23}$$

$$\rho_{Le} = \text{average gyro radius} = \frac{\sqrt{\frac{2 X T_{e\perp}}{m_e}}}{\Omega_e} \tag{C-24}$$

$$k_\pm = k_x \mp i k_y \tag{C-25}$$

$$\xi_\pm = \xi_x \mp i \xi_y \tag{C-26}$$

$$\xi_{x,y} = -\frac{m_e g_{eo} E_{x,y}}{X T_{e\perp}} + \left(\frac{dg_{eo}}{dv_z} + \frac{m_e v_z g_{eo}}{X T_{e\perp}}\right)$$

$$\cdot \left(\frac{k_z E_{x,y}}{\omega} - \frac{k_{x,y} E_z}{\omega}\right) \tag{C-27}$$

$$I_n = I_n(\lambda) = i^{-n} J_n(i\lambda) \tag{C-28}$$

$$\xi_z = E_z \frac{dg_{eo}}{dv_z} \tag{C-29}$$

The Bessel functions, $J_n(i\lambda)$ and $I_n(\lambda)$, in Eqn (C-28) are respectively the ordinary and modified Bessel functions of the first kind. After the distribution in the z direction is specified as the following Maxwellian with a zero drift velocity:

$$g_{eo}(v_z) = \left[\frac{m_e}{2\pi X T_{e\parallel}}\right]^{1/2} e^{-\frac{m_e v_z^2}{2 X T_{e\parallel}}} \tag{C-30}$$

the total spatial average of the first order distribution becomes

$$\int_{-\infty}^{\infty} d\vec{v}\, f_{e1} = \int_{-\infty}^{\infty} dv_z \langle f_{e1} \rangle_\perp = -\frac{e}{m} e^{-\lambda}\, 2 n_{eo} \left[\frac{m_e}{2 \times T_{e//}} \right]^{3/2}$$

$$\cdot \sum_{n=-\infty}^{\infty} I_m \left\{ -\frac{T_{e//}}{T_{e\perp}} \frac{n \Omega_e}{h_x h_z} E_x F_0(\alpha_n) + \left[\frac{n \Omega_e}{\omega} \left(\frac{E_x}{h_x} \right. \right. \right.$$

$$\left. \left. - \frac{E_z}{h_z} \right) \left(\frac{T_{e//}}{T_{e\perp}} - 1 \right) + \frac{E_z}{h_z} \right] F_1(\alpha_n) \tag{C-31}$$

where $\qquad h_y = E_y = 0 \tag{C-32}$

$$F_0(\alpha_n) = -i\, Z(\alpha_n) \tag{C-33}$$

$$F_1(\alpha_n) = \sqrt{\frac{2 \times T_{e//}}{m_e}} \left[-i + \alpha_n F_0(\alpha_n) \right] \tag{C-34}$$

$$\alpha_n = \frac{\omega + n \Omega_e}{h_z} \sqrt{\frac{m_e}{2 \times T_{e//}}} \tag{C-35}$$

$$Z(\alpha_n) = \text{plasma dispersion} \atop \text{function (Ref 17)} = \frac{1}{\sqrt{\pi}} \int_L \frac{dz\, e^{-z^2}}{z - \alpha_n} \tag{C-36}$$

The electric field is assumed to be electrostatic so

$$\vec{E}(\vec{h}, \omega) = -i\, \vec{h}\, \phi(\vec{h}, \omega) \tag{C-37}$$

where ϕ is the electrostatic potential. When Eqns (C-37) and (C-31) are combined with the Fourier transformed Poisson's equation,

$$i\, \vec{h} \cdot \vec{E}(\vec{h}, \omega) = 4\pi \sum_\alpha q_\alpha e \int_{-\infty}^{\infty} d\vec{v}\, f_{\alpha1}(\vec{v}, \vec{h}, \omega) \tag{C-38}$$

the following form of the electron dielectric results:

$$\epsilon_e = \frac{\omega_{pe}^2}{h^2 c_{ex}^2} \left\{ \frac{T_{ex}}{T_{ez}} (\lambda - 1) \frac{\omega}{h_z \sqrt{2}\, c_{ez}} Z(\alpha_0) - \frac{T_{ex}}{T_{ez}} \right.$$

$$-\frac{\lambda}{2} \frac{1}{\sqrt{2} c_{ez}} \frac{1}{h_z} \left[\left(\frac{T_{ex}}{T_{ez}} (\omega + \Omega_e) - \Omega_e \right) Z(\alpha_1) \right.$$

110

$$+ \left(\frac{T_{ex}}{T_{ez}} \left(\omega - \Omega_e \right) + \Omega_e \right) \frac{1}{7} \left(\alpha_{-1} \right) \Biggr] \Biggr\} \tag{C-39}$$

where ω_{pe} = plasma frequency = $\sqrt{\dfrac{4\pi n_{eo} e^2}{m_e}}$ (C-40)

$$T_{ex} = T_{e\perp} \tag{C-41}$$

$$T_{ez} = T_{e//} \tag{C-42}$$

$c_{ex,z}$ = thermal speed = $\sqrt{\dfrac{X T_{ex,z}}{m_e}}$ (C-43)

The infinite sum has been eliminated by assuming

$$\lambda \ll 1 \tag{C-44}$$

so $I_o(\lambda) = 1$ (C-45)

$$I_{\pm 1}(\lambda) = \frac{\lambda}{2} \tag{C-46}$$

$I_{|n| \geq 2}(\lambda)$ is of order λ^2 or higher (C-47)

Only the zero and first order terms in λ are retained in Eqn (C-39). This result is also valid for damped modes because the definition of the plasma dispersion function includes the analytic continuation.

Equation (C-39) appears to be singular for propagation exactly perpendicular to the ambient magnetic field. However, the limit of the dielectric as $k_z \rightarrow 0$ is

$$\lim_{k_z \rightarrow 0} \epsilon_e = \frac{\omega_{pe}^2}{k^2 c_{ex}^2} \lambda \frac{\Omega_e^2}{\omega^2 - \Omega_e^2} \tag{C-48}$$

which is well behaved.

111

Appendix D

Analytical Form of the Field-Free Dielectrics

An analytical form of the field-free dielectric integrals in Eqn
(9) results when the following two-temperature Maxwellian is used:

$$f_{\alpha o}(\vec{v}) = n_{\alpha o} \frac{m_\alpha}{2\pi X}\left[\frac{1}{T_{\alpha x} T_{\alpha z}}\right]^{1/2} e^{-\frac{m_\alpha(v_x - V_\alpha)^2}{2 X T_{\alpha x}} - \frac{m_\alpha v_z^2}{2 X T_{\alpha z}}} \quad (D-1)$$

where the streaming velocity, V_α, is assumed to be in the x direction.
To begin the derivation, Equation (9) is rewritten as

$$1 - \sum_\alpha \frac{\omega_{p\alpha}^2}{k^2}\int_L d\vec{v}\, \frac{\vec{k}\cdot\vec{G}_{\alpha o}(\vec{v},t)}{[\vec{k}\cdot\vec{v} - \omega(\vec{k},t)]} = 1 - \sum_\alpha \frac{\omega_{p\alpha}^2}{k^2} I_\alpha = 0 \quad (D-2)$$

where $\omega_{p\alpha}^2 = $ (species plasma frequency)$^2 = \dfrac{4\pi q_\alpha^2 e^2 n_{\alpha o}}{m_\alpha}$ (D-3)

$$\vec{G}_{\alpha o}(\vec{v},t) = \frac{1}{n_{\alpha o}}\frac{\partial f_{\alpha o}(\vec{v},t)}{\partial \vec{v}} \quad (D-4)$$

When Equation (D-1) is inserted into Eqn (D-4) and the result is
multiplied by $\vec{k}$,

$$\vec{k}\cdot\vec{G}_{\alpha o}(\vec{v},t) = -\frac{1}{2\pi}\frac{1}{c_{\alpha x}c_{\alpha z}}\left[k_x \frac{v_x - V_\alpha}{c_{\alpha x}^2} + k_z \frac{v_z}{c_{\alpha z}^2}\right]$$

$$\cdot e^{-\frac{(v_x - V_\alpha)^2}{2 c_{\alpha x}^2} - \frac{v_z^2}{2 c_{\alpha z}^2}} \quad (D-5)$$

where the one-dimensional root-mean-square thermal velocities in the x
and z directions are defined as

$$c_{\alpha x, z} = \sqrt{\frac{X T_{\alpha x, z}}{m_\alpha}} \quad (D-6)$$

The most convenient way to do the integral I_α in Eqn (D-2) is to
perform a coordinate rotation in the v_x-v_z plane to align the new v_x
axis ($v_{x'}$) with the wave propagation direction. Then, the singularly
in the denominator appears only in the $v_{x'}$ coordinate so the integration

112

in $v_{z'}$ can be done directly. The relationships between the wave $\vec{k}$ and velocity vectors in the old and new systems are

$$\begin{pmatrix} v_x \\ v_z \end{pmatrix}; \begin{pmatrix} k_x \\ k_z \end{pmatrix} = \begin{pmatrix} \cos\theta & -\sin\theta \\ \sin\theta & \cos\theta \end{pmatrix} \begin{pmatrix} v_{x'} \\ v_{z'} \end{pmatrix}; \begin{pmatrix} k_{x'} \\ k_{z'} \end{pmatrix} \tag{D-7}$$

When these relations are used along with the fact that the Jacobian for a rotation is unity, the result after much algebra is

$$I_\alpha = -\frac{|\vec{k}|}{2\pi} \frac{1}{c_{dx}^3 c_{dz}^3} \int_L dv_{x'} dv_{z'} \frac{\left[c_{d\theta}^2 v_{x'} + (c_{dx}^2 - c_{dz}^2) \cdot \cos\theta\sin\theta\, v_{z'} - V_d c_{dz}^2 \cos\theta \right]}{\omega - |\vec{k}| v_{x'}}$$

$$\cdot \exp\left\{ \frac{\left[c_{d\theta}^2 v_{x'}^2 - 2V_d c_{dz}^2 v_{x'}\cos\theta + 2v_{x'} v_{dz'}(c_{dx}^2 - c_{dz}^2) \cdot \cos\theta\sin\theta + c_{d\theta}^2 v_{z'}^2 + 2V_d c_{dz}^2 v_{z'}\sin\theta + V_d^2 c_{dz}^2 \right]}{2\, c_{dx}^2\, c_{dz}^2} \right\} \tag{D-8}$$

where

$$c_{d\theta}^2 = c_{dx}^2 \cos^2\theta + c_{dz}^2 \sin^2\theta \tag{D-9}$$

$$c_{d\theta}^2 = c_{dx}^2 \sin^2\theta + c_{dz}^2 \cos^2\theta \tag{D-10}$$

The angle θ is that between $\vec{k}$ and the v_x axis. After the integral in $v_{z'}$ is done and the result is simplified, the following simple expression appears

$$I_\alpha = \frac{1}{\sqrt{2\pi}\, c_{d\theta}^3} \int_L dv_{x'} \frac{(v_{x'} - V_d\cos\theta)}{v_{x'} - \omega/|\vec{k}|} e^{-\frac{(v_{x'} - V_d\cos\theta)^2}{2 c_{d\theta}^2}} \tag{D-11}$$

This form is related to the derivative of the plasma dispersion function as defined by Fried and Conte (Ref 17). This derivative is

$$Z_1'(z_\alpha) = -\frac{2}{\sqrt{\pi}} \int_L \frac{du\, u\, e^{-u^2}}{u - z_\alpha} \tag{D-12}$$

Hence, the final form of the dispersion relation results when Eqns (D-2), (D-11), and (D-12) are combined:

$$1 - \sum_\alpha \epsilon_\alpha = 1 - \sum_\alpha \frac{\omega_{pd}^2}{2k^2 c_{d\theta}^2} Z_1'(z_\alpha) = 0 \tag{D-13}$$

113

where $c_{\alpha\theta}$ is the root-mean-square thermal width in the θ direction from Eqn (D-9) and

$$z_\alpha = \frac{\omega/|\vec{k}| - v_\alpha \cos\theta}{\sqrt{2}\, c_{\alpha\theta}} \qquad (D\text{-}14)$$

Note $\omega_{p\alpha}^2/c_{\alpha\theta}^2$ can be rewritten in terms of the species Debye length in the θ direction because

$$\frac{\omega_{p\alpha}^2}{c_{\alpha\theta}^2} = \frac{1}{\lambda_{D\alpha\theta}^2} \qquad (D\text{-}15)$$

Incidentally, the dispersion relation, Eqn (D-13), has the same form as a one-dimensional dispersion relation.

The dispersion relation is valid for all values of the complex frequency because the definition of the plasma dispersion function contains the analytic continuation across the ω_r axis into the lower half of the complex frequency plane. This continuation is equivalent to conducting the integration in Eqn (D-12) along the Landau contour.

Appendix E

The Derivation of the Anomalous Transport Coefficients

The calculation of the anomalous transport coefficients for momentum and energy transfer is done using the formulas derived below. These formulas are obtained from the first three velocity moments of the spatially averaged Vlasov equation, Eqn (A-9). This process gives the standard fluid equations of continuity, momentum transfer, and energy balance with anomalous collision terms instead of the normal collision terms due to binary interactions.

In the derivation, the following definitions are used:

$$n_{\alpha 0}(t) = \int_{-\infty}^{\infty} d\vec{v}\, f_{\alpha 0}(\vec{v}, t) \tag{E-1}$$

$$n_{\alpha 1}(\vec{x}, t) = \int_{-\infty}^{\infty} d\vec{v}\, f_{\alpha 1}(\vec{x}, \vec{v}, t) \tag{E-2}$$

$$n_{\alpha 0}\vec{V}_{\alpha}(t) = \int_{-\infty}^{\infty} d\vec{v}\, \vec{v}\, f_{\alpha 0}(\vec{v}, t) \tag{E-3}$$

$$(n\vec{V})_{\alpha 1}(\vec{x}, t) = \int_{-\infty}^{\infty} d\vec{v}\, \vec{v}\, f_{\alpha 1}(\vec{x}, \vec{v}, t) \tag{E-4}$$

$$\frac{3}{2} n_{\alpha 0} \times T_{\alpha}(t) = \frac{1}{2} m_{\alpha} \int_{-\infty}^{\infty} d\vec{v}\, w^2 f_{\alpha 0}(\vec{v}, t) \tag{E-5}$$

where T_α is in degrees Kelvin, and

$$\vec{w} = \text{random velocity} = \vec{v} - \vec{V}_{\alpha} \tag{E-6}$$

For convenience, Eqn (A-9) is repeated here:

$$\frac{\partial f_{\alpha 0}}{\partial t} = -\frac{q_\alpha}{m_\alpha} \left\langle \vec{E} \cdot \frac{\partial f_{\alpha 1}}{\partial \vec{v}} \right\rangle \tag{E-7}$$

The velocity-to-the-zero-power moment simply gives the equation of

115

continuity which is not of interest because the plasma is assumed to be initially homogeneous. The next two moments are done using the methods in Seshadri (Ref 7: 27-45).

The velocity-to-the-first-power moment of Eqn (E-7) is

$$\frac{\partial}{\partial t}\left[n_{\alpha o} \, m_{\alpha} \, \vec{V}_{\alpha} \right] = - \frac{q_{\alpha} e}{m_{\alpha}} \int_{-\infty}^{\infty} d\vec{v} \, m_{\alpha} \, \vec{v} \left\langle \vec{E} \cdot \frac{\partial f_{\alpha 1}}{\partial \vec{v}} \right\rangle \qquad \text{(E-8)}$$

$$= q_{\alpha} e \left\langle \vec{E} \, n_{\alpha 1} \right\rangle \qquad \text{(E-9)}$$

where the chain rule, the divergence theorem, and Eqns (E-2) and (E-3) have been used. Equation (E-9) is the momentum transfer equation with the right hand side representing the anomalous change in momentum density due to wave-particle interactions.

The third moment of Eqn (E-7) is

$$\frac{\partial}{\partial t}\left[\frac{1}{2} m_{\alpha} \int_{-\infty}^{\infty} d\vec{v} \, w^2 \, f_{\alpha o} \right] = - \frac{q_{\alpha} e}{2} \int_{-\infty}^{\infty} d\vec{v} \, w^2 \left\langle \vec{E} \cdot \frac{\partial f_{\alpha 1}}{\partial \vec{v}} \right\rangle \qquad \text{(E-10)}$$

$$\frac{\partial}{\partial t}\left[\frac{3}{2} n_{\alpha o} \times T_{\alpha} \right] = \frac{q_{\alpha} e}{2} \left\langle \vec{E} \cdot \int_{-\infty}^{\infty} d\vec{v} \, f_{\alpha 1} \frac{\partial}{\partial \vec{v}}\left[(\vec{v} - \vec{V}_{\alpha})^2 \right] \right\rangle \qquad \text{(E-11)}$$

where the above procedures and Eqn (E-5) have been used. Continuing,

$$\frac{3}{2} n_{\alpha o} \frac{\partial \times T_{\alpha}}{\partial t} = q_{\alpha} e \left\langle \vec{E} \cdot \left[\int_{-\infty}^{\infty} d\vec{v} \, \vec{v} \, f_{\alpha 1} - \vec{V}_{\alpha} \int_{-\infty}^{\infty} d\vec{v} \, f_{\alpha 1} \right] \right\rangle \qquad \text{(E-12)}$$

$$= q_{\alpha} e \left\langle \vec{E} \cdot \left[(n\vec{V})_{\alpha 1} - \vec{V}_{\alpha} \, n_{\alpha 1} \right] \right\rangle \qquad \text{(E-13)}$$

where Eqns (E-2) and (E-4) have been used. Equation (E-13) is the energy or heating equation with the right hand side giving the anomalous heating rate.

Equations (E-9) and (E-13) are put into a more convenient form by using the Fourier transformed Poisson's equation, Eqn (A-29),

$$i h E(\vec{h}, t) = 4\pi \sum_{\alpha} q_{\alpha} e \int_{-\infty}^{\infty} d\vec{v} \, f_{\alpha 1}(\vec{h}, \vec{v}, t) \qquad \text{(E-14)}$$

and the dispersion relation,

$$1 = \sum_{\alpha} \epsilon_{\alpha} \qquad \text{(E-15)}$$

The plasma dielectric, ϵ_{α}, from Eqn (9) is

$$\epsilon_{\alpha} = \frac{4\pi q_{\alpha}^2 e^2}{m_{\alpha} h^2} \int_{L} d\vec{v} \, \frac{\vec{h} \cdot \frac{\partial f_{\alpha 0}(\vec{v}, t)}{\partial \vec{v}}}{[\vec{h} \cdot \vec{v} - \omega(\vec{h}, t)]} \qquad \text{(E-16)}$$

When both sides of Eqn (E-15) are multiplied by $ikE(\vec{k}, t)$, Eqn (E-14) used, and corresponding terms of the sums equated;

$$n_{\alpha 1}(\vec{h}, t) = \int_{-\infty}^{\infty} d\vec{v} \, f_{\alpha 1}(\vec{h}, \vec{v}, t) = \frac{i h E(\vec{h}, t) \epsilon_{\alpha}(\omega/h), \vec{h})}{4\pi q_{\alpha} e} \qquad \text{(E-17)}$$

This equation along with the definition of spectral wave energy, Eqn (A-35), are the main equations used to recast the anomalous collision terms. In addition to these equations, the integral form of the delta function,

$$\delta(\vec{h} + \vec{h}') = \frac{1}{(2\pi)^3} \int_{-\infty}^{\infty} d\vec{x} \, e^{i(\vec{h} + \vec{h}') \cdot \vec{x}} \qquad \text{(E-18)}$$

and the symmetry of the dielectric,

$$\epsilon_{\alpha}(-\vec{h}, t) = \epsilon_{\alpha}^{*}(\vec{h}, t) \qquad \text{(E-19)}$$

are used. Equation (E-19) follows from Eqn (E-16) broken into its real and imaginary parts and from Eqn (A-26). Therefore, from Eqn (E-9),

$$\frac{\partial}{\partial t}\left[n_{\alpha 0} m_{\alpha} \vec{V}_{\alpha} \right] = q_{\alpha} e \left\langle \frac{1}{(2\pi)^3} \int_{-\infty}^{\infty} d\vec{h}' \, e^{i\vec{h}' \cdot \vec{x}} \vec{E}(\vec{h}', t) \right.$$

$$\left. \cdot \frac{1}{(2\pi)^3} \int_{-\infty}^{\infty} d\vec{h} \, e^{i\vec{h} \cdot \vec{x}} n_{\alpha 1}(\vec{h}, t) \right\rangle \qquad \text{(E-20)}$$

117

$$= 2i \int d\vec{h} \, \vec{h} \, \mathcal{E}(\vec{h},t) \, \epsilon_\alpha(\omega(\vec{h},t),\vec{h}) \qquad \text{(E-21)}$$

$$= 2 \int d\vec{h} \, \vec{h} \, \mathcal{E}(\vec{h},t) \, Im\left[\epsilon_\alpha(\omega(\vec{h},t),\vec{h})\right] \qquad \text{(E-22)}$$

and from Eqn (E-13),

$$\frac{3}{2} n_{1o} \frac{\partial XT_\alpha}{\partial t} = q_\alpha e \left\langle \vec{E} \cdot (n\vec{v})_{\alpha 1} \right\rangle - q_\alpha e \left\langle \vec{E} \cdot \vec{V}_\alpha \, n_{\alpha 1} \right\rangle \qquad \text{(E-23)}$$

$$= q_\alpha e \left\langle \frac{1}{(2\pi)^3} \int d\vec{h}' e^{i\vec{h}'\cdot\vec{n}} \vec{E}(\vec{h}',t) \frac{1}{(2\pi)^3} \int d\vec{h} \, e^{i\vec{h}\cdot\vec{n}} (n\vec{v})_\alpha(\vec{h},t) \right\rangle$$

$$- q_\alpha e \left\langle \int d\vec{h}' e^{i\vec{h}'\cdot\vec{n}} \vec{E}(\vec{h}',t) \frac{\vec{V}_\alpha}{(2\pi)^3} \int d\vec{h} \, e^{i\vec{h}\cdot\vec{n}} n_{\alpha 1}(\vec{h},t) \right\rangle \qquad \text{(E-24)}$$

$$= 2i \int d\vec{h} \, \mathcal{E}(\vec{h},t) \, \omega(\vec{h},t) \, \epsilon_\alpha(\omega(\vec{h},t),\vec{h})$$

$$- 2i \int d\vec{h} \, \mathcal{E}(\vec{h},t) \, \vec{h}\cdot\vec{V}_\alpha \, \epsilon_\alpha(\omega(\vec{h},t),\vec{h}) \qquad \text{(E-25)}$$

$$= -2 \int_{-\infty}^{\infty} d\vec{h} \, \mathcal{E}(\vec{h},t) \left\{ \omega_i(\vec{h},t) \, Re\left[\epsilon_\alpha(\omega(\vec{h},t),\vec{h})\right] \right.$$

$$\left. + (\omega_r(\vec{h},t) - \vec{h}\cdot\vec{V}_\alpha) \, Im\left[\epsilon_\alpha(\omega(\vec{h},t),\vec{h})\right] \right\} \qquad \text{(E-26)}$$

where in the first term on the right hand side of Eqn (E-23), Eqn (A-28) without the free streaming terms and Eqn (B-10) were used to obtain Eqn (E-26). Equations (E-22) and (E-26) are the normal fluid momentum transfer and energy balance equations for a collisionless homogeneous plasma with added anomalous collision terms on the right hand sides. Because the plasma is homogeneous, all of the changes in the momentum and energy densities are due to anomalous transport.

Although the above derivation assumes the plasma is magnetic field

118

free, the generalization to a plasma with a uniform magnetic field is
very straight forward. In fact, the resulting anomalous transport
coefficients are the same as those in Eqns (E-22) and (E-26). With the
addition of the magnetic field, Equation (E-22) becomes

$$\frac{\partial}{\partial t}\left[n_{\alpha 0}\, m_\alpha \vec{V}_\alpha\right] - n_{\alpha 0}\, q_\alpha\, e\; \frac{\vec{V}_\alpha \times \vec{B}_0}{c}$$

$$= -2\int_{-\infty}^{\infty} d\vec{k}\; \vec{k}\; \mathcal{E}(\vec{k}, t)\; Im\left[\epsilon_\alpha\left(\omega(\vec{k}, t), \vec{k}\right)\right] \quad \text{(E-27)}$$

where $\vec{B}_0$ is the magnetic field. The energy balance equation is
unchanged.

Appendix F

Numerical Form of the Quasilinear Equations

In this appendix, the quasilinear equations are each cast into their numerical forms by the extensive use of symmetries. The resulting equations are the ones put into the solution program controlled by IONION. The diffusion equation is discussed first.

The diffusion equation is solved only on the upper half of the computer solution velocity plane shown in Fig. 6 because the equation is symmetric with respect to reflection across the v_x axis. This half plane is mapped onto a rectangle (the computer mesh) with its lower left and upper right corners at (-1,0) and (1,1) respectively. This mapping is described by the following relations:

$$v_x = \frac{v_{xo}\, \mu_x}{\sqrt{1 - \mu_x^2}} - V_{DA} \qquad (F\text{-}1)$$

$$v_z = \frac{v_{zo}\, \mu_z}{\sqrt{1 - \mu_z^2}} \qquad (F\text{-}2)$$

where $\quad -1 \leq \mu_x \leq 1 \qquad (F\text{-}3)$

$$0 \leq \mu_z \leq 1 \qquad (F\text{-}4)$$

The variables u_x and u_z are the mesh coordinates. Three separate sets of the three transformation parameters; v_{xo}, v_{zo}, and V_{DA}; are used for each of the plasma species; debris, air, and electrons. Therefore, a given value of a mesh coordinate refers to three separate velocities depending on which species is being referenced.

The transformation parameters are determined from the initial species Maxwellians and are held fixed throughout the time evolution. The parameter V_{DA} is chosen so the computer mesh is centered on the

120

electron distribution, or for the ions, is centered one thermal width in the v_x direction away from the distribution peak on the side toward the other distribution. The scale parameters v_{xo} and v_{zo} are respectively set equal to three times the species thermal width in the v_x direction and that in the v_z direction. These settings of the transformation parameters cause the majority of the mesh points to correspond to the velocities of the interesting parts of the species distributions.

For good numerical results, the mesh spacing (the number of mesh points used) in the u_x and u_z directions are chosen so at least a few mesh points correspond to the resonant region (where Eqn (18) holds). The mesh spacing is also chosen to insure sufficient accuracy of the dispersion relation integrals described later. This spacing is fairly critical because the mode growth rates depend on the distribution slopes.

An interesting result of the above mesh transformation procedures is that a given plasma species appears the same on the mesh regardless of its temperature, mean velocity, or density. For example, a sketch of the initial debris Maxwellian is shown in Fig. F-1. Therefore, the numerical accuracy of the evolution is relatively unaffected by changes in the plasma distribution.

The diffusion equation for growing modes, after expansion of the dot products and conversion into the mesh coordinate system, is

$$\frac{\partial f_{do}(\vec{u},t)}{\partial t} = D_{xx}(\vec{u},t) \frac{(1-u_x^2)^3}{v_{xo}^2} \frac{\partial^2 f_{do}(\vec{u},t)}{\partial u_x^2}$$

$$+ 2 D_{xz}(\vec{u},t) \frac{[(1-u_x^2)(1-u_z^2)]^{3/2}}{v_{xo} v_{zo}} \frac{\partial^2 f_{do}(\vec{u},t)}{\partial u_x \partial u_z} \qquad .$$

$$+ D_{zz}(\vec{u},t) \frac{(1-u_z^2)^3}{v_{zo}^2} \frac{\partial^2 f_{do}(\vec{u},t)}{\partial u_z^2}$$
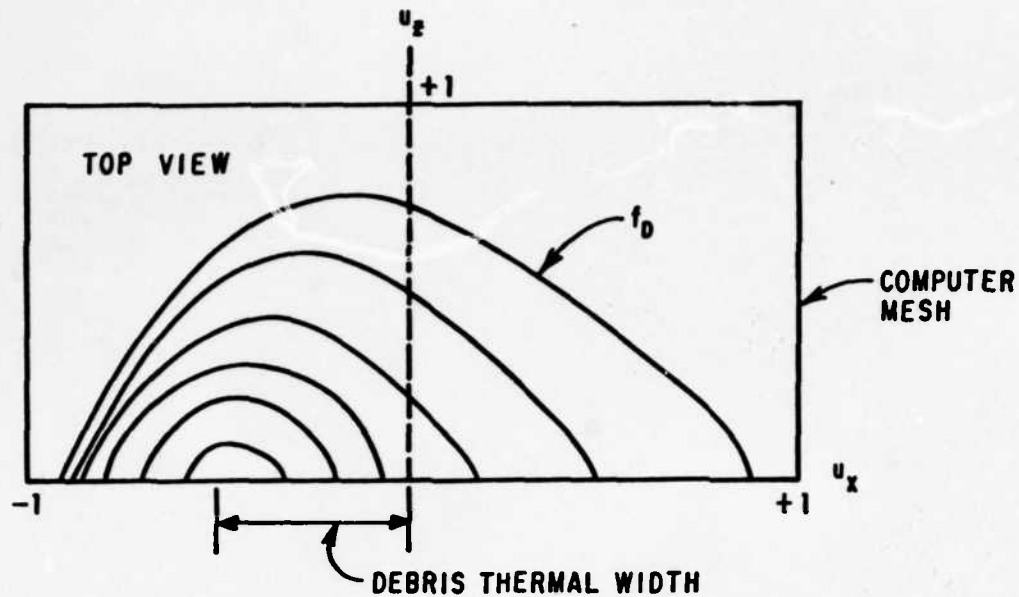
Fig. F-1. Initial Debris Maxwellian Distribution on the Computer Mesh.

$$+\left\{G_{xxxz}(\vec{u},t)\frac{(1-u_x^2)^{3/2}}{\nu_{xo}} - D_{xx}(\vec{u},t)\right.$$

$$\left. \cdot \frac{3u_x(1-u_x^2)^2}{\nu_{xo}^2}\right\}\frac{\partial f_{do}(\vec{u},t)}{\partial u_x} + \left\{G_{xzzz}(\vec{u},t)\right.$$

$$\left. \cdot \frac{(1-u_z^2)^{3/2}}{\nu_{zo}} - D_{zz}(\vec{u},t)\frac{3u_z(1-u_z^2)^2}{\nu_{zo}^2}\right\}\frac{\partial f_{do}(\vec{u},t)}{\partial u_z} \qquad \text{(F-5)}$$

where $D_{xx}(\vec{u},t) = 8\pi\left(\frac{q_d e}{m_d}\right)^2 \iint_{-\infty}^{\infty} d\vec{k}\,\frac{\mathcal{E}(\vec{k},t)\,k_x^2\,\omega_i(\vec{k},t)}{\left[(\vec{k}\cdot\vec{v}(\vec{u})-\omega_r(\vec{k},t))^2 + \omega_i^2(\vec{k},t)\right]k^2}$ (F-6)

$D_{xz}(\vec{u},t) = 8\pi\left(\frac{q_d e}{m_d}\right)^2\iint_{-\infty}^{\infty} d\vec{k}\,\frac{\mathcal{E}(\vec{k},t)\,k_x\,k_z\,\omega_i(\vec{k},t)}{\left[(\vec{k}\cdot\vec{v}(\vec{u})-\omega_r(\vec{k},t))^2 + \omega_i^2(\vec{k},t)\right]k^2}$ (F-7)

$D_{zz}(\vec{u},t) = 8\pi\left(\frac{q_d e}{m_d}\right)^2\iint_{-\infty}^{\infty} d\vec{k}\,\frac{\mathcal{E}(\vec{k},t)\,k_z^2\,\omega_i(\vec{k},t)}{\left[(\vec{k}\cdot\vec{v}(\vec{u})-\omega_r(\vec{k},t))^2 + \omega_i^2(\vec{k},t)\right]k^2}$ (F-8)

$G_{xxxz}(\vec{u},t) = -16\pi\left(\frac{q_d e}{m_d}\right)^2\iint_{-\infty}^{\infty} d\vec{k}\,\frac{\mathcal{E}(\vec{k},t)\,k_x\,\omega_i(\vec{k},t)}{\left[(\vec{k}\cdot\vec{v}(\vec{u})-\omega_r(\vec{k},t))^2 + \omega_i^2(\vec{k},t)\right]^2}$ (F-9)

$G_{xzzz}(\vec{u},t) = -16\pi\left(\frac{q_d e}{m_d}\right)^2\iint_{-\infty}^{\infty} d\vec{k}\,\frac{\mathcal{E}(\vec{k},t)\,k_z\,\omega_i(\vec{k},t)}{\left[(\vec{k}\cdot\vec{v}(\vec{u})-\omega_r(\vec{k},t))^2 + \omega_i^2(\vec{k},t)\right]^2}$ (F-10)

AFIT/DS/PH/78-1

Equations (F-9) and (F-10) resulted from the combination of the velocity derivatives of the diffusion coefficients given by Eqns (F-6) to (F-8). Equation (F-5) appears to be an elliptical-parabolic equation with two spatial variables, u_x and u_z. The right hand side is elliptic because the coefficients to the second order terms are positive definite, and

$$\left[D_{xx} \frac{(1-u_x^2)^3}{N_{x_0}^2} \right] \left[D_{zz} \frac{(1-u_z^2)^3}{N_{z_0}^2} \right] > \left[D_{xz} \frac{[(1-u_x^2)(1-u_z^2)]^{3/2}}{N_{x_0} N_{z_0}} \right]^2 \quad (F-11)$$

For damped modes or a combination of damped and growing modes, Eqn (F-5) must be analytically continued. This process is numerically very difficult and is not necessary because the growing modes dominate the solution for the times of interest. (The fastest growing modes build up the largest wave energies which modify the distribution the most.) A mixture of damped and growing modes appears only late in the calculation anyway.

Because the plasma species distributions all go to zero as v_x or v_z goes to infinity, the boundary conditions for the diffusion equation are relatively simple:

$$f_{\alpha 0}(u_x = 1, u_z, t) = 0 \quad (F-12)$$

$$f_{\alpha 0}(u_x = -1, u_z, t) = 0 \quad (F-13)$$

$$f_{\alpha 0}(u_x, u_z = 1, t) = 0 \quad (F-14)$$

The symmetry of the upper and lower half planes determines the boundary condition on the mesh bottom. The initial condition for each distribution is the initial Maxwellian,

$$f_{\alpha 0}(\vec{u}, t = 0) = \frac{n_{d0}}{2\pi C_{\alpha x} C_{\alpha z}} e^{-\frac{(N_x - V_d)^2}{2 C_{\alpha x}^2} - \frac{N_z^2}{2 C_{\alpha z}^2}} \quad (F-15)$$

123

AFIT/DS/PH/78-1

where v_x and v_z are given by Eqns (F-1) and (F-2).

In the method of lines, the spatial derivatives on the right hand side of Eqn (F-5) are written in terms of finite differences, and the resulting set of simultaneous ordinary differential equations is evolved in time by the GEARB package. The interior including the bottom of the mesh is broken up into a series of vertical lines of mesh points with the points sequentially numbered. The resulting numbering scheme is shown in Fig. F-2 for a n_x by n_z mesh where n_x and n_z are respectively the numbers of mesh points in the u_x and u_z directions. A finite difference equation is written for each of the numbered points using the following finite difference formulas:

$$\frac{\partial^2 f_{d0}}{\partial u_x^2} = \frac{f_{i+n_z} - 2f_i + f_{i-n_z}}{h_x^2} \tag{F-16}$$

$$\frac{\partial^2 f_{d0}}{\partial u_x \partial u_z} = \frac{f_{i+1+n_z} - f_{i+1-n_z} - f_{i-1+n_z} + f_{i-1-n_z}}{4 h_x h_z} \tag{F-17}$$

$$\frac{\partial^2 f_{d0}}{\partial u_z^2} = \frac{f_{i+1} - 2f_i + f_{i-1}}{h_z^2} \tag{F-18}$$

$$\frac{\partial f_{d0}}{\partial u_x} = \frac{f_{i+n_z} - f_{i-n_z}}{2 h_x} \tag{F-19}$$

$$\frac{\partial f_{d0}}{\partial u_z} = \frac{f_{i+1} - f_{i-1}}{2 h_z} \tag{F-20}$$

where h_x and h_z are the uniform mesh spacings, and i is the mesh point of interest. As shown in Fig. F-2, this is a nine point differencing scheme. For the difference terms on the top and sides of the mesh, the boundary conditions, Eqns (F-12) to (F-14), are used. The equations for the bottom mesh points use the symmetry of the distribution. For these points, Eqns (F-16) and (F-19) are unchanged, Eqns (F-17) and (F-20)

124

u_z

$(n_z - 1)$ $2(n_z - 1)$

$(n_x - 3)$
$\cdot (n_z - 1)$

$(n_x - 2)$
$\cdot (n_z - 1)$

$(n_x - 4)$
$\cdot (n_z - 1)$
$+3$

$(n_x - 3)$
$\cdot (n_z - 1)$
$+3$

3 $(n_z - 1) + 3$

$(n_x - 4)$
$\cdot (n_z - 1)$
$+2$

$(n_x - 3)$
$\cdot (n_z - 1)$
$+2$

2 $(n_z - 1) + 2$

$(n_x - 4)$
$\cdot (n_z - 1)$
$+1$

$(n_x - 3)$
$\cdot (n_z - 1)$
$+1$

1 $(n_z - 1) + 1$

u_x

number of z mesh points

number of x mesh points

sample
part of
mesh
around
i^{th} point

$i - (n_z - 1) + 1$ $i + 1$ $i + (n_z - 1) + 1$

$i - (n_z - 1)$ i $i + (n_z - 1)$

$i - (n_z - 1) - 1$ $i - 1$ $i + (n_z - 1) - 1$
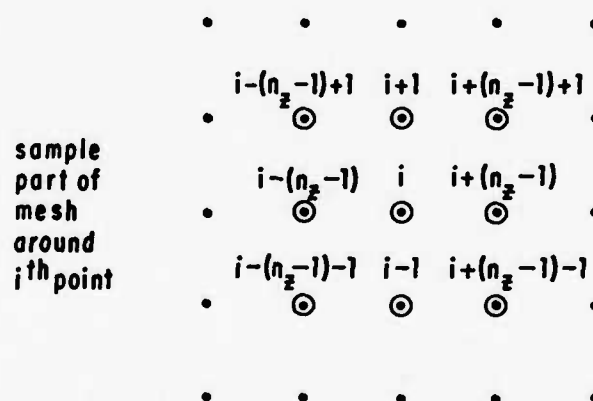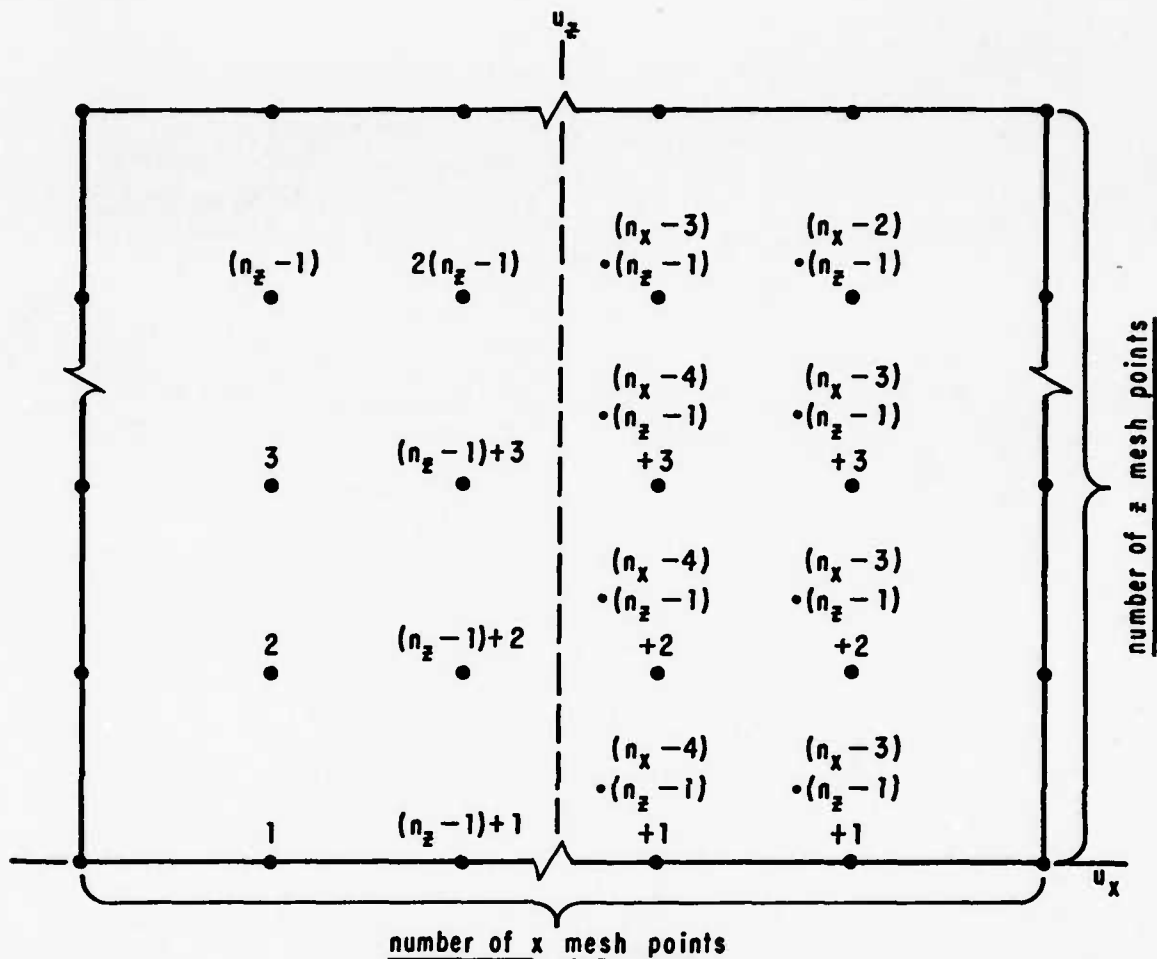
(ALL NINE POINTS ARE USED IN THE FINITE DIFFERENCE EQUATION FOR THE ith POINT)

Fig. F-2. Mesh Point Numbering Scheme in the Method of Lines.

vanish, and Eqn (F-18) becomes

$$\frac{\partial^2 f_{d0}}{\partial \mu_z^2}\bigg|_{bottom} = \frac{2 f_{i+1} - 2 f_i}{h_z^2} \tag{F-21}$$

The finite difference equation coefficients are always evaluated at the point of interest.

The equation for mesh point i from Eqns (F-5), (F-12) to (F-14), and (F-16) to (F-21) is

$$\frac{\partial f_{di}}{\partial t} = V_{dxz\,i}\, f_{d\,i-1-m_z} + VM_{dxi}\, f_{d\,i-m_z}$$

$$- V_{dxz\,i}\, f_{d\,i+1-m_z} + VM_{dzi}\, f_{d\,i-1} - V_{di}\, f_{di}$$

$$+ VP_{dzi}\, f_{d\,i+1} - V_{dxz\,i}\, f_{d\,i-1+m_z} + VP_{dxi}\, f_{d\,i+m_z}$$

$$+ V_{dxz\,i}\, f_{d\,i+1+m_z} \tag{F-22}$$

or $\dfrac{\partial f_{di}}{\partial t}\bigg|_{bottom} = VM_{dxi}\, f_{d\,i-m_z} - V_{di}\, f_{di} + V_{dzi}\, f_{d\,i+1} + VP_{dxi}\, f_{d\,i+m_z}$ (F-23)

where $VP_{dxi} = \left\{ \dfrac{1}{h_x^2} D_{xx} \dfrac{(1-\mu_x^2)^3}{\nu_{xo}^2} \right\} + \left\{ \dfrac{1}{2h_x} \left[G_{xxxz} \dfrac{(1-\mu_x^2)^{3/2}}{\nu_{xo}} - D_{xx} \dfrac{3\mu_x(1-\mu_x^2)^2}{\nu_{xo}^2} \right] \right\}$ (F-24)

$$VM_{dxi} = \Big\{\ same\ \Big\} - \Big\{\ same\ \Big\} \tag{F-25}$$

$$VP_{dzi} = \left\{ \dfrac{1}{h_z^2} D_{zz} \dfrac{(1-\mu_z^2)^3}{\nu_{zo}^2} \right\} + \left\{ \dfrac{1}{2h_z} \left[G_{zzzz} \dfrac{(1-\mu_z^2)^{3/2}}{\nu_{zo}} - D_{zz} \dfrac{3\mu_z(1-\mu_z^2)^2}{\nu_{zo}^2} \right] \right\} \tag{F-26}$$

$$VM_{dzi} = \Big\{\ same\ \Big\} - \Big\{\ same\ \Big\} \tag{F-27}$$

$$V_{dxzi} = \frac{1}{4h_x h_z}\, 2 D_{xz}\, \frac{\left[(1-\mu_x^2)(1-\mu_z^2) \right]^{3/2}}{\nu_{xo}\, \nu_{zo}} \tag{F-28}$$

126

$$V_{\alpha i} = \frac{2}{h_x^2} D_{xx} \frac{(1-\mu_x^2)^3}{N_{x_0}^2} + \frac{2}{h_z^2} D_{zz} \frac{(1-\mu_z^2)^3}{N_{z_0}^2} \qquad (F\text{-}29)$$

$$V_{\alpha z i} = \frac{2}{h_z^2} D_{zz} \frac{(1-\mu_z^2)^3}{N_{z_0}^2} \qquad (F\text{-}30)$$

The set of simultaneous ordinary differential equations each given by Eqn (F-22) or (F-23) is the set which is solved by the GEARB package using backward difference formulas. The set is stiff because the coefficients contain the exponentially growing spectral energies of the wave modes and because the method of lines usually results in a stiff set of equations (Ref 23). The set is of the form:

$$\dot{\overrightarrow{FJ}} = \overset{\Leftrightarrow}{J} \, \overrightarrow{FJ} \qquad (F\text{-}31)$$

where

$$\dot{\overrightarrow{FJ}} = \begin{bmatrix} \dfrac{\partial f_{\alpha 1}}{\partial t} \\[4pt] \dfrac{\partial f_{\alpha 2}}{\partial t} \\[4pt] \vdots \\[4pt] \dfrac{\partial f_{\alpha NJ}}{\partial t} \end{bmatrix} \qquad (F\text{-}32)$$

$$\overrightarrow{FJ} = \begin{bmatrix} f_{\alpha 1} \\ f_{\alpha 2} \\ \vdots \\ f_{\alpha NJ} \end{bmatrix} \qquad (F\text{-}33)$$

The system matrix and Jacobian, $\overset{\Leftrightarrow}{J}$, are the same and are defined as

$$J_{ij} = \frac{\partial FJ^i}{\partial FJ_j} \qquad (F\text{-}34)$$

The matrix and Jacobian have the banded structure shown in Fig. F-3. This banded structure is exploited in the GEARB routines to save computer storage and to increase computational speed. The total number of equations, NJ, is

127
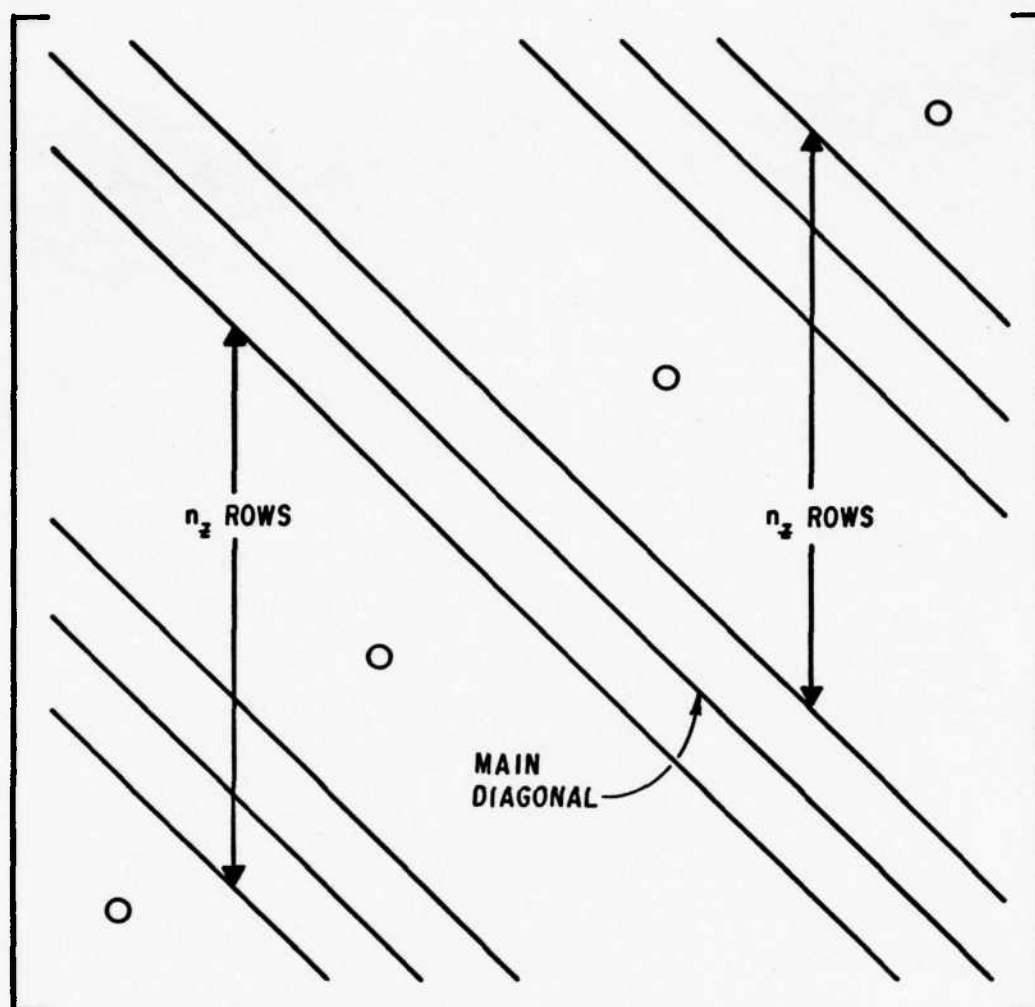
Fig. F-3. Banded System Matrix and Jacobian of the Ordinary
Differential Equation Set.

$$NJ = (n_x - 2)(n_z - 1) \tag{F-35}$$

and the total bandwidth of the Jacobian, MW, is

$$MW = 2n_z + 1 \tag{F-36}$$

The lines in the method of lines are taken in the vertical direction
because normally $n_z < n_x$ so the bandwidth is minimized.

The Jacobian elements contain the diffusion coefficients, Eqns
(F-6) to (F-10), which are integrals over the entire k_x-k_z plane. These

128

integrals are done numerically using a wave $\vec{k}$ grid determined during the solutions of the dispersion relation for the initial plasma distribution. At that time, the location of the grid in the first quadrant of the $\vec{k}$ plane is determined by locating the area of suitable unstable growing wave modes. The boundaries of the grid are constrained so that

$$0 < k_x < \infty \tag{F-37}$$

$$0 \leq k_z < \infty \tag{F-38}$$

The k_z axis must be avoided because the dispersion relation used is singular there. The grid is chosen to be as small as possible so only the significant wave modes are considered.

The first quadrant grid is sufficient to do all of the integrals. The waves propagating in other directions, and thereby, having wave k's in the other quadrants are incorporated into the integrals by the use of these two symmetries of the diffusion coefficient integrands: (1) The integrands are symmetric with respect to inversion in $\vec{k}$, and (2) the integrand in the fourth quadrant is that in the first with the signs of the k_z terms reversed. These symmetries are rigorously true for unmagnetized ions and electrons. They also hold approximately when the electrons are magnetized. The symmetries result from the physical equivalence of waves propagating in the θ, $-\theta$, $\theta + \pi$, and $-\theta + \pi$ directions. Thus,

$$\omega_r(k_x, k_z, t) = \omega_r(k_x, -k_z, t) = -\omega_r(-k_x, k_z, t) = -\omega_r(-k_x, -k_z, t) \tag{F-39}$$

$$\omega_i(k_x, k_z, t) = \omega_i(k_x, -k_z, t) = \omega_i(-k_x, k_z, t) = \omega_i(-k_x, -k_z, t) \tag{F-40}$$

$$E(k_x, k_z, t) = E(k_x, -k_z, t) = E(-k_x, k_z, t) = E(-k_x, -k_z, t) \tag{F-41}$$

129

$$\mathcal{E}_\alpha(k_x, k_z, t) = \mathcal{E}_\alpha(k_x, -k_z, t) = \mathcal{E}_\alpha^*(-k_x, k_z, t) = \mathcal{E}_\alpha^*(-k_x, -k_z, t) \quad \text{(F-42)}$$

where the symmetry of the species distributions about the v_x axis and Eqn (A-26) have been used. These symmetries are also used in the conversion of the dispersion relation into its numerical form.

Because the frequencies and growth rates are assumed to be constant during each phase of the evolution, the only time variation in the diffusion coefficients during a given phase is through the spectral energy, $\mathcal{E}(\vec{k}, t)$. Equation (11) can then be easily integrated to give:

$$\mathcal{E}(\vec{k}, t) = \mathcal{E}(\vec{k}, t = t_0) \, e^{2\omega_i(\vec{k}, t_0)(t - t_0)} \quad \text{(F-43)}$$

where t_0 is the beginning time of the current phase of the evolution and $\mathcal{E}(\vec{k}, t = t_0)$ is the spectral energy accumulated from the previous phases. This result is inserted directly into the diffusion coefficient integrands.

An initial thermal spectral wave energy, $\mathcal{E}(\vec{k}, t = 0)$, is used to begin an evolution. This energy is assumed to be constant over the $\vec{k}$ grid and equal to the plasma thermal energy divided by the available volume in space for electric fields, the Debye sphere. (A point charge is unshielded by the rest of the plasma inside the Debye sphere, and hence, random electric fields can exist only within that volume.) Therefore,

$$\iint_{-\infty}^{\infty} d\vec{k} \, \mathcal{E}(\vec{k}, t = 0) \sim \frac{\frac{3}{2} \times T_{\alpha \, max}}{\frac{4}{3} \pi \lambda_{D\alpha \, max}^3} = \frac{9 \times T_{\alpha \, max}}{8 \pi \lambda_{D\alpha \, max}^3} \quad \left(\frac{ergs}{cm^7}\right) \quad \text{(F-44)}$$

$$\mathcal{E}(\vec{k}, t = 0) \sim \frac{1}{4} \frac{9 \times T_{\alpha \, max}}{8 \pi \lambda_{D\alpha \, max}^3} \frac{1}{\Delta k_{x \, grid} \Delta k_{z \, grid}} \left(\frac{ergs}{cm}\right) \quad \text{(F-45)}$$

where the Δk's are the lengths of the grid sides and the factor of one

quarter accounts for the energy in the other quadrants. The exact value of this small thermal wave energy is not important. In fact, it is usually increased a few orders of magnitude in the beginning of the evolution calculation to save computer time.

Two separate procedures are used to evaluate the dispersion relation dielectrics. The first is used only on the initial Maxwellian species distributions and is the faster of the two. In this procedure, the analytical form of the plasma dielectrics given by Eqn (20) or (32) is used. The plasma dispersion function is numerically computed. In the second procedure, the integrals in Eqn (9) are numerically evaluated for evolved non Maxwellian ion distributions. Note the analytical procedure can always be used for the electron dielectrics because the electrons are adiabatic.

The numerical integrals in the ion dielectrics are done assuming that $\omega_i(\vec{k},t) \neq 0$. The integral for species α, I_α, is

$$I_\alpha = \int\!\!\!\int_{-\infty}^{\infty} d\vec{v} \; \frac{(\vec{k} \cdot \frac{\partial f_{\alpha 0}}{\partial \vec{v}})(\omega_r(\vec{k},t) - \vec{k} \cdot \vec{v})}{(\omega_r(\vec{k},t) - \vec{k} \cdot \vec{v})^2 + \omega_i^2(\vec{k},t)}$$

$$- i \int\!\!\!\int_{-\infty}^{\infty} d\vec{v} \; \frac{(\vec{k} \cdot \frac{\partial f_{\alpha 0}}{\partial \vec{v}}) \, \omega_i(\vec{k},t)}{(\omega_r(\vec{k},t) - \vec{k} \cdot \vec{v})^2 + \omega_i^2(\vec{k},t)}$$

$$- 2\pi i \; \Theta(-\omega_i) \int_{-\infty}^{\infty} dv_z \left[\frac{\partial f_{\alpha 0}}{\partial v_x} + \frac{\partial f_{\alpha 0}}{\partial v_z} \tan\theta \right] \Bigg| \qquad \text{(F-46)}$$

$$v_x = \frac{\omega_r}{k\cos\theta} - v_z \tan\theta$$

where $\quad \Theta(g) = 1 \qquad g > 0$

$$\qquad\qquad\quad = 0 \qquad g < 0 \qquad\qquad\qquad\qquad \text{(F-47)}$$

The angle between $\vec{k}$ and the v_x axis is Θ. The last term of Eqn (F-46) is the analytic continuation for negative growth rates. It is derived using the residue of the integrand numerator in Eqn (9) at the singular-

131

ity assuming

$$\omega_i(\vec{h},t) << \omega_n(\vec{h},t) \tag{F-48}$$

The resulting residue integral, $I_{\alpha R}$, is

$$I_{\alpha R} = 2\pi i \iint_{-\infty}^{\infty} d\vec{v} \; \vec{h} \cdot \frac{\partial f_{do}}{d\vec{v}} \; \delta(\vec{h}\cdot\vec{v} - \omega_n(\vec{h},t)) \tag{F-49}$$

It reduces to the form in Eqn (F-46) after the coordinate rotation procedure in Appendix D is used. This rotation allows the delta function to be integrated in the v_x direction of the rotated frame of reference.

Equation (F-46) after the coordinate transforms, Eqns (F-1) and (F-2) are applied is

$$I_\alpha = \iint_{mesh} d\vec{u} \; \frac{\left\{ h_x \frac{v_{zo}}{(1-u_z^2)^{3/2}} \frac{\partial f_{do}}{\partial u_x} + h_z \frac{v_{xo}}{(1-u_x^2)^{3/2}} \frac{\partial f_{do}}{\partial u_z} \right\}}{\left\{ (\omega_n(\vec{h},t) - \vec{h}\cdot\vec{v}(\vec{u}))^2 + \omega_i^2(\vec{h},t) \right\}}$$

$$\cdot \; (\omega_n(\vec{h},t) - \vec{h}\cdot\vec{v}(\vec{u}))$$

$$- i \iint_{mesh} d\vec{u} \; \frac{\left\{ \begin{array}{c} same \end{array} \right\}}{\left\{ \begin{array}{c} same \end{array} \right\}} \cdot \omega_i(\vec{h},t) - 2\pi i \; \Theta(-\omega_i(\vec{h},t))$$

$$\cdot \int_0^1 du_z \left\{ \frac{v_{zo}}{v_{xo}} \left(\frac{1-u_x^2}{1-u_z^2}\right)^{3/2} \frac{\partial f_{do}}{\partial u_x} + \frac{\partial f_{do}}{\partial u_z} \tan\theta \right\} \Bigg|_{u_x = \frac{R}{(v_{xo}^2 + R^2)^{1/2}}}$$

$$+ \left\{ \begin{array}{l} \text{three similar terms with reversed signs in} \\ \partial f_{do}/\partial u_z \text{ and } v_z \end{array} \right\} \tag{F-50}$$

where $\quad R = \frac{\omega_n(\vec{h},t)}{h \cos\theta} \mp \frac{v_{zo} u_z}{\sqrt{1-u_z^2}} \tan\theta - V_{DA}$ $\qquad$ (F-51)

The first three terms on the right hand side of Eqn (F-50) correspond to the integrals over the upper half of the velocity plane, and the second three correspond to those over the lower half. The signs in

132

Eqn (F-51) refer respectively to the upper and lower half planes.

The numerical version of the ion dielectrics is, therefore,

$$\epsilon_\alpha = \frac{4\pi g_\alpha^2 e^2}{m_\alpha \hbar^2} I_\alpha \qquad \text{(F-52)}$$

with I_α given by Eqn (F-50). With this equation, the conversion of the quasilinear equations into forms suitable for numerical solution is complete.

Appendix G

The Solution Program

The quasilinear equations for the ion-ion instability in the form
of Eqns (F-6) to (F-10), (F-31) to (F-34), (F-43), and Eqn (9) with the
dielectrics from Eqn (20), (32), or (F-52) are solved by a set of
computer routines controlled by a master program, IONION. IONION sets
up the problem by reading in the initial distribution parameters and
initializing the variables needed by the solution routines. It then
controls the solution of the problem by calling the proper routines in
turn finally terminating when the solution is complete. The program is
also set up to handle magnetic-field-free electron-ion instabilities such
as the ion acoustic instability, but this feature has never been tested.

The unmagnetized versus the magnetized approach is selected by
setting the input magnetic field to zero or not. Once this selection is
made, the program automatically uses the proper form of the electron
dielectric.

A block diagram of the entire program showing the routines called
by IONION in the order they are called is in Fig. G-1. The figure shows
all of the routines or groups of routines used in the solution. Each of
these routines is discussed below in the order in which it is first
called. The discussions include brief explanations on what the routines
do and how they work.

The first routine called is PLASMA. This routine sets the reference
frame and calculates the fundamental plasma parameters needed throughout
the rest of the program. The reference frame is that shown in Fig. 6.

The next routine is GRIDLOC which locates the region in the first
quadrant of the k_x-k_z plane where significant wave growth occurs. It

134
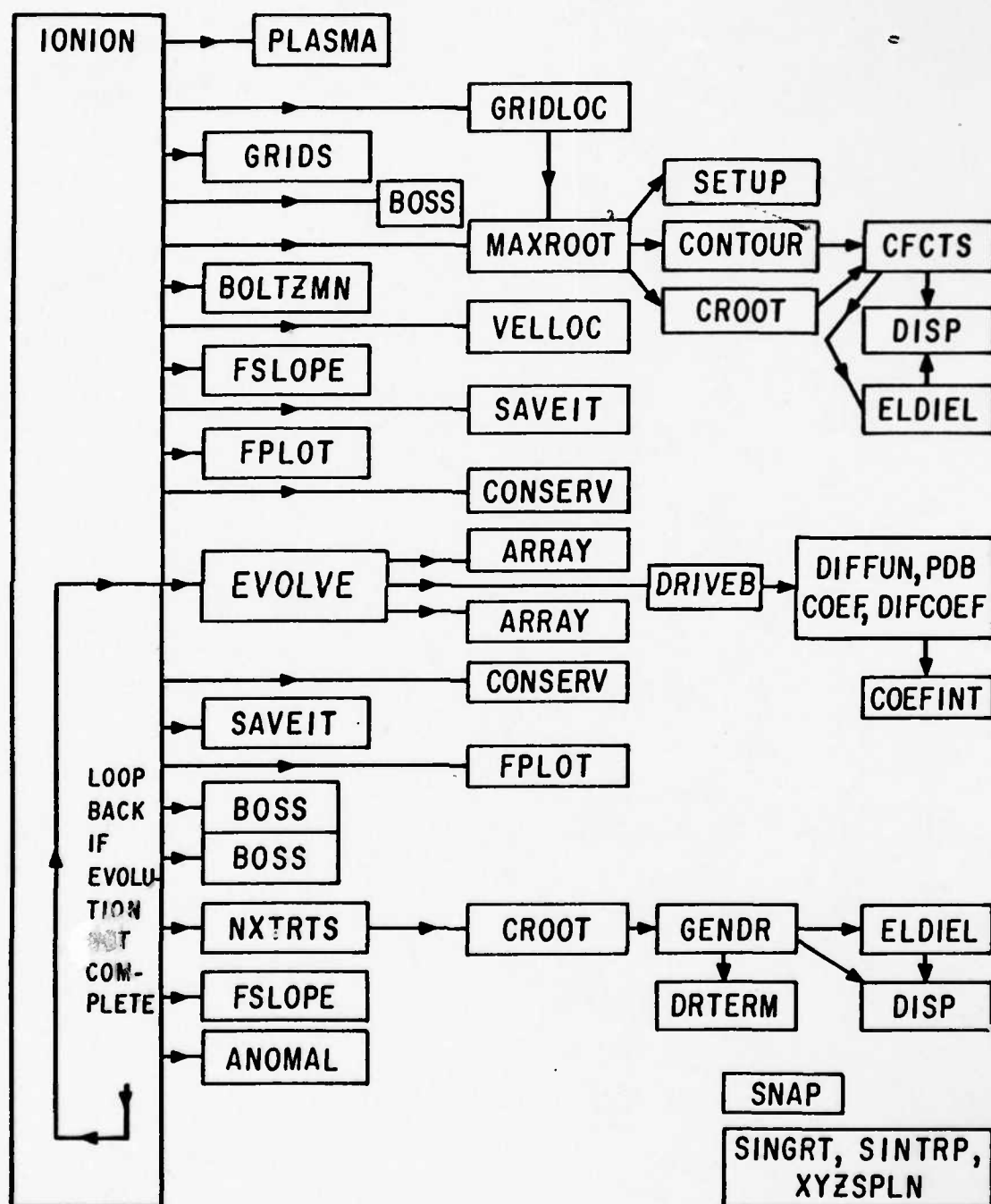
Fig. G-1. Block Diagram of the Computer Program.

attempts to locate in k_x, k_z, and in the radial direction as precisely as possible the exact boundaries of the significant growth region.

GRIDLOC calls MAXROOT which controls the linear dispersion relation solution for each trial k_x and k_z from GRIDLOC. Of the wave modes found, MAXROOT saves the one with the largest growth rate. Usually, the input parameters are adjusted so that the root finding routines look only for growing modes.

The routine SETUP is called by MAXROOT to convert parameters such as wave $\vec{k}$ and Debye length from rectangular to polar form. This form is needed by the dispersion relation routines called by the root finders.

The next set of routines, CONTOUR, SEEK, and ANGLER, called by MAXROOT locates the dispersion relation roots by searching over a large area of the complex frequency plane. The set, developed by Giri and Baum (Ref 24), divides up the plane into a series of boxes, does a contour integration around each box, and then uses an extension of the Cauchy residue theorem to locate the roots in each box.

MAXROOT then calls CROOT which uses a second order Newton-Raphson iteration scheme to improve on the roots located by the CONTOUR set. CROOT needs reasonably accurate initial guesses so it cannot be used alone. CROOT is also called later in the program to periodically update the wave modes of the evolved distributions. In this capacity, it uses the previously calculated modes as initial guesses.

The root finding routines call CFCTS which is the analytical dispersion relation. CFCTS uses the analytical form of the ion and electron dielectrics given by Eqns (20) and (32). Therefore, CFCTS can only be used in the location of the roots of the initial Maxwellian distributions.

CFCTS calls the set of routines DISP, DISPPR, DISPA, DISPI, DISPF,

136

DISPS, GQINTM, and ERF which evaluates the plasma dispersion function. This is the function tabulated by Fried and Conte.

If the magnetized approach has been selected, CFCTS calls ELDIEL which computes the magnetized version of the electron dielectric, Eqn (20). ELDIEL also calls the DISP package.

When GRIDLOC is finished having determined the boundaries of the $\vec{k}$ plane grid, control returns to the main program, IONION. IONION then calls the routine GRIDS which calculates the $\vec{k}$ plane grid for the diffusion coefficient integrals and the velocity mesh for the species distributions. All three distributions use the same velocity mesh, and their corresponding transformations are described in Appendix F. Thus, the same mesh point refers to three different velocities depending on which distribution is being referenced. The $\vec{k}$ grid and velocity mesh are uniform and held fixed throughout the rest of the program.

BOSS is the next routine called. This routine times an activity and is called once when entering the activity and again when leaving it. The routine determines the amount computer time remaining when entering the activity and terminates the program execution if the activity is expected to take too long. For this determination, BOSS keeps a running average of the time the activity takes. In IONION, the activity timed is one phase of the evolution.

Next, MAXROOT is called directly from IONION for each wave $\vec{k}$ on the grid. The fastest growing mode for each $\vec{k}$ is saved for the evolution calculation. If no suitable mode is found at a given $\vec{k}$, a dummy root with

$$\omega_\sim = \omega_{po} \tag{G-1}$$

$$\omega_i = 0 \tag{G-2}$$

137

is substituted. The dummy roots zero the values of the diffusion coeffi-
cient integrands at their corresponding locations on the $\vec{k}$ grid. Hence,
only significantly growing modes will build up in energy and cause diffu-
sion of particles. This part of the program completes the linear insta-
bility problem solution.

The next routine called is BOLTZMN which places the initial Maxwell-
Boltzman species distributions in their arrays. Each value of a distri-
bution in its array corresponds to a particular velocity mesh point.

VELLOC is called next to locate the evolution control velocity mesh
point. This point is two thermal widths from the initial maximum of the
air distribution and is at the same angle to the negative v_x axis as the
propagation angle of the initially fastest growing wave mode. The dis-
tribution slope at this point, which lies in the upper resonant region
shown in Fig. 4, is used to control the evolution. The less dense air
distribution is used because it evolves faster. FSLOPE is then called
to compute $\frac{\partial f_{Ao}}{\partial v_z}$ or $\frac{\partial f_{Ao}}{\partial v_x}$ depending on whether the propagation angle is
greater than 45 degrees or not. The change in the distribution slope is
a good measure of the change in the growth rate of the fastest growing
mode. The slope computed at this time is periodically compared with the
slope during the evolution of the air distribution. When the slope
change becomes too large, the air evolution is stopped so the debris
evolution can be brought up to date and the wave modes can be updated.

The restart file routines SAVEIT, ALTER, and EXTEND are called next.
The program can be restarted after the linear solution or after any
phase of the evolution using the information on the restart file. The
plotting routine, FPLOT, is also called at this time. This routine calls
several plotting routines in the AFWL computer system library, METALIB.

138

The resulting plots are three-dimensional perspective views of the plasma distributions.

CONSERV is called next. This routine checks for conservation of matter, momentum, and energy. It also calculates the individual velocity moments of the distributions. It is called in each phase of the evolution to check on the progress of the program.

The next routine, EVOLVE, controls the solutions of the species diffusion equations. These solutions are the time evolutions of the species distributions. EVOLVE first calls ARRAY for the air distribution to convert its two-dimensional format into the one-dimensional format needed by the method of lines. It then calls up the GEARB package by calling DRIVEB and controls the progress of the air evolution by periodic calls to FSLOPE. When the current phase of the air evolution is finished, ARRAY is called again to put it back into its original two-dimensional format. Then, the debris distribution is evolved in a similar manner up to the same ending time as the air by successive calls to ARRAY, DRIVEB, and ARRAY. This step completes a phase of the evolution.

The GEARB package consists of the routines DRIVEB, INTERP, STIFFB, COSET, PSETB, DECBR, and SOLBR. These routines solve the ordinary differential equation set derived in Appendix F. These routines in turn call the set of routines DIFFUN, PDB, COEF, DIFCOEF, and COEFINT which define the equation, the coefficients, and the Jacobian. The integrands for the diffusion coefficients are constructed in DIFCOEF, and the integrations are done by COEFINT. COEFINT is designed to run extremely rapidly because millions of diffusion coefficient integrals must be done in a typical evolution.

When a phase of the evolution is complete; CONSERV, SAVEIT, FPLOT,

139

and BOSS are called to check, save, and output the results. BOSS is called again to start timing the next phase.

The phase begins by the recalculation of the wave modes using NXTRTS. Because the ion distributions are no longer Maxwellian, the numerical form of their dielectrics must be used. NXTRTS controls this updating by calls to CROOT which locates the new roots. CROOT calls the routine GENDR which is the dispersion relation. GENDR calls DRTERM which does the ion dielectric integrals, Eqn (F-50). The electron dielectric is computed by GENDR using the same procedures which are used by CFCTS.

FSLOPE is then called to update the slope of the air distribution. Finally, the anomalous transport coefficients are computed using ANOMAL. If significantly growing wave modes still exist and the transport coefficients are still increasing, the program loops back to the EVOLVE call to continue this phase of the evolution. Otherwise execution terminates as the program is finished.

Two groups of utility routines are called throughout the program. The first group is the SNAP set which outputs the value of a variable at the time the call to SNAP is made. This set is a very useful diagnostic aid. The other group is SINGRT, SINTRP, and XYZSPLN. These routines fit a smooth cubic polynomial surface to a function defined by values in an array. The routines then integrate, differentiate, or interpolate on that surface. All of the program numerical integrations except those for the diffusion coefficients are done in this manner.

Appendix H

Tables of the Dissertation Plasma Distributions

Below are tabulated all of the plasma distributions used in the dissertation. The parameters listed in the tables are as follows:

n - number density

q - units of charge

AMU - atomic mass units (atomic weight)

V - velocity (in the computer reference frame shown in Fig. 6)

T_x - temperature in the x direction

T_z - temperature in the z direction

λ_{Dx} - Debye length in the x direction

λ_{Dz} - Debye length in the z direction

ω_p - plasma frequency

Ω - gyro frequency

ω_{LH} - lower hybrid frequency

ρ_L - Larmor radius (gyro radius)

v_{ac} - ion acoustic speed

v_{alf} - Alfvén speed

c_x - thermal speed in the x direction

c_z - thermal speed in the z direction

V_R - relative velocity between the debris and air

B - magnetic field

β_e - electron beta

A given distribution is uniquely determined by the selection of densities, charges, atomic weights, and temperatures for the debris and air; by the selection of the electron temperatures; and by the selection of the relative velocity and magnetic field strength. The remaining para-

141

meters are computed assuming charge neutrality, zero current, and the individual debris, air, and electron distributions are Maxwellian.

The air densities and air atomic weight in the last four tables, Tables H-VI to H-IX, are representative of an assumed predominately atomic oxygen atmosphere of the earth existing at 200 and 600 km. The debris atomic weight in these four tables is that of aluminum which conveniently represents an average of all the materials in the debris of a high altitude nuclear explosion. The remaining parameters which uniquely determine these simulation distributions are chosen to approximate the conditions which could be found in the debris-air mixing region shown in Fig. 1.

Table H-I

Equal and Opposite Cold Beam Distribution

	n (cm^{-3})	q (units)	AMU (AMU)	V (cm/sec)
Debris	5.1(10^{10})	1	20	-9.9(10^6)
Air	5.0(10^{10})	1	20	1.0(10^7)
Electron	1.0(10^{11})	-	-	0
	T_x (eV)	T_z (eV)	λ_{Dx} (cm)	λ_{Dz} (cm)
Debris	1	1	3.3(10^{-3})	3.3(10^{-3})
Air	1	1	3.3(10^{-3})	3.3(10^{-3})
Electron	2.8(10^4)	2.8(10^4)	3.9(10^{-1})	3.9(10^{-1})
	ω_p (sec^{-1})	Ω (sec^{-1})	ω_{LH} (sec^{-1})	ρ_L (cm)
Debris	6.7(10^7)	0	0	∞
Air	6.6(10^7)	0	0	∞
Electron	1.8(10^{10})	0	-	∞
	v_{ac} (cm/sec)	v_{alf} (cm/sec)	c_x (cm/sec)	c_z (cm/sec)
Debris	2.6(10^7)	0	2.2(10^5)	2.2(10^5)
Air	2.6(10^7)	0	2.2(10^5)	2.2(10^5)
Electron	-	-	7.0(10^9)	7.0(10^9)

V_R (cm/sec) = 2.0(10^7)

B (guass) = 0

β_e = ∞

Table H-II

Bump-on-the-Tail Distribution

	n (cm^{-3})	q (units)	AMU (AMU)	V (cm/sec)
Debris	$1.0(10^{11})$	1	20	$-5.0(10^5)$
Air	$1.0(10^9)$	1	20	$5.0(10^7)$
Electron	$1.0(10^{11})$	-	-	0

	T_x (eV)	T_z (eV)	λ_{Dx} (cm)	λ_{Dz} (cm)
Debris	10^3	10^3	$7.4(10^{-2})$	$7.4(10^{-2})$
Air	10^2	10^2	$2.4(10^{-1})$	$2.4(10^{-1})$
Electron	$2.8(10^4)$	$2.8(10^4)$	$3.9(10^{-1})$	$3.9(10^{-1})$

	ω_p (sec^{-1})	Ω (sec^{-1})	ω_{LH} (sec^{-1})	ρ_L (cm)
Debris	$9.3(10^7)$	0	0	∞
Air	$9.3(10^6)$	0	0	∞
Electron	$1.8(10^{10})$	0	-	∞

	v_{ac} (cm/sec)	v_{alf} (cm/sec)	c_x (cm/sec)	c_z (cm/sec)
Debris	$3.9(10^7)$	0	$6.9(10^6)$	$6.9(10^6)$
Air	$5.3(10^6)$	0	$2.2(10^6)$	$2.2(10^6)$
Electron	-	-	$7.0(10^9)$	$7.0(10^9)$

V_R (cm/sec) = $5.0(10^7)$

B (guass) = 0

β_e = ∞

Table H-III

Magnetized Equal Beam Distribution

	n (cm^{-3})	q (units)	AMU (AMU)	V (cm/sec)
Debris	$5.1(10^{10})$	1	20	$-9.9(10^6)$
Air	$5.0(10^{10})$	1	20	$1.0(10^7)$
Electron	$1.0(10^{11})$	-	-	0

	T_x (eV)	T_z (eV)	λ_{Dx} (cm)	λ_{Dz} (cm)
Debris	1	1	$3.3(10^{-3})$	$3.3(10^{-3})$
Air	1	1	$3.3(10^{-3})$	$3.3(10^{-3})$
Electron	10^{-2}	10^{-2}	$2.3(10^{-4})$	$2.3(10^{-4})$

	ω_p (sec^{-1})	Ω (sec^{-1})	ω_{LH} (sec^{-1})	ρ_L (cm)
Debris	$6.7(10^7)$	$4.8(10^5)$	$4.7(10^7)$	$2.1(10^1)$
Air	$6.6(10^7)$	$4.8(10^5)$	$4.7(10^7)$	$2.1(10^1)$
Electron	$1.8(10^{10})$	$1.8(10^{10})$	-	$3.4(10^{-4})$

	v_{ac} (cm/sec)	v_{alf} (cm/sec)	c_x (cm/sec)	c_z (cm/sec)
Debris	$3.8(10^5)$	$2.2(10^8)$	$2.2(10^5)$	$2.2(10^5)$
Air	$3.8(10^5)$	$2.2(10^8)$	$2.2(10^5)$	$2.2(10^5)$
Electron	-	-	$4.2(10^6)$	$4.2(10^6)$

V_R (cm/sec) $\approx 2.0(10^7)$

B (guass) $\approx 1.0(10^3)$

$\rho_e \approx 4.1(10^{-8})$

Table H-IV

Initial Bump-on-the-Tail Distribution for the Test Evolution

	n	q	AMU	V
	(cm^{-3})	(units)	(AMU)	(cm/sec)
Debris	$1.0(10^{1 \cdots})$	1	20	$-3.0(10^5)$
Air	$1.0(10^9)$	1	20	$3.0(10^7)$
Electron	$1.0(10^{11})$	-	-	0

	T_x	T_z	λ_{Dx}	λ_{Dz}
	(eV)	(eV)	(cm)	(cm)
Debris	10^3	10^3	$7.4(10^{-2})$	$7.4(10^{-2})$
Air	10^2	10^2	$2.4(10^{-1})$	$2.4(10^{-1})$
Electron	$2.8(10^4)$	$2.8(10^4)$	$3.9(10^{-1})$	$3.9(10^{-1})$

	ω_p	Ω	ω_{LH}	ρ_L
	(sec^{-1})	(sec^{-1})	(sec^{-1})	(cm)
Debris	$9.3(10^7)$	0	0	∞
Air	$9.3(10^6)$	0	0	∞
Electron	$1.8(10^{10})$	0	-	∞

	v_{ac}	v_{alf}	c_x	c_z
	(cm/sec)	(cm/sec)	(cm/sec)	(cm/sec)
Debris	$3.9(10^7)$	0	$6.9(10^6)$	$6.9(10^6)$
Air	$5.3(10^6)$	0	$2.2(10^6)$	$2.2(10^6)$
Electron	-	-	$7.0(10^9)$	$7.0(10^9)$

V_R (cm/sec) = $3.0(10^7)$

B (guass) = 0

β_e = ∞

146

Table H-V

Large Relative Velocity Bump-on-the-Tail Distribution

	n (cm^{-3})	q (units)	AMU (AMU)	V (cm/sec)
Debris	$1.0(10^{11})$	1	20	$-9.9(10^5)$
Air	$1.0(10^9)$	1	20	$9.9(10^7)$
Electron	$1.1(10^{11})$	-	-	0

	T_x (eV)	T_z (eV)	λ_{Dx} (cm)	λ_{Dz} (cm)
Debris	10^3	10^3	$7.4(10^{-2})$	$7.4(10^{-2})$
Air	10^2	10^2	$2.4(10^{-1})$	$2.4(10^{-1})$
Electron	$2.8(10^4)$	$2.8(10^4)$	$3.9(10^{-1})$	$3.9(10^{-1})$

	ω_p (sec^{-1})	Ω (sec^{-1})	ω_{LH} (sec^{-1})	ρ_L (cm)
Debris	$9.3(10^7)$	0	0	∞
Air	$9.3(10^6)$	0	0	∞
Electron	$1.8(10^{10})$	0	-	∞

	v_{ac} (cm/sec)	v_{alf} (cm/sec)	c_x (cm/sec)	c_z (cm/sec)
Debris	$3.9(10^7)$	0	$6.9(10^6)$	$6.9(10^6)$
Air	$5.3(10^6)$	0	$2.2(10^6)$	$2.2(10^6)$
Electron	-	-	$7.0(10^9)$	$7.0(10^9)$

V_R (cm/sec) = $1.0(10^8)$

B (guass) = 0

β_e = ∞

Table H-VI

Low Relative Velocity Distribution Simulating 200 km

	n	q	AMU	V
	(cm^{-3})	(units)	(AMU)	(cm/sec)
Debris	$2.0(10^{10})$	1	27	$-6.7(10^6)$
Air	$1.0(10^{10})$	1	16	$1.3(10^7)$
Electron	$3.0(10^{10})$	-	-	0
	T_x	T_z	λ_{Dx}	λ_{Dz}
	(eV)	(eV)	(cm)	(cm)
Debris	$5.0(10^2)$	$5.0(10^2)$	$1.2(10^{-1})$	$1.2(10^{-1})$
Air	$5.0(10^2)$	$5.0(10^2)$	$1.7(10^{-1})$	$1.7(10^{-1})$
Electron	$1.0(10^4)$	$1.0(10^4)$	$4.3(10^{-1})$	$4.3(10^{-1})$
	ω_p	Ω	ω_{LH}	ρ_L
	(sec^{-1})	(sec^{-1})	(sec^{-1})	(cm)
Debris	$3.6(10^7)$	0	0	∞
Air	$3.3(10^7)$	0	0	∞
Electron	$9.8(10^9)$	0	-	∞
	v_{ac}	v_{alf}	c_x	c_z
	(cm/sec)	(cm/sec)	(cm/sec)	(cm/sec)
Debris	$1.7(10^7)$	0	$4.2(10^6)$	$4.2(10^6)$
Air	$1.7(10^7)$	0	$5.5(10^6)$	$5.5(10^6)$
Electron	-	-	$4.2(10^9)$	$4.2(10^9)$

V_R (cm/sec) = $2.0(10^7)$

B (guass) = 0

β_e = ∞

Table H-VII

High Relative Velocity Distribution Simulating 200 km

	n (cm^{-3})	q (units)	AMU (AMU)	V (cm/sec)
Debris	$2.0(10^{10})$	1	27	$-2.3(10^7)$
Air	$1.0(10^{10})$	1	16	$4.7(10^7)$
Electron	$3.0(10^{10})$	-	-	0

	T_x (eV)	T_z (eV)	λ_{Dx} (cm)	λ_{Dz} (cm)
Debris	$1.0(10^3)$	$1.0(10^3)$	$1.7(10^{-1})$	$1.7(10^{-1})$
Air	$1.0(10^3)$	$1.0(10^3)$	$2.4(10^{-1})$	$2.4(10^{-1})$
Electron	$1.0(10^4)$	$1.0(10^4)$	$4.3(10^{-1})$	$4.3(10^{-1})$

	ω_p (sec^{-1})	Ω (sec^{-1})	ω_{LH} (sec^{-1})	ρ_L (cm)
Debris	$3.6(10^7)$	0	0	∞
Air	$3.3(10^7)$	0	0	∞
Electron	$9.8(10^9)$	0	-	∞

	v_{ac} (cm/sec)	v_{alf} (cm/sec)	c_x (cm/sec)	c_z (cm/sec)
Debris	$1.9(10^7)$	0	$6.0(10^6)$	$6.0(10^6)$
Air	$2.0(10^7)$	0	$7.8(10^6)$	$7.8(10^6)$
Electron	-	-	$4.2(10^9)$	$4.2(10^9)$

V_R (cm/sec) = $7.0(10^7)$

B (guass) = 0

β_e = ∞

149

Table H-VIII

Low Relative Velocity Distribution Simulating 600 km

	n (cm^{-3})	q (units)	AMU (AMU)	V (cm/sec)
Debris	$2.0(10^7)$	1	27	$-6.7(10^6)$
Air	$1.0(10^7)$	1	16	$1.3(10^7)$
Electron	$3.0(10^7)$	-	-	0
	T_x (eV)	T_z (eV)	λ_{Dx} (cm)	λ_{Dz} (cm)
Debris	$5.0(10^2)$	$5.0(10^2)$	3.7	3.7
Air	$5.0(10^2)$	$5.0(10^2)$	5.3	5.3
Electron	$1.0(10^3)$	$1.0(10^4)$	4.3	$1.4(10^1)$
	ω_p (sec^{-1})	Ω (sec^{-1})	ω_{LH} (sec^{-1})	ρ_L (cm)
Debris	$1.1(10^6)$	$1.8(10^4)$	$1.1(10^6)$	$3.7(10^2)$
Air	$1.0(10^6)$	$3.0(10^4)$	$9.9(10^5)$	$4.4(10^2)$
Electron	$3.1(10^8)$	$8.8(10^8)$	-	2.1
	v_{ac} (cm/sec)	v_{alf} (cm/sec)	c_x (cm/sec)	c_z (cm/sec)
Debris	$1.4(10^7)$	$4.7(10^8)$	$4.2(10^6)$	$4.2(10^6)$
Air	$1.4(10^7)$	$8.7(10^8)$	$5.5(10^6)$	$5.5(10^6)$
Electron	-	-	$1.3(10^9)$	$4.2(10^9)$

V_R (cm/sec) $= 2.0(10^7)$

B (guass) $= 5.0(10^1)$

β_e $\quad = 4.8(10^{-4})$

Table H-IX

High Relative Velocity Distribution Simulating 600 km

	n (cm^{-3})	q (units)	AMU (AMU)	V (cm/sec)
Debris	$2.0(10^7)$	1	27	$-2.3(10^7)$
Air	$1.0(10^7)$	1	16	$4.7(10^7)$
Electron	$3.0(10^7)$	-	-	0

	T_x (eV)	T_z (eV)	λ_{Dx} (cm)	λ_{Dz} (cm)
Debris	$1.0(10^3)$	$1.0(10^3)$	5.3	5.3
Air	$1.0(10^3)$	$1.0(10^3)$	7.4	7.4
Electron	$1.0(10^3)$	$1.0(10^4)$	4.3	$1.4(10^1)$

	ω_p (sec^{-1})	Ω (sec^{-1})	ω_{LH} (sec^{-1})	ρ_L (cm)
Debris	$1.1(10^6)$	$1.8(10^4)$	$1.1(10^6)$	$1.3(10^3)$
Air	$1.0(10^6)$	$3.0(10^4)$	$9.9(10^5)$	$1.5(10^3)$
Electron	$3.1(10^8)$	$8.8(10^8)$	-	2.1

	v_{ac} (cm/sec)	v_{alf} (cm/sec)	c_x (cm/sec)	c_z (cm/sec)
Debris	$1.5(10^7)$	$4.7(10^8)$	$6.0(10^6)$	$6.0(10^6)$
Air	$1.7(10^7)$	$8.7(10^8)$	$7.8(10^6)$	$7.8(10^6)$
Electron	-	-	$1.3(10^9)$	$4.2(10^9)$

V_R (cm/sec) = $7.0(10^7)$

B (guass) = $5.0(10^1)$

β_e = $4.8(10^{-4})$

Appendix I

Evolution of the Bump-on-the-Tail Instability

The analytical quasilinear solution for the bump-on-the-tail
instability is done using a combined debris and air ion distribution.
The same procedures are used which are employed by Davidson (Ref 14: 174-
182) in his solution of the equivalent electron bump-on-the-tail problem.
For the test ion problem shown in Table H-IV, the electron temperature is
large enough so the electron dielectric which goes like $1/k^2 \lambda_{De}^2$ (See
Eqns (53), (57), and (58).) is less than one. Therefore, the electrons
can be ignored because their contribution to the dispersion relation,
and hence to the unstable waves causing the time evolution of the ion
distribution, is negligible.

The equations of interest for the ions are from Eqns (10), (11),
and (12):

$$\frac{\partial f_0(v,t)}{\partial t} = \frac{\partial}{\partial v}\left[D(v,t) \frac{\partial f_0(v,t)}{\partial v}\right] \tag{I-1}$$

$$\frac{\partial \mathcal{E}(k,t)}{\partial t} = 2\omega_i(k,t)\,\mathcal{E}(k,t) \tag{I-2}$$

$$D(v,t) = 8\pi \frac{q^2 e^2}{m^2}\int_k dk \frac{\mathcal{E}(k,t)\,\omega_i(k,t)}{[kv - \omega_r(k,t)]^2 + \omega_i^2(k,t)} \tag{I-3}$$

where the subscript α has been dropped and the equations are written in
a one-dimensional form.

The diffusion coefficient has two different approximate forms with-
in and outside the resonant region. In the resonant region,

$$kv - \omega_r(k,t) \approx 0 \tag{I-4}$$

so the corresponding coefficient is

$$D_r(v,t) = 8\pi^2 \frac{q^2 e^2}{m^2} \int_{-\infty}^{\infty} dk \, \mathcal{E}(k,t) \, \delta(kv - \omega_r(k,t)) \quad \text{(I-5)}$$

where Eqn (F-37), $\omega_i(k,t) \geq 0$, and

$$\lim_{\omega_i \to 0^+} \frac{\omega_i(k,t)}{[kv - \omega_r(k,t)]^2 + \omega_i^2(k,t)} = \pi \delta(kv - \omega_r(k,t)) \quad \text{(I-6)}$$

have been used. Outside the resonant region,

$$[kv - \omega_r(k,t)]^2 \gg \omega_i^2(k,t) \quad \text{(I-7)}$$

so the nonresonant form of the coefficient is

$$D_{nr}(v,t) = 8\pi \frac{q^2 e^2}{m^2} \int_{-\infty}^{\infty} dk \, \frac{\mathcal{E}(k,t)\,\omega_i(k,t)}{[kv - \omega_r(k,t)]^2} \quad \text{(I-8)}$$

The resonant form after the symmetries in Eqns (A-24) and (A-26) are applied is

$$D_r(v,t) = 16\pi^2 \frac{q^2 e^2}{m^2} \int_{0}^{\infty} dk \, \mathcal{E}(k,t) \, \delta(kv - \omega_r(k,t)) \quad \text{(I-9)}$$

This integration is done by assuming

$$\omega_r(k,t) \sim \omega_{pi} \sim \omega_{po} \quad \text{(I-10)}$$

so

$$D_r(v,t) = 16\pi^2 \frac{q^2 e^2}{m^2} \frac{1}{v} \left[\mathcal{E}(k,t) \right] \Big|_{k = \frac{\omega_{po}}{v}} \geq 0 \quad \text{(I-11)}$$

This diffusion coefficient is negligible outside the resonant region because the wave spectral energy does not grow above the background thermal levels.

The approximation in Eqn (I-10) is valid for long wavelength modes so all but the first term on the right hand side of

$$\omega_r(k,t) = \pm \omega_{pi} \left(1 + \frac{3}{2} k^2 \lambda_{Di} + \cdots \right) \quad \text{(I-12)}$$

can be ignored. This is the real part of the Bohm-Gross dispersion relation which is derived for electrons in Krall and Trivelpiece (Ref

19: 383-392). The corresponding imaginary part is

$$\omega_i(h,t) = \frac{\pi}{2}\,\omega_r\,\frac{\omega_{pi}^2}{h^2}\left[\frac{\partial f_o(v,t)}{\partial v}\right]\Bigg|_{v=\frac{\omega_r}{h}} \quad (I\text{-}13)$$

The long wavelength approximation is a good one for the test distribution as

$$h^2\lambda_{Di}^2 \sim 5(10^{-2}) << 1 \quad (I\text{-}14)$$

for the growing modes of interest.

The resonant form of Eqn (I-1) is

$$\frac{\partial f_o(v,t)}{\partial t} = \frac{\partial}{\partial v}\left[D_r(v,t)\,\frac{\partial f_o(v,t)}{\partial v}\right] \quad (I\text{-}15)$$

where D_r is given by Eqn (I-11). The time derivative of Eqn (I-11) combined with Eqns (I-2), (I-10), and (I-13) is

$$\frac{\partial D_r(v,t)}{\partial t} = \pi\,\omega_{po}\,v^2\left[D_r(v,t)\,\frac{\partial f_o(v,t)}{\partial v}\right] \quad (I\text{-}16)$$

where Eqn (I-11) has been used again to eliminate the spectral energy term. The integral of Eqn (I-16) is

$$D_r(v,t) = D_r(v,t=0)\,e^{\left[\pi\,\omega_{po}\,v^2\int_o^t dt'\,\frac{\partial f_o(v,t')}{\partial v}\right]} \quad (I\text{-}17)$$

When Eqns (I-15) and (I-16) are combined and integrated,

$$\frac{\partial f_o(v,t)}{\partial t} = \frac{\partial}{\partial v}\left[\frac{1}{\pi\,\omega_{po}v^2}\,\frac{\partial D_r(v,t)}{\partial t}\right] \quad (I\text{-}18)$$

$$f_o(v,t) = f_o(v,t=0) + \frac{\partial}{\partial v}\left[\frac{D_r(v,t)-D_r(v,t=0)}{\pi\,\omega_{po}\,v^2}\right] \quad (I\text{-}19)$$

Although Eqns (I-17) and (I-19) are the resonant solution, they still are not in a form suitable for a hand calculation. The best approach is to find the time asymptotic solution.

154

AFIT/DS/PH/78-1

The first step in the asymptotic solution is to multiply Eqn (I-15) by $f_0(v,t)$ and integrate with respect to v:

$$\int_{-\infty}^{\infty} dv\, f_0(v,t)\, \frac{\partial f_0(v,t)}{\partial t} = \int_{-\infty}^{\infty} dv\, f_0(v,t) \frac{\partial}{\partial v}\left[D_n(v,t)\, \frac{\partial f_0(v,t)}{\partial v}\right] \quad (I-20)$$

$$\frac{1}{2}\frac{d}{dt}\int_{-\infty}^{\infty} dv\left[f_0(v,t)\right]^2 = -\int_{-\infty}^{\infty} dv\, D_n(v,t)\left[\frac{\partial f_0(v,t)}{\partial v}\right]^2 \leqq 0 \quad (I-21)$$

The integrated part resulting from the right hand side of Eqn (I-20) vanishes because resonant diffusion is negligible outside the resonant region. Because the time rate of change of a positive quantity is negative for all time,

$$D_n(v, t\to\infty)\left[\frac{\partial f_0(v, t\to\infty)}{\partial v}\right] \stackrel{must}{=} 0 \quad (I-22)$$

Either or both terms can be zero. If

$$D_n(v, t\to\infty) = 0 \quad (I-23)$$

then from Eqn (I-17),

$$\frac{\partial f_0(v, t\to\infty)}{\partial v} < 0 \quad (I-24)$$

so the growth rate from Eqn (I-13) becomes negative. Equations (I-19) and (I-23) also imply

$$f_0(v, t\to\infty) = f_0(v, t=0) - \frac{\partial}{\partial v}\left[\frac{D_n(v, t=0)}{\pi\,\omega_{po}\,v^2}\right] \quad (I-25)$$

Because the particle energy is much larger than the initial wave energy, the initial diffusion should be small. Therefore, the second term can be neglected and

$$\frac{\partial f_0(v, t\to\infty)}{\partial v} = \frac{\partial f_0(v, t=0)}{\partial v} > 0 \quad (I-26)$$

Equations (I-24) and (I-26) contradict so Eqn (I-23) must be incorrect and

$$\frac{\partial f_0(v, t \to \infty)}{\partial v} = 0 \tag{I-27}$$

Thus, the asymptotic behavior of the distribution in the resonant region is to form a plateau with the wave growth rates going to zero.

The nonresonant diffusion coefficient, Eqn (I-8), is used to determine the behavior of the bulk of the distribution (the debris distribution). Because the phase velocities of the growing waves lie in the resonant velocity range which is much greater than the thermal velocity of the bulk distribution,

$$\left[\omega(k, t) - k v \right]^2 \sim \omega(k, t) \sim \omega_{p0} \sim \omega_p \tag{I-28}$$

Therefore, Equation (I-8) becomes

$$D_m(v, t) = 8\pi \frac{q^2 e^2}{m^2 \omega_p^2} \int_{-\infty}^{\infty} dk \, \mathcal{E}(k, t) \, \omega_i(k, t) \tag{I-29}$$

$$D_m(v, t) = \frac{1}{nm} \frac{\partial}{\partial t} \int_{-\infty}^{\infty} dk \, \mathcal{E}(k, t) \tag{I-30}$$

Note the coefficient is independent of velocity. The nonresonant form of Eqn (I-1) is then:

$$\frac{\partial f_0(v, t)}{\partial t} = D_m(t) \frac{\partial^2 f_0(v, t)}{\partial v^2} \tag{I-31}$$

When $T(t)$ is defined as

$$T(t) = \frac{2}{n} \int_{-\infty}^{\infty} dk \, \mathcal{E}(k, t) \tag{I-32}$$

Equation (I-31) becomes

$$\frac{\partial f_0(v, T)}{\partial T} = \frac{1}{2m} \frac{\partial^2 f_0(v, T)}{\partial v^2} \tag{I-33}$$

156

The Green's function solution of this equation with an initial Maxwellian distribution for the bulk plasma is

$$f_0(v, t) = \left\{ \frac{m}{2\pi [\chi T + T(t)]} \right\}^{1/2} e^{-\left\{ \frac{mv^2}{2[\chi T + T(t)]} \right\}} \quad (\text{I-34})$$

where T is the bulk ion temperature. Note that

$$T(t) >> T(0) \qquad \text{for} \quad t >> \omega_i^{-1} \quad (\text{I-35})$$

has been assumed. The nonresonant solution, Eqns (I-32) and (I-34), shows that the effective temperature of the bulk of the ions increases as the wave energy increases. This increase is due to bulk plasma oscillations induced by the electrostatic waves. A sketch of the final time asymptotic ion distribution showing both the resonant and non-resonant changes is included in Fig. 7.

The growth of the wave energies and the growth of the bulk plasma oscillations is fed by a loss in the energy of the resonant particles in the bump. In fact, (Ref 19: 527-532)

$$\begin{bmatrix} \text{change in} \\ \text{nonresonant} \\ \text{particle} \\ \text{energy} \end{bmatrix} = \begin{bmatrix} \text{change} \\ \text{in total} \\ \text{wave} \\ \text{energy} \end{bmatrix} = -\frac{1}{2} \times \begin{bmatrix} \text{change in} \\ \text{resonant} \\ \text{particle} \\ \text{energy} \end{bmatrix} \quad (\text{I-36})$$

Appendix J

Tables of the Linear Dispersion Relation Solutions

The linear dispersion relation solutions for growing wave modes
are tabulated for all of the distributions which are evolved. The
solutions are for Maxwellian debris, air, and electron distributions so
they are the wave modes which exist at the beginning of an evolution.
An additional dispersion relation solution table, Table J-V, is included
to show a possible mixture of modified two-stream and ion-ion modes.
This table is discussed in the section on magnetized evolutions in
Chapter IV.

In all of the tables, only the growing wave modes in the first
quadrant of the k_x-k_z plane where

$$0 < k_x < \infty \qquad \text{(J-1)}$$

$$0 \leq k_z < \infty \qquad \text{(J-2)}$$

are included. The modes propagating in the other quadrants of this
plane are related to those tabulated by the equations in Appendix F,
Eqns (F-39), (F-40), and (F-42).

In the tables below, the headings are the components of the wave $\vec{k}$
in the x and z directions; the real and imaginary parts of the wave
frequency; and the debris, air, and electron dielectrics evaluated at
the wave frequency. The dielectrics are complex so both the real and
imaginary parts are listed. The row marked with an asterisk is the wave
mode with the largest growth rate. This mode dominates the evolution.

Table J-1

Linear Solutions for the Bump-on-the-Tail Test Case

KX (1/CM)	KZ (1/CM)	FREQUENCY (1/SEC)		DDIELECTRIC		ADIELECTRIC		EDIELECTRIC	
6.5E-01	0.	1.9E+07	1.4E+06	3.0E+01	-6.1E+00	-1.4E+01	6.2E+00	-1.6E+01	-7.9E-02
6.5E-01	3.1E-01	1.9E+07	8.4E+05	3.2E+01	-5.0E+00	-1.8E+01	5.1E+00	-1.3E+01	-5.9E-02
1.2E+00	0.	3.3E+07	2.7E+06	9.3E+00	-2.1E+00	-3.6E+00	2.1E+00	-4.7E+00	-2.4E-02
1.2E+00	3.1E-01	3.4E+07	2.4E+06	9.4E+00	-2.0E+00	-4.0E+00	2.0E+00	-4.4E+00	-2.2E-02
1.2E+00	6.3E-01	3.4E+07	1.6E+06	9.8E+00	-1.7E+00	-5.1E+00	1.7E+00	-3.7E+00	-1.7E-02
1.2E+00	9.4E-01	3.4E+07	2.7E+05	1.1E+01	-1.6E+00	-7.0E+00	1.6E+00	-2.9E+00	-1.2E-02
1.7E+00	0.	4.8E+07	4.2E+06	4.6E+00	-1.1E+00	-1.3E+00	1.2E+00	-2.2E+00	-1.1E-02
1.7E+00	3.1E-01	4.8E+07	4.0E+06	4.6E+00	-1.1E+00	-1.4E+00	1.1E+00	-2.2E+00	-1.1E-02
1.7E+00	6.3E-01	4.8E+07	3.5E+06	4.6E+00	-1.1E+00	-1.7E+00	1.1E+00	-2.0E+00	-9.3E-03
1.7E+00	9.4E-01	4.9E+07	2.6E+06	4.8E+00	-9.9E-01	-2.1E+00	1.0E+00	-1.7E+00	-7.7E-03
1.7E+00	1.3E+00	4.9E+07	1.4E+06	5.1E+00	-9.4E-01	-2.6E+00	9.4E-01	-1.5E+00	-6.1E-03
2.2E+00	0.	6.1E+07	5.6E+06	2.8E+00	-7.6E-01	-5.2E-01	7.7E-01	-1.3E+00	-6.3E-03
2.2E+00	3.1E-01	6.1E+07	5.5E+06	2.8E+00	-7.6E-01	-5.5E-01	7.7E-01	-1.3E+00	-6.1E-03
2.2E+00	6.3E-01	6.1E+07	5.3E+06	2.8E+00	-7.5E-01	-6.2E-01	7.6E-01	-1.2E+00	-5.7E-03
2.2E+00	9.4E-01	6.2E+07	4.8E+06	2.9E+00	-7.4E-01	-7.5E-01	7.4E-01	-1.1E+00	-5.0E-03
2.2E+00	1.3E+00	6.3E+07	4.0E+06	2.9E+00	-7.2E-01	-9.2E-01	7.2E-01	-9.9E-01	-4.3E-03
2.2E+00	1.6E+00	6.3E+07	2.8E+06	3.0E+00	-7.1E-01	-1.1E+00	7.1E-01	-8.8E-01	-3.6E-03
2.2E+00	1.9E+00	6.4E+07	1.4E+06	3.2E+00	-7.2E-01	-1.4E+00	7.2E-01	-7.7E-01	-3.0E-03
2.8E+00	0. *	7.3E+07	6.4E+06	2.0E+00	-5.4E-01	-1.5E-01	5.5E-01	-8.5E-01	-4.0E-03
2.8E+00	3.1E-01	7.3E+07	6.4E+06	2.0E+00	-5.5E-01	-1.6E-01	5.5E-01	-8.4E-01	-3.9E-03
2.8E+00	6.3E-01	7.3E+07	6.2E+06	2.0E+00	-5.5E-01	-1.9E-01	5.5E-01	-8.1E-01	-3.7E-03
2.8E+00	9.4E-01	7.4E+07	6.0E+06	2.0E+00	-5.6E-01	-2.4E-01	5.6E-01	-7.6E-01	-3.4E-03
2.8E+00	1.3E+00	7.5E+07	5.6E+06	2.0E+00	-5.6E-01	-3.1E-01	5.6E-01	-7.1E-01	-3.1E-03

Table J-I (Continued)

KX (1/CM)	KZ (1/CM)	FREQUENCY (1/SEC)	DDIELECTRIC	ADIELECTRIC	EDIELECTRIC
2.8E+00	1.6E+00	7.5E+07 5.0E+06	2.0E+00 -5.7E-01	-3.9E-01 5.7E-01	-6.5E-01 -2.7E-03
2.8E+00	1.9E+00	7.6E+07 4.1E+06	2.1E+00 -5.8E-01	-4.9E-01 5.8E-01	-5.8E-01 -2.4E-03
3.3E+00	0.	8.4E+07 6.1E+06	1.6E+00 -3.9E-01	4.0E-02 3.9E-01	-6.0E-01 -2.7E-03
3.3E+00	3.1E-01	8.4E+07 6.1E+06	1.6E+00 -3.9E-01	3.5E-02 3.9E-01	-5.9E-01 -2.7E-03
3.3E+00	6.3E-01	8.4E+07 6.1E+06	1.6E+00 -4.0E-01	2.1E-02 4.0E-01	-5.8E-01 -2.6E-03
3.3E+00	9.4E-01	8.5E+07 6.0E+06	1.6E+00 -4.1E-01	-2.8E-03 4.1E-01	-5.5E-01 -2.4E-03
3.3E+00	1.3E+00	8.5E+07 5.9E+06	1.6E+00 -4.2E-01	-3.5E-02 4.2E-01	-5.2E-01 -2.3E-03
3.3E+00	1.6E+00	8.6E+07 5.6E+06	1.6E+00 -4.3E-01	-7.4E-02 4.4E-01	-4.9E-01 -2.1E-03
3.3E+00	1.9E+00	8.7E+07 5.1E+06	1.6E+00 -4.5E-01	-1.2E-01 4.5E-01	-4.5E-01 -1.9E-03

* DOMINANT MODE

160

Table J-II

Linear Solutions for the Large Relative Velocity Bump-on-the-Tail Distribution

KX (1/CM)	KZ (1/CM)	FREQUENCY (1/SEC)		DDIELECTRIC		ADIELECTRIC		EDIELECTRIC	
2.0E-01	6.0E-01	1.9E+07	1.6E+06	2.8E+01	-6.4E+00	-1.1E+01	6.5E+00	-1.6E+01	-8.7E-02
3.5E-01	1.1E+00	3.3E+07	2.8E+06	9.4E+00	-2.2E+00	-3.4E+00	2.2E+00	-5.0E+00	-2.6E-02
5.0E-01	1.1E+00	4.2E+07	4.2E+06	5.3E+00	-1.2E+00	3.1E-01	1.3E+00	-4.6E+00	-2.9E-02
5.0E-01	1.6E+00	4.6E+07	4.2E+06	4.8E+00	-1.2E+00	-1.4E+00	1.2E+00	-2.4E+00	-1.2E-02
5.0E-01	2.1E+00	4.8E+07	9.6E+05	5.4E+00	-9.6E-01	-3.0E+00	9.7E-01	-1.5E+00	-6.0E-03
6.5E-01	1.6E+00	5.5E+07	5.5E+06	3.2E+00	-7.6E-01	1.1E-01	7.8E-01	-2.3E+00	-1.3E-02
6.5E-01	2.1E+00	5.9E+07	5.5E+06	3.0E+00	-8.0E-01	-5.7E-01	8.1E-01	-1.4E+00	-6.9E-03
6.5E-01	2.5E+00	6.1E+07	2.9E+06	3.2E+00	-7.3E-01	-1.2E+00	7.3E-01	-9.5E-01	-4.0E-03
8.0E-01	2.1E+00	6.7E+07	5.9E+06	2.2E+00	-5.0E-01	1.4E-01	5.0E-01	-1.3E+00	-7.3E-03
8.0E-01	2.5E+00 *	7.1E+07	6.3E+06	2.1E+00	-5.8E-01	-2.0E-01	5.8E-01	-9.2E-01	-4.4E-03
8.0E-01	3.0E+00	7.3E+07	4.5E+06	2.2E+00	-5.9E-01	-5.1E-01	6.0E-01	-6.7E-01	-2.8E-03
8.0E-01	3.5E+00	7.5E+07	1.4E+06	2.4E+00	-6.4E-01	-8.6E-01	6.4E-01	-5.1E-01	-1.9E-03
9.5E-01	2.5E+00	7.8E+07	5.3E+06	1.7E+00	-3.2E-01	1.9E-01	3.2E-01	-8.9E-01	-4.6E-03
9.5E-01	3.0E+00	8.1E+07	6.3E+06	1.6E+00	-4.2E-01	3.7E-03	4.3E-01	-6.5E-01	-3.0E-03
9.5E-01	3.5E+00	8.4E+07	5.3E+06	1.7E+00	-4.8E-01	-1.7E-01	4.8E-01	-5.0E-01	-2.1E-03
1.1E+00	3.0E+00	8.8E+07	3.1E+06	1.4E+00	-1.6E-01	2.3E-01	1.6E-01	-6.3E-01	-3.1E-03
1.1E+00	3.5E+00	9.1E+07	5.1E+06	1.4E+00	-2.9E-01	1.2E-01	3.0E-01	-4.8E-01	-2.2E-03

* DOMINANT MODE

Table J-III

Linear Solutions for the Low Relative Velocity 200-km Simulation

KX (1/CM)	KZ (1/CM)	FREQUENCY (1/SEC)	DDIELECTRIC	ADIELECTRIC	EDIELECTRIC
2.2E-02	0.	8.6E+04 8.1E+04	1.2E+04 -2.3E+04	2.2E+02 2.3E+04	-1.2E+04 -1.4E+01
8.0E-01	0.	3.2E+06 2.9E+06	8.9E+00 -1.7E+01	5.8E-01 1.7E+01	-8.4E+00 -1.0E-02
8.0E-01	3.6E-01	3.4E+06 2.5E+06	9.1E+00 -1.8E+01	-1.0E+00 1.8E+01	-7.0E+00 -8.0E-03
8.0E-01	7.2E-01	4.0E+06 1.2E+06	1.1E+01 -1.8E+01	-5.3E+00 1.8E+01	-4.7E+00 -5.2E-03
1.6E+00	0.	6.1E+06 4.9E+06	2.7E+00 -4.7E+00	4.6E-01 4.7E+00	-2.2E+00 -2.5E-03
1.6E+00	3.6E-01	6.1E+06 4.7E+06	2.7E+00 -4.7E+00	3.4E-01 4.7E+00	-2.1E+00 -2.3E-03
1.6E+00	7.2E-01	6.4E+06 4.1E+06	2.8E+00 -4.8E+00	1.8E-02 4.8E+00	-1.8E+00 -2.0E-03
1.6E+00	1.1E+00	6.8E+06 3.0E+06	3.0E+00 -5.0E+00	-4.9E-01 5.0E+00	-1.5E+00 -1.6E-03
1.6E+00	1.4E+00	7.5E+06 1.4E+06	3.4E+00 -5.1E+00	-1.2E+00 5.1E+00	-1.2E+00 -1.3E-03
2.4E+00	0. *	8.7E+06 5.7E+06	1.5E+00 -2.2E+00	4.3E-01 2.2E+00	-9.7E-01 -1.1E-03
2.4E+00	3.6E-01	8.7E+06 5.6E+06	1.5E+00 -2.3E+00	4.0E-01 2.3E+00	-9.5E-01 -1.0E-03
2.4E+00	7.2E-01	8.8E+06 5.2E+06	1.6E+00 -2.3E+00	3.3E-01 2.3E+00	-8.9E-01 -9.5E-04
2.4E+00	1.1E+00	9.1E+06 4.5E+06	1.6E+00 -2.3E+00	2.2E-01 2.3E+00	-8.1E-01 -8.4E-04
2.4E+00	1.4E+00	9.5E+06 3.5E+06	1.6E+00 -2.4E+00	6.5E-02 2.4E+00	-7.1E-01 -7.3E-04
2.4E+00	1.8E+00	1.0E+07 2.0E+06	1.7E+00 -2.5E+00	-1.3E-01 2.5E+00	-6.2E-01 -6.2E-04
2.4E+00	2.2E+00	1.1E+07 2.4E+05	1.9E+00 -2.6E+00	-3.6E-01 2.6E+00	-5.3E-01 -5.3E-04
3.1E+00	0.	1.1E+07 5.3E+06	1.1E+00 -1.4E+00	4.2E-01 1.4E+00	-5.5E-01 -5.7E-04
3.1E+00	3.6E-01	1.1E+07 5.2E+06	1.1E+00 -1.4E+00	4.1E-01 1.4E+00	-5.4E-01 -5.6E-04
3.1E+00	7.2E-01	1.1E+07 4.9E+06	1.1E+00 -1.4E+00	3.8E-01 1.4E+00	-5.2E-01 -5.4E-04
3.1E+00	1.1E+00	1.1E+07 4.4E+06	1.1E+00 -1.4E+00	3.4E-01 1.4E+00	-4.9E-01 -5.0E-04
3.1E+00	1.4E+00	1.1E+07 3.6E+06	1.2E+00 -1.4E+00	2.9E-01 1.4E+00	-4.6E-01 -4.5E-04
3.1E+00	1.8E+00	1.2E+07 2.6E+06	1.2E+00 -1.5E+00	2.2E-01 1.5E+00	-4.2E-01 -4.0E-04
3.1E+00	2.2E+00	1.2E+07 1.2E+06	1.2E+00 -1.5E+00	1.4E-01 1.5E+00	-3.7E-01 -3.6E-04

Table J-III (Continued)

KX (1/CM)	KZ (1/CM)	FREQUENCY (1/SEC)		DDIELECTRIC		ADIELECTRIC		EDIELECTRIC	
3.9E+00	0.	1.3E+07	3.7E+06	9.5E-01	-9.2E-01	4.1E-01	9.2E-01	-3.5E-01	-3.5E-04
3.9E+00	3.6E-01	1.3E+07	3.6E+06	9.5E-01	-9.3E-01	4.0E-01	9.3E-01	-3.5E-01	-3.4E-04
3.9E+00	7.2E-01	1.3E+07	3.3E+06	9.5E-01	-9.4E-01	3.9E-01	9.4E-01	-3.4E-01	-3.3E-04
3.9E+00	1.1E+00	1.3E+07	2.9E+06	9.6E-01	-9.5E-01	3.7E-01	9.5E-01	-3.3E-01	-3.2E-04
3.9E+00	1.4E+00	1.3E+07	2.3E+06	9.6E-01	-9.7E-01	3.5E-01	9.7E-01	-3.1E-01	-3.0E-04
3.9E+00	1.8E+00	1.4E+07	1.5E+06	9.8E-01	-1.0E+00	3.2E-01	1.0E+00	-2.9E-01	-2.7E-04
3.9E+00	2.2E+00	1.4E+07	4.3E+05	9.9E-01	-1.0E+00	2.8E-01	1.0E+00	-2.7E-01	-2.5E-04
4.7E+00	0.	1.5E+07	9.1E+05	8.5E-01	-6.7E-01	4.0E-01	6.7E-01	-2.5E-01	-2.3E-04
4.7E+00	3.6E-01	1.5E+07	8.5E+05	8.5E-01	-6.7E-01	4.0E-01	6.7E-01	-2.4E-01	-2.3E-04
4.7E+00	7.2E-01	1.5E+07	6.4E+05	8.5E-01	-6.7E-01	3.9E-01	6.7E-01	-2.4E-01	-2.2E-04
4.7E+00	1.1E+00	1.5E+07	2.8E+05	8.5E-01	-6.8E-01	3.8E-01	6.8E-01	-2.3E-01	-2.1E-04

* DOMINANT MODE

AFIT/DS/PH/78-1

Table J-IV

Linear Solutions for the High Relative Velocity 200-km Simulation

KX (1/CM)	KZ (1/CM)	FREQUENCY (1/SEC)	DDIELECTRIC	ADIELECTRIC	EDIELECTRIC
1.3E-01	1.8E-01	1.4E+06 9.3E+05	6.5E+01 -4.7E+01	4.6E+01 4.8E+01	-1.1E+02 -2.1E-01
3.3E-01	5.8E-01	3.8E+06 2.7E+06	8.4E+00 -9.1E+00	4.7E+00 9.1E+00	-1.2E+01 -2.0E-02
3.3E-01	9.9E-01	5.0E+06 9.3E+05	7.2E+00 -1.1E+01	-1.2E+00 1.1E+01	-5.0E+00 -7.2E-03
5.2E-01	5.8E-01	5.0E+06 1.2E+06	5.7E+00 -1.4E+00	4.2E+00 1.4E+00	-8.9E+00 -1.7E-02
5.2E-01	9.9E-01	6.0E+06 3.8E+06	3.5E+00 -3.7E+00	1.9E+00 3.7E+00	-4.4E+00 -7.0E-03
5.2E-01	1.4E+00	7.0E+06 2.2E+06	3.1E+00 -4.2E+00	3.7E-01 4.2E+00	-2.5E+00 -3.5E-03
7.2E-01	9.9E-01	7.3E+06 3.1E+06	2.7E+00 -1.4E+00	1.9E+00 1.4E+00	-3.7E+00 -6.5E-03
7.2E-01	1.4E+00 *	8.1E+06 4.2E+06	2.1E+00 -2.0E+00	1.1E+00 2.0E+00	-2.2E+00 -3.4E-03
7.2E-01	1.8E+00	9.0E+06 2.6E+06	1.9E+00 -2.3E+00	5.3E-01 2.3E+00	-1.5E+00 -2.0E-03
9.1E-01	1.4E+00	9.2E+06 3.3E+06	1.8E+00 -9.3E-01	1.2E+00 9.3E-01	-2.0E+00 -3.3E-03
9.1E-01	1.8E+00	1.0E+07 3.8E+06	1.5E+00 -1.3E+00	8.3E-01 1.3E+00	-1.3E+00 -2.0E-03
9.1E-01	2.2E+00	1.1E+07 2.2E+06	1.4E+00 -1.5E+00	5.3E-01 1.5E+00	-9.6E-01 -1.3E-03
1.1E+00	1.8E+00	1.1E+07 2.5E+06	1.4E+00 -6.4E-01	8.7E-01 6.4E-01	-1.2E+00 -1.9E-03
1.1E+00	2.2E+00	1.2E+07 2.6E+06	1.2E+00 -8.6E-01	6.8E-01 8.6E-01	-9.0E-01 -1.3E-03
1.1E+00	2.6E+00	1.2E+07 8.8E+05	1.2E+00 -1.0E+00	5.0E-01 1.0E+00	-6.8E-01 -8.9E-04
1.3E+00	2.2E+00	1.2E+07 6.7E+05	1.1E+00 -4.4E-01	7.0E-01 4.4E-01	-8.3E-01 -1.2E-03
1.3E+00	2.6E+00	1.3E+07 5.3E+05	1.1E+00 -6.1E-01	5.9E-01 6.1E-01	-6.4E-01 -8.6E-04

* DOMINANT MODE

164

Table J-V

Linear Solutions Showing a Mixture of Modified Two-Stream and Ion-Ion Modes

KX (1/CM)	KZ (1/CM)	FREQUENCY (1/SEC)		DDIELECTRIC		ADIELECTRIC		EDIELECTRIC	
1.2E-03	0.	5.8E+03	7.4E+03	1.5E+03	-5.4E+03	-1.5E+03	5.4E+03	-1.2E-01	-1.4E-11
2.8E-02	0.	1.3E+05	1.5E+05	3.6E+00	-1.1E+01	-2.5E+00	1.1E+01	-1.2E-01	-6.1E-09
2.8E-02	1.0E-04	2.5E+05	1.1E+04	9.3E+00	-1.1E+00	-2.3E+01	3.1E+01	1.5E+01	-3.0E+01
5.4E-02	0.	2.3E+05	2.4E+05	1.4E+00	-3.4E+00	-2.8E-01	3.4E+00	-1.2E-01	-1.7E-08
5.4E-02	1.0E-04	3.5E+05	1.8E+05	2.2E+00	-2.2E+00	-1.6E+00	4.6E+00	4.5E-01	-2.4E+00
8.0E-02	0. *	3.1E+05	2.6E+05	9.9E-01	-1.8E+00	1.3E-01	1.8E+00	-1.2E-01	-2.6E-08
8.0E-02	1.0E-04	4.1E+05	2.4E+05	1.1E+00	-1.3E+00	-1.9E-01	2.1E+00	5.7E-02	-7.2E-01
1.1E-01	0.	3.8E+05	2.2E+05	8.5E-01	-1.1E+00	2.7E-01	1.1E+00	-1.2E-01	-2.7E-08
1.1E-01	1.0E-04	4.6E+05	2.3E+05	8.4E-01	-9.2E-01	1.3E-01	1.3E+00	2.8E-02	-3.3E-01
1.1E-01	2.1E-04	6.2E+05	1.9E+05	8.6E-01	-5.7E-01	-1.5E-01	1.5E+00	2.9E-01	-9.7E-01
1.1E-01	3.1E-04	7.6E+05	7.2E+04	8.5E-01	-2.4E-01	-5.4E-01	2.1E+00	6.8E-01	-1.8E+00
1.3E-01	0.	4.4E+05	1.4E+05	7.9E-01	-8.0E-01	3.3E-01	8.0E-01	-1.2E-01	-2.0E-08
1.3E-01	1.0E-04	5.1E+05	1.7E+05	7.2E-01	-6.8E-01	2.5E-01	8.5E-01	3.0E-02	-1.7E-01
1.3E-01	2.1E-04	6.6E+05	1.6E+05	6.8E-01	-4.6E-01	1.0E-01	1.0E+00	2.2E-01	-5.5E-01
1.3E-01	3.1E-04	8.1E+05	8.9E+04	6.6E-01	-2.5E-01	-5.9E-02	1.2E+00	4.0E-01	-1.0E+00
1.6E-01	0.	4.9E+05	1.7E+04	7.6E-01	-5.8E-01	3.6E-01	5.8E-01	-1.2E-01	-2.6E-09
1.6E-01	1.0E-04	5.3E+05	7.3E+04	6.7E-01	-5.4E-01	3.0E-01	6.0E-01	3.2E-02	-6.2E-02
1.6E-01	2.1E-04	6.9E+05	9.8E+04	5.9E-01	-3.7E-01	2.0E-01	7.0E-01	2.1E-01	-3.3E-01
1.6E-01	3.1E-04	8.4E+05	5.1E+04	5.5E-01	-2.2E-01	1.1E-01	8.5E-01	3.3E-01	-6.3E-01

* DOMINANT MODE

Table J-VI

Linear Solutions for the Low Relative Velocity 600-km Simulation

KX (1/CM)	KZ (1/CM)	FREQUENCY (1/SEC)		DDIELECTRIC		ADIELECTRIC		EDIELECTRIC	
9.0E-03	0.	4.3E+04	5.4E+04	2.8E+01	-1.0E+02	-2.7E+01	1.0E+02	-1.2E-01	-7.3E-10
9.0E-03	1.0E-02	5.1E+04	3.2E+03	9.9E+01	-1.4E+02	-6.8E+01	1.4E+02	-3.0E+01	-4.6E-02
3.3E-02	0.	1.5E+05	1.7E+05	2.7E+00	-8.3E+00	-1.6E+00	8.3E+00	-1.2E-01	-8.2E-09
3.3E-02	1.0E-02	1.3E+05	1.1E+05	5.7E+00	-1.1E+01	6.8E-02	1.1E+01	-4.8E+00	-1.8E-02
3.3E-02	2.0E-02	1.4E+05	8.2E+04	6.1E+00	-1.1E+01	-1.2E+00	1.1E+01	-3.8E+00	-7.8E-03
3.3E-02	3.0E-02	1.6E+05	3.8E+04	7.1E+00	-1.1E+01	-3.3E+00	1.1E+01	-2.8E+00	-4.4E-03
5.6E-02	0.	2.3E+05	2.5E+05	1.3E+00	-3.2E+00	-2.2E-01	3.2E+00	-1.2E-01	-1.8E-08
5.6E-02	1.0E-02	2.1E+05	1.6E+05	2.3E+00	-3.8E+00	4.3E-01	3.8E+00	-1.8E+00	-1.1E-02
5.6E-02	2.0E-02	2.2E+05	1.4E+05	2.4E+00	-3.9E+00	2.6E-01	3.9E+00	-1.6E+00	-5.0E-03
5.6E-02	3.0E-02	2.3E+05	1.2E+05	2.4E+00	-4.0E+00	-6.9E-03	4.0E+00	-1.4E+00	-3.0E-03
5.6E-02	4.0E-02	2.4E+05	8.7E+04	2.6E+00	-4.1E+00	-3.6E-01	4.1E+00	-1.2E+00	-2.1E-03
5.6E-02	5.0E-02	2.6E+05	4.0E+04	2.8E+00	-4.2E+00	-8.1E-01	4.2E+00	-1.0E+00	-1.5E-03
8.0E-02	0.	3.1E+05	2.6E+05	1.0E+00	-1.8E+00	1.3E-01	1.8E+00	-1.2E-01	-2.6E-08
8.0E-02	1.0E-02	2.9E+05	1.7E+05	1.5E+00	-2.0E+00	4.5E-01	2.0E+00	-9.5E-01	-7.1E-03
8.0E-02	2.0E-02	2.9E+05	1.6E+05	1.5E+00	-2.1E+00	4.1E-01	2.1E+00	-9.1E-01	-3.4E-03
8.0E-02	3.0E-02	3.0E+05	1.4E+05	1.5E+00	-2.1E+00	3.3E-01	2.1E+00	-8.5E-01	-2.2E-03
8.0E-02	4.0E-02	3.0E+05	1.2E+05	1.5E+00	-2.2E+00	2.3E-01	2.2E+00	-7.8E-01	-1.5E-03
8.0E-02	5.0E-02	3.1E+05	9.0E+04	1.6E+00	-2.2E+00	1.1E-01	2.2E+00	-7.0E-01	-1.1E-03
8.0E-02	6.0E-02	3.3E+05	5.0E+04	1.7E+00	-2.3E+00	-3.9E-02	2.3E+00	-6.3E-01	-8.9E-04
1.0E-01	0.	3.7E+05	2.3E+05	8.6E-01	-1.2E+00	2.6E-01	1.2E+00	-1.2E-01	-2.8E-08
1.0E-01	1.0E-02	3.5E+05	1.4E+05	1.2E+00	-1.3E+00	4.5E-01	1.3E+00	-6.2E-01	-5.2E-03
1.0E-01	2.0E-02	3.5E+05	1.4E+05	1.2E+00	-1.3E+00	4.3E-01	1.3E+00	-6.0E-01	-2.5E-03
1.0E-01	3.0E-02	3.6E+05	1.2E+05	1.2E+00	-1.3E+00	4.0E-01	1.3E+00	-5.8E-01	-1.6E-03

Table J-VI (Continued)

KX (1/CM)	KZ (1/CM)	FREQUENCY (1/SEC)		DDIELECTRIC		ADIELECTRIC		EDIELECTRIC	
1.0E-01	4.0E-02	3.6E+05	1.1E+05	1.2E+00	-1.4E+00	3.6E-01	1.4E+00	-5.4E-01	-1.2E-03
1.0E-01	5.0E-02	3.7E+05	8.2E+04	1.2E+00	-1.4E+00	3.1E-01	1.4E+00	-5.1E-01	-9.0E-04
1.0E-01	6.0E-02	3.8E+05	5.2E+04	1.2E+00	-1.4E+00	2.5E-01	1.4E+00	-4.7E-01	-7.1E-04
1.3E-01	0.	4.3E+05	1.6E+05	8.0E-01	-8.7E-01	3.2E-01	8.7E-01	-1.2E-01	-2.2E-08
1.3E-01	1.0E-02	4.1E+05	8.0E+04	1.0E+00	-9.0E-01	4.4E-01	9.1E-01	-4.5E-01	-4.0E-03
1.3E-01	2.0E-02	4.1E+05	7.4E+04	1.0E+00	-9.1E-01	4.4E-01	9.1E-01	-4.4E-01	-2.0E-03
1.3E-01	3.0E-02	4.1E+05	6.5E+04	1.0E+00	-9.2E-01	4.2E-01	9.3E-01	-4.3E-01	-1.3E-03
1.3E-01	4.0E-02	4.2E+05	5.0E+04	1.0E+00	-9.4E-01	4.0E-01	9.4E-01	-4.1E-01	-9.3E-04
1.3E-01	5.0E-02	4.2E+05	3.1E+04	1.0E+00	-9.6E-01	3.8E-01	9.6E-01	-4.0E-01	-7.2E-04
1.3E-01	6.0E-02	4.3E+05	7.3E+03	1.0E+00	-9.9E-01	3.5E-01	9.9E-01	-3.8E-01	-5.8E-04
1.5E-01	0.	4.8E+05	6.3E+04	7.7E-01	-6.5E-01	3.5E-01	6.5E-01	-1.2E-01	-9.6E-09

* DOMINANT MODE

167

Table J-VII

Linear Solutions for the High Relative Velocity 600-km Simulation

KX (1/CM)	KZ (1/CM)	FREQUENCY (1/SEC)		DDIELECTRIC		ADIELECTRIC		EDIELECTRIC	
3.0E-03	0.	4.4E+04	9.7E+04	6.7E+00	-5.8E+01	-5.5E+00	5.8E+01	-1.2E-01	-1.4E-09
9.9E-03	0.	1.4E+05	2.9E+05	1.1E+00	-5.7E+00	3.1E-02	5.7E+00	-1.2E-01	-1.3E-08
9.9E-03	1.3E-02	1.1E+05	6.3E+04	1.2E+01	-7.7E+00	8.7E+00	7.7E+00	-2.0E+01	-4.7E-02
9.9E-03	2.7E-02	1.4E+05	5.6E+04	7.4E+00	-1.1E+01	3.1E-01	1.1E+01	-6.7E+00	-1.0E-02
1.7E-02	0.	2.3E+05	4.2E+05	7.4E-01	-2.2E+00	3.9E-01	2.2E+00	-1.2E-01	-3.1E-08
1.7E-02	2.7E-02	1.8E+05	1.1E+05	3.9E+00	-3.1E+00	2.6E+00	3.1E+00	-5.5E+00	-1.1E-02
1.7E-02	4.0E-02	2.1E+05	1.0E+05	3.0E+00	-3.9E+00	8.8E-01	3.9E+00	-2.9E+00	-4.6E-03
2.4E-02	0. *	3.1E+05	4.8E+05	6.5E-01	-1.2E+00	4.8E-01	1.2E+00	-1.2E-01	-4.7E-08
2.4E-02	2.7E-02	2.0E+05	1.8E+03	3.3E+00	-2.7E-01	2.0E+00	2.8E-01	-4.3E+00	-9.5E-03
2.4E-02	4.0E-02	2.5E+05	1.3E+05	2.2E+00	-1.6E+00	1.4E+00	1.6E+00	-2.5E+00	-4.8E-03
2.4E-02	5.3E-02	2.8E+05	1.1E+05	1.9E+00	-2.0E+00	7.6E-01	2.0E+00	-1.6E+00	-2.5E-03
2.4E-02	6.7E-02	3.2E+05	2.6E+04	1.8E+00	-2.2E+00	2.5E-01	2.2E+00	-1.1E+00	-1.5E-03
3.1E-02	0.	3.8E+05	4.7E+05	6.1E-01	-7.3E-01	5.1E-01	7.3E-01	-1.2E-01	-5.7E-08
3.1E-02	4.0E-02	2.8E+05	3.1E+04	1.9E+00	-4.2E-01	1.3E+00	4.2E-01	-2.2E+00	-4.4E-03
3.1E-02	5.3E-02	3.2E+05	1.1E+05	1.5E+00	-9.7E-01	9.5E-01	9.8E-01	-1.5E+00	-2.5E-03
3.1E-02	6.7E-02	3.4E+05	8.9E+04	1.4E+00	-1.2E+00	6.6E-01	1.2E+00	-1.0E+00	-1.5E-03
3.1E-02	8.0E-02	3.7E+05	1.2E+04	1.4E+00	-1.4E+00	4.0E-01	1.4E+00	-7.6E-01	-1.0E-03
3.8E-02	0.	4.5E+05	3.8E+05	6.0E-01	-4.1E-01	5.3E-01	4.1E-01	-1.2E-01	-5.5E-08
3.8E-02	6.7E-02	3.7E+05	5.8E+04	1.2E+00	-6.2E-01	7.4E-01	6.2E-01	-9.6E-01	-1.5E-03
3.8E-02	8.0E-02	4.0E+05	3.5E+04	1.1E+00	-8.0E-01	5.9E-01	8.0E-01	-7.2E-01	-1.0E-03
4.5E-02	0.	5.1E+05	6.3E+04	6.0E-01	-5.5E-02	5.3E-01	5.5E-02	-1.2E-01	-1.0E-08

* DOMINANT MODE

Vita

Robert Carl Backstrom was born on 9 June 1947 in Seattle, Washington, the son of Bert Harold Backstrom and Jean Oliver Backstrom. After graduating from high school in Kirkland, Washington in 1965, he entered the University of Washington. In March 1969 he married the former Conra Sue Randall. In April 1969 he was selected as a member of the College All American Rifle Team. He graduated from the University of Washington Cum Laude in June 1969 with the degree of Bachelor of Science in Physics and was elected to Phi Beta Kappa. He was commissioned that same month as a Second Lieutenant in the United States Air Force and entered active duty in August 1969 assigned to the Air Force Institute of Technology (AFIT) resident school. He graduated from AFIT with distinction in June 1971 with the degree of Master of Science in Physics. His thesis was "An Experimental Evaluation of Theoretical Solar Flare Models." He then served as a space environments forecaster working in the North American Aerospace Defense Command Cheyenne Mountain Complex. Concurrently with that assignment, he was trained and certified as a civilian flight instructor. He returned to AFIT in May 1974 to begin work in the doctoral program.

Permanent address: 11215 Champagne Point Road
Kirkland, Washington 98033

REPORT DOCUMENTATION PAGE		READ INSTRUCTIONS BEFORE COMPLETING FORM
1. REPORT NUMBER AFIT/DS/PH/78-1	2. GOVT ACCESSION NO.	3. RECIPIENT'S CATALOG NUMBER
4. TITLE (and Subtitle) ANOMALOUS TRANSPORT COEFFICIENTS DUE TO THE ION-ION TWO-STREAM PLASMA MICROINSTABILITY		5. TYPE OF REPORT & PERIOD COVERED PhD Dissertation
		6. PERFORMING ORG. REPORT NUMBER
7. AUTHOR(s) Robert C. Backstrom Captain		8. CONTRACT OR GRANT NUMBER(s)
9. PERFORMING ORGANIZATION NAME AND ADDRESS Air Force Institute of Technology (AFIT-EN) Wright-Patterson AFB, Ohio 45433		10. PROGRAM ELEMENT, PROJECT, TASK AREA & WORK UNIT NUMBERS
11. CONTROLLING OFFICE NAME AND ADDRESS Air Force Weapons Laboratory (AFWL/DYC) Kirtland AFB, New Mexico 87117		12. REPORT DATE 6 June 1978
		13. NUMBER OF PAGES 185
14. MONITORING AGENCY NAME & ADDRESS(if different from Controlling Office)		15. SECURITY CLASS. (of this report) Unclassified
		15a. DECLASSIFICATION/DOWNGRADING SCHEDULE

16. DISTRIBUTION STATEMENT (of this Report)

Approved for public release; distribution unlimited

17. DISTRIBUTION STATEMENT (of the abstract entered in Block 20, if different from Report)

18. SUPPLEMENTARY NOTES

Approved for public release, IAW AFR 190-17

JERRAL F. GUESS, Captain, USAF
Director of Information

19. KEY WORDS (Continue on reverse side if necessary and identify by block number)

High Altitude Nuclear Burst Debris-Air Coupling
Ion-Ion Plasma Instability
Quasilinear Plasma Theory
Plasma Instability

20. ABSTRACT (Continue on reverse side if necessary and identify by block number)

Improved calculations of the anomalous transport coefficients due to the ion-ion two-stream plasma instability are presented. The coefficients describe the transfer of momentum and energy between the ion species by the electric fields generated by unstable waves. The calculations use electrostatic quasilinear theory in two dimensions to trace the time evolutions of the two ion species. The evolutions are continued until the transport coefficients reach their maximum values. The evolutions are done for homogeneous plasmas with warm ion beams and a single hot electron background distribution. The electrons may or

DD FORM 1473 EDITION OF 1 NOV 65 IS OBSOLETE
1 JAN 73

may not be magnetized by a uniform magnetic field perpendicular to the ion streaming motion. The results of the evolutions indicate that a fair amount of momentum transfer from the debris to the air occurs when the relative velocity between them is less than the characteristic wave phase velocity of the plasma, the ion acoustic speed or the Alfven speed (respectively for unmagnetized or magnetized electrons). On the other hand, little transfer occurs when the relative velocity is higher than the characteristic speed.

FILMED

9-7